CLOUD CHAMBER STUDIES OF THE PHOTODISINTEGRATION OF LIGHT NUCIEI.

By

Douglas R. O. Morrison

Thesis submitted for the degree of Ph. D. from the University of Glasgow.

PREFACE

This thesis describes work carried out on the photodisintegration of the light nuclei, helium, nitrogen and neon, in the Natural Philosophy Department of Glasgow University, between October 1951 and September 1954.

Experiments on and theories of photodisintegration are critically reviewed in Chapter I. The need for further information on the photodisintegration of light nuclei and on the emission of charged particles is found. The advantages of cloud chamber studies are discussed.

The basic technique established by Mr. J.R. Atkinson, Mr. J.M. Reid and Mr. I.F. Wright, is outlined and the photodisintegration of helium is briefly described in the second chapter. The author assisted in the preparation for a second "run" with helium and did almost all the analysis. The results were interpreted jointly with Mr. I.F. Wright.

The photodisintegration of nitrogen described in Chapter III was next investigated by Mr. I.F. Wright and the author jointly. The preparations for the experiment were shared out between the workers, while the photography and measuring of the films were performed jointly.

The photodisintegration of neon is described in

Chapter IV. This work was performed in collaboration with Mr. G.I. Crawford, Miss M. McClements, Mr. I. Preston and Mr. I.F. Wright. The technique was further improved by Mr. I.F. Wright and the author. The preparation and photography were carried out with Mr. G.I. Crawford's assistance. The analysis was initiated by the author and performed latterly by Mr. G.I. Crawford, Miss M. McClements and Mr. I. Preston. The results which were interpreted jointly, tested the charge independence hypothesis by means of the isotopic spin selection rules as well as providing further information on photodisintegration.

The range-energy relations employed were taken from a review by the author of the range-velocity relations for ions. This is given in the Appendix.

The author is glad to acknowledge the direction and encouragement given by Professor P.I. Dee, Professor J.C. Gunn and Mr. J.R. Atkinson, He is also indebted to Mr. J.M. Reid, Dr. K.G. McNeil, Dr. D. Green and Mr. J.C.W. Telfer for their unstinted help in operating the synchrotron. The author also wishes to thank the Department of Scientific and Industrial Research for the award of a maintenance grant which made this work possible.

CHAPTER I.

REVIEW OF PHOTONUCLEAR EXPERIMENTS AND THEORY.

1.1 Introduction.

After the successful operation of the Cockroft-Walton accelerator, it was generally considered that the nucleus could best be studied by bombarding it with particles and observing its modes of disintegration. On the basis of such particle-induced reactions several models of the nucleus have been devised, but so far no one model explains all the experimental evidence. A study of photo-nuclear reactions yields further information of a different character as the "absorption" of the radiation depends on electro-magnetic rather than nuclear forces.

In the low energy region (< 50 MeV) the models of the nucleus may be appreciated by considering two rather extreme examples. These two models differ in the description of the motion of a nucleon in nuclear matter.

In the first case, the Independent Particle Model, each nucleon is considered to be able to travel appreciable distances in nuclear matter before colliding with another nucleon, being only slightly perturbed by the other nucleons. Thus an incident particle can interact directly with a nucleon and eject it from the nucleus. Assuming a mean free path/

path for the incident particle for collision with a nucleon, allows calculations of the reaction cross-section, angular distribution and energy distribution of the emitted particles. Reactions in which several particles are emitted can be described by considering the possibility of each nucleon colliding again (Goldhaber or "Monte Carlo" method). In this 'direct' interaction the emitted particles will mainly have high energies and the angular distribution will be non-isotropic. Thus we can say the "mean free path", λ, of a nucleon in nuclear matter is long — greater than or of the order of the nuclear radius, R.

In the other case, the Collective Model of the nucleus, collisions between nucleons are very frequent i.e. λ is much smaller than the nuclear radius, R, so that an energetic nucleon shares its energy among the other nucleons very quickly. This intermediate state, called the compound nucleus, can last for an appreciable time until the energy is so distributed that a nucleon or radiation can be emitted, these processes being of a statistical nature. The essential feature is that the state of the compound nucleus (its energy, angular momentum and parity) and its manner of re-emitting energy are both independent of its mode of formation.

A compound state with an energy, E, distributed among/

among the colliding nucleons until one has sufficient energy to be emitted, may be likened to the surface of a liquid at a high temperature in which the molecules are colliding with one another until one has enough energy to escape. Thus the decay of the compound nucleus is similar to the 'evaporation' of nucleons according to the nuclear 'temperature' and the energy distribution is approximately Maxwellian except that transitions to the ground state or to the first few excited states of the product nucleus will appear as discrete resonances.

The assumptions on which this model is based, are that the energy is not too high (< 50 Mev) and that the mean free path is much smaller than the nuclear radius. This latter condition implies that the nucleons interact strongly with very short range forces so that an incident particle has several collisions and loses its energy in a short distance in nuclear matter. Bohr's liquid drop model is similar as it has short range internal forces and shows saturation effects. This picture is in contrast to the Independent Particle Model in which the forces between nucleons are weak and long range and it is assumed there are correlations between nucleons.

Early work on the radiative capture of neutrons favoured the compound nucleus theory (e.g. Feshback and Weisskopf/

Weisskopf, 1949) in which the total capture cross section decreases montonically with energy, but more detailed experiments revealed a considerable number of "undulations" varying systematically throughout the Periodic Table. In view of this, Weisskopf and his co-workers (Feshbach et.al. 1953) assumed an optical model of the nucleus in which the incident neutron was only slowly absorbed in the nucleus. The 'undulations' were then accounted for by the interaction of the incoming wave with the wave of the nucleon in nuclear matter. This 'absorption' requires a very much longer mean free path of the nucleon in nuclear matter, the actual value being 2×10^{-12}cm. This implies that the particle can exist for an appreciable time in the nucleus as an "independent particle" until, after several collisions, a compound nucleus state is formed.

Further support for the Independent Particle Model is the success of the Shell Model. It was observed that when the number of neutrons or protons in the nucleus was one of the "magic" numbers, 2, 8, 14, 20, 28, 50, 82 and 126, the binding energy of that nucleus was very low (e.g. He^4, O^{16} and Si^{28} are doubly magic i.e. N = Z = magic number, and are very stable). Other evidence (not all independant) is that the magic numbers appear in the number of isotopes and isotones occurring for a "magic" Z and N respectively/

respectively; the abundance of the elements in nature; range of radioactive alpha particles; energy of beta-ray emitters (these above all depend on the low binding energy); density of levels, which also leads to minima in the cross sections for (n,γ) reactions; spin; magnetic moment; quadruple moment of nuclei.

In the Shell Model it is assumed that there exist orbits in the nucleus with well defined quantum numbers. This is only possible if the nucleon can travel appreciable distances in the nucleus unperturbed by its neighbours, i.e. that the mean free path is long. This model again neglects correlations between nuclei and surface effects.

Thus the present position is that there are several nuclear models, all of which have their successes -- and their failures. The two main descriptions are firstly, of a collective motion of the nucleons and secondly, of each nucleon moving independently and only slightly perturbed by its neighbours.

The experiments in photodisintegration performed to date will be initially reviewed and an experimental description of various reactions will be built up and compared with the detailed theories of phtodisintegration. These theories are based on the models described above, and it will be shown that when more experiments have been performed/

performed it should be possible to decide between them.

Experimental measurements of (γ,n) reactions will be considered first, as most work has been done on them and as they are the most probable photo-reactions for medium and heavy nuclei as the emission of charged particles is inhibited by the Coulomb barrier. Results for (γ,p), (γ,α), (γ,d), (γ,γ) and other reactions are then considered successively and an experimental picture of photodisintegration is constructed. This picture is compared with the various theoretical predictions and explanations based on the models described above.

The need for experiments on the photodisintegration of light elements is shown and in particular the advantages of using a cloud chamber are demonstrated.

I.2. Gamma-Ray Sources

Photodisintegration studies are severely limited by the lack of well calibrated gamma-ray sources. Up to the present, only two methods of producing gamma-rays have been used.

(a) Gamma-rays from nuclear reactions.

Apart from early experiments on the photodisintegration of the deuteron which has an extremely low threshold (2.23 Mev) so that natural radio-active γ-rays could be used, almost the only γ-ray source employed has been the 17.6 MeV γ-rays from the $Li^7(\gamma,p)$ reaction.

This/

This reaction also emits 14 and 12 MeV γ-rays which complicate the interpretation of the results. The early experiments (before 1948) were performed with the Li^7 $(p\gamma)$-rays.

(b) A source of γ-rays with a continuous energy spectrum was provided by the development of high energy electron accelerators (Betatron, synchrotron and linear accelerator). The electron beam strikes a target made of material of a high Atomic Number and emits bremsstrahlung. Although these machines can produce X-rays of any desired energy, the shape of the energy spectrum is not well known. This is discussed in more detail below.

Recently there have been reports of a photon monochronometer. The energy of the recoil electron is measured and from this, the energy of the photon produced can be calculated. Using a very fast coincidence circuit, the reaction induced by this photon, can be studied. The resolving time required is so short and the X-ray beam has to be run at such low intensity that this technique has not been applied yet.

I.3. Gamma-Neutron Reactions

Experiments on (γ,n) reactions will be classified into two main types -- measurement of the radioactivity of the product nucleus and measurement of the neutron yield. A number of related measurements have been made which provide useful/

useful checks but little else.

(a) Measurement of the Radio-Active Product.

In (γ,p), (γ,pn), (γ,d) and (γ,α) reactions in natural elements, the product is usually stable but in (γ,n) and $(\gamma,2n)$ reactions the product nucleus is normally unstable and measurement of its beta-activity allows the reaction cross section to be measured. The great advantage of this method is that since the counting is done after the beam has passed and when the background is small, whereas other techniques involve counting when the X-ray beam is passing so that the background of photons and electrons is large. The method is then to measure the yield of the unstable product nucleus at successively higher peak energies of the bremsstrahlung — usually in half MeV steps.

The X-ray beam is passed through a monitor and through the sample in front of which is an absorber (e.g. 4 cms. of Lucite) which is chosen such that the photon beam is in equilibrium with its secondary electrons (this allows the energy response to be calculated simply). The sample is removed and its induced γ-activity is measured. A standard Victoreen r-meter is put in place of the sample and the monitor is calibrated in terms of it. Corrections are made for geometrical effects, self-absorption and back-scattering — these corrections are often large. This procedure is repeated at other energies and the activity curve as a function of the peak X-ray is then constructed.

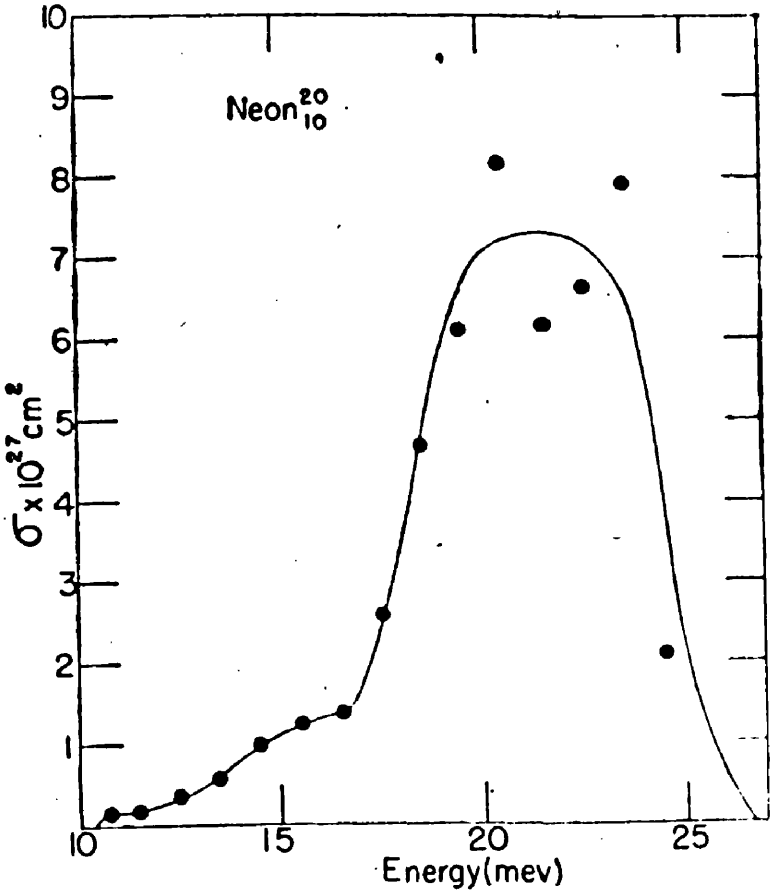
Neon$^{20}_{10}$
$\sigma \times 10^{27} cm^2$
Energy(mev)
10
9
8
7
6
5
4
3
2
1
10
15
20
25

Fig. I.1

Fig. I.3

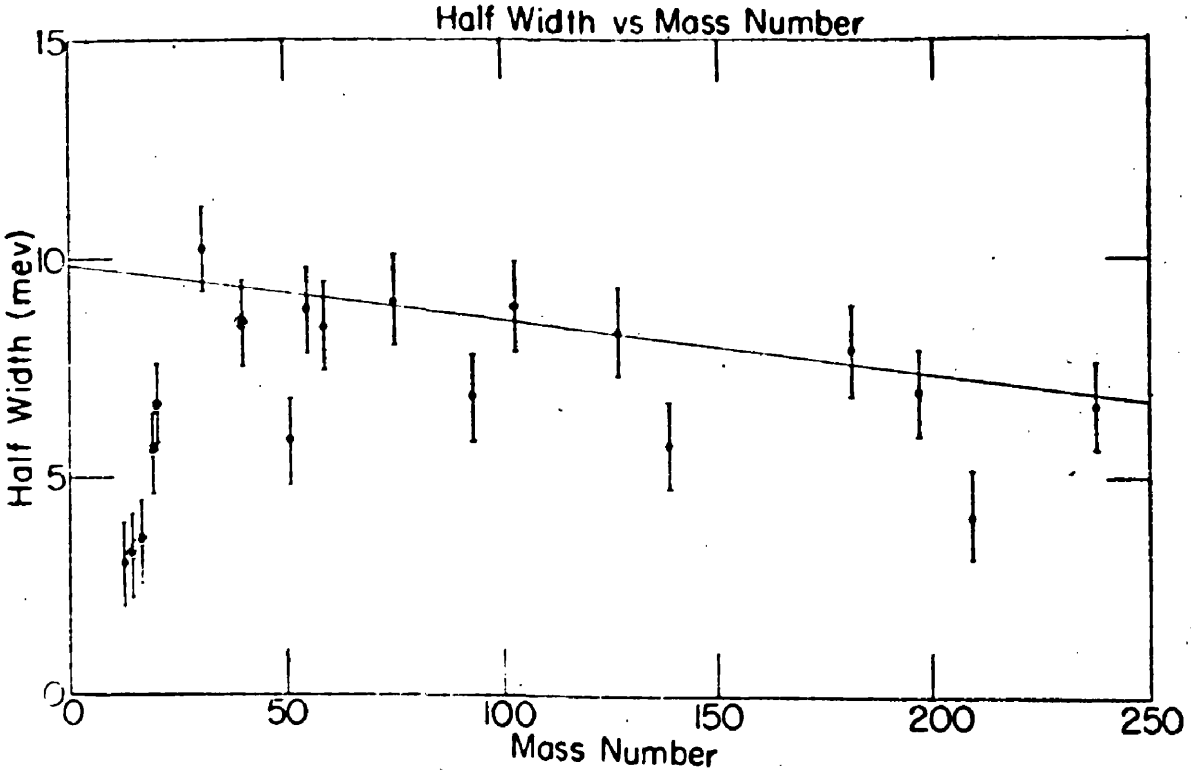
Half Width vs Mass Number
Half Width (mev)
Mass Number
15
10
5
0
0
50
100
150
200
250

The normal method of calculating cross-sections used is the "photon difference" calculations of Katz and Cameron (1951).

If the normalised activities are A_1, A_2, ..., at energies E_1, E_2, ..., where E_o, is the reaction threshold and if P_{ij} is the number of photons in the energy interval centred on $E_{i-\frac{1}{2}}$ where E_j is the peak X-ray energy then,

$$A_1 = \sigma_{\frac{1}{2}} P_{11}$$

$$A_2 = \sigma_{\frac{1}{2}} P_2 + \sigma_{\frac{3}{2}} P_{22}$$

where $\sigma_{\frac{1}{2}}$, $\sigma_{\frac{3}{2}}$, ... , are the cross sections averaged over the intervals E_o to E_1, E_1 to E_2, ... Solution of these equations gives the cross sectional values.

This method of obtaining cross sections is liable to large errors although the activity measurements are quite accurate statistically (3%).

This can be seen by considering the graph of cross section with energy as the "differential" curve obtained from the "integral" curve of the activity measurements. If one value of the cross section has been over-estimated, this will affect the succeeding values the next one being too low etc. so that the values will oscillate e.g. Fig. I.1 for $Ne(\gamma,n)$. The integrated cross section will, however, only vary slightly.

Katz and Cameron (1951) have used an "improved" method in which the activity curve is not now drawn through the experimental points to give the best fit, but is chosen to be such that its first and second derivations are continuous. This certainly avoids any oscillations of the cross section measurement but is really only preventing the errors of their method appearing in the final graph.

It will be noted that this technique and method of analysis tends to conceal the existence of any "fine structure" or levels that may exist.

However, it was found by the Saskatchewan group (Katz et. al., 1954, Goldemberg and Katz, 1954) that when the activity curve is measured in very small energy steps (5 KeV) the yield curve exhibited very definite 'breaks'. which could be interpreted as energy levels. This was only possible due to the exceptional energy stability of the betatron (<5 KeV daily).

The 'breaks' occur at different energies for different targets thus showing that they were not due to machine irregularities.

The Saskatchewan results for $O^{16}(\gamma,n)O^{15}$ have been confirmed by other workers (Penfold and Spicer, 1955, and Collie, 1954).

The success of this method was rather surprising but is now considered definite.

(b) Neutron Yield Measurements.

The advantage of measuring the yield of photoneutrons directly

is that reactions in which the end-products are stable can be studied. This method has the disadvantage that neutrons are sometimes counted from several reactions e.g. one count would be received from (γ,n) or (γ,pn) and two counts from $(\gamma,2n)$ reactions. Another difficulty is that the neutrons are being recorded while the X-ray beam is passing so that it is difficult to separate photoneutrons from the target from background events.

The most widely employed method was to slow down the neutrons from the target in a paraffin box and then measure them by the activity they induced in a Rh. foil (Price and Kerst, 1950) or by means of BF_3 counters (Montalbetti, Katz and Goldenberg, 1953), Jones and Terwilliger (1953), Nathans and Halpern (1954). Neutrons from other directions were slowed down by paraffin and captured with B_4C or Cd foil. The calibration of these measurements was not exact so that while the relative measurements of any one group are reasonably consistent, the absolute values are in doubt.

It was frequently found that the neutron yield cross section could be interpreted as the summation of two reactions. With a judicious use of reaction thresholds and subtraction of previous (γ,n) measurements it was possible to obtain estimates of (γ,pn) and $(\gamma,2n)$ reactions.

The variation of cross section with energy was obtained as before and so was subject to appreciable absolute errors. As the (γ,pn) and $(\gamma,2n)$ cross sections were obtained by subtraction the

errors in them were appreciable.

The energy distribution of the photoneutrons cannot be measured by this method. Angular distributions cannot be measured with the BF_3 counters due to their large size, but Price and Kerst (1950) have obtained some angular distributions with their smaller Rh foil. Poss (1950) has measured the angular distribution of high energy neutrons, detecting them by the activity they produce in an aluminium foil by the $Al^{27}(n,p)Mg^{27}$ reaction which has a threshold of 4.6 MeV.

Energy and angular distributions have, however, been obtained by observing recoiling protons in photographic plates but background neutrons may yield anomalous results e.g. see Section III.5.

(c) Results for the (γ,n) Reaction

The early experiments of Bothe and Gentner (1932) using 17.6 MeV gamma rays gave large variations in yield. The experiments of Baldwin and Klaiber (1948) using a betatron then showed that in all elements, there existed a large maximum in the cross section at about 15 to 20 MeV, which was several MeV wide. This was called the "Giant Resonance". The fact that this giant resonance appeared to occur with all elements suggested that this was a fundamental property of the nucleus and resulted in many more experiments being performed. The experimental conclusions are:

1) There exists a giant resonance in all photoneutron reactions.

2) The giant resonance has been found to be symmetrical in all cases

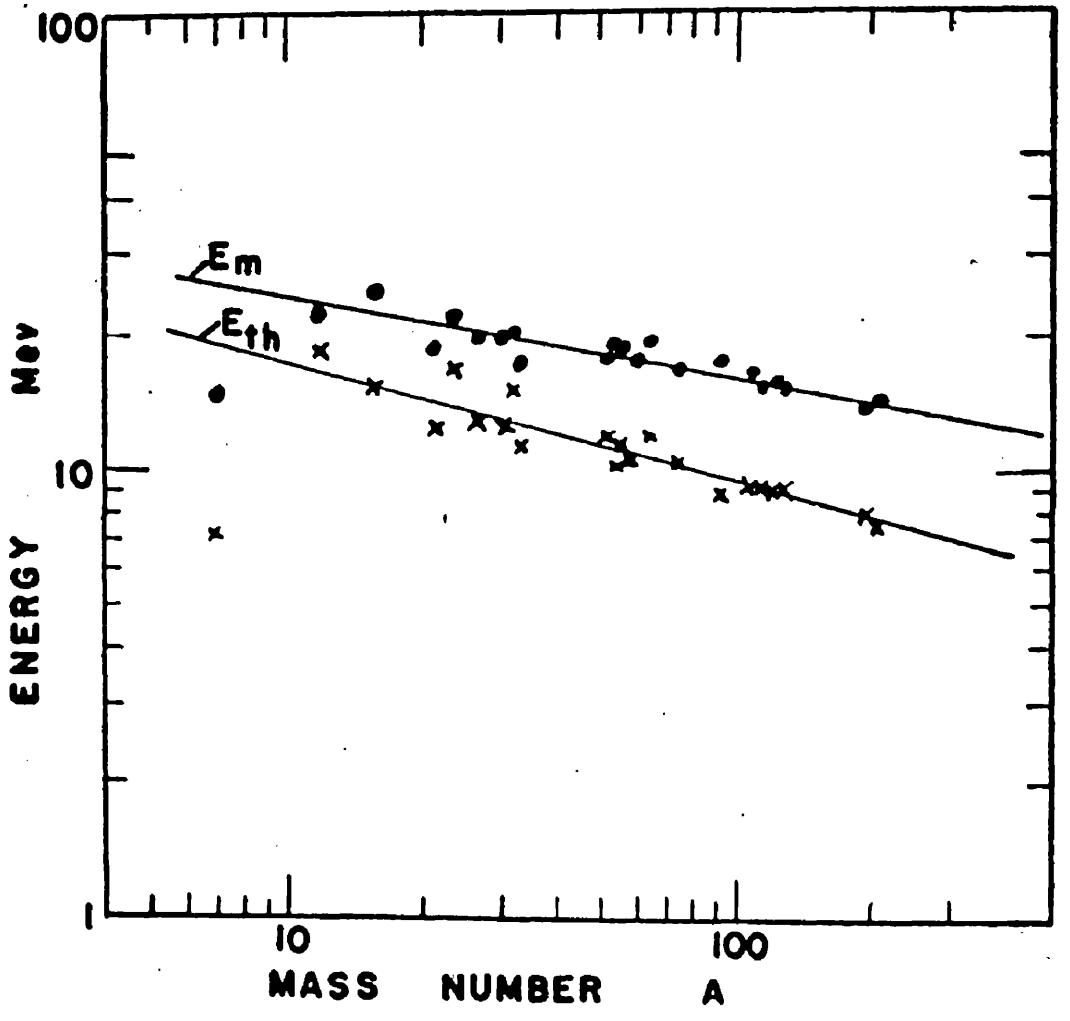

Fig. I.2.

except for C^{12} and Fe^{54} which have high (γ,n) thresholds.

3) The energy, E_m, at which the (γ,n) cross section is a maximum, varies uniformly with A as shown in Fig. I.2. Nathans and Halpern (1954) found that

$$E_m = 38.5.\ A^{-0.186 \pm 0.011}$$

while Montalbetti et. al. (1954) gave

$$E_m = 37 \times A^{-0.184}$$

The errors in the measurement of E_m are appreciable (e.g. see Fig. I.1) and the errors in the powers of A do seem optimistic e.g. it has been suggested that E_m is constant for low values of A.

4) As shown in Fig. I.2, E_m has a constant value above the (γ,n) threshold energy E_{th}. This agreement, however, is probably fortuitous.

5) The width, Γ, at half-maximum of the giant resonance is normally about 6 MeV, but it was noted by Nathans and Halpern (1954) that when the number of neutrons was magic (i.e. with Carbon, Vanadium, Columbium, Lanthanum and Bismuth), the giant resonance is much narrower. It has also been found that Γ is less for the light elements as shown in Fig. I.3.

6) The integrated yields, $\int \sigma.dE$, are a smooth function of A except that the (γ,n) yield in Nickel is low. The $N^{14}(\gamma,n)$ yield was also found to be anomalously low, as shown in Fig. III.1. It is expected from the Sum Rule, see Section I.10, that the integrated yield should be a function of $\frac{NZ}{A}$. A plot of $\frac{\int \sigma.dE}{NZ/A}$ is shown in Fig. I.4. It was found that the light elements fell well below the expected values. This can

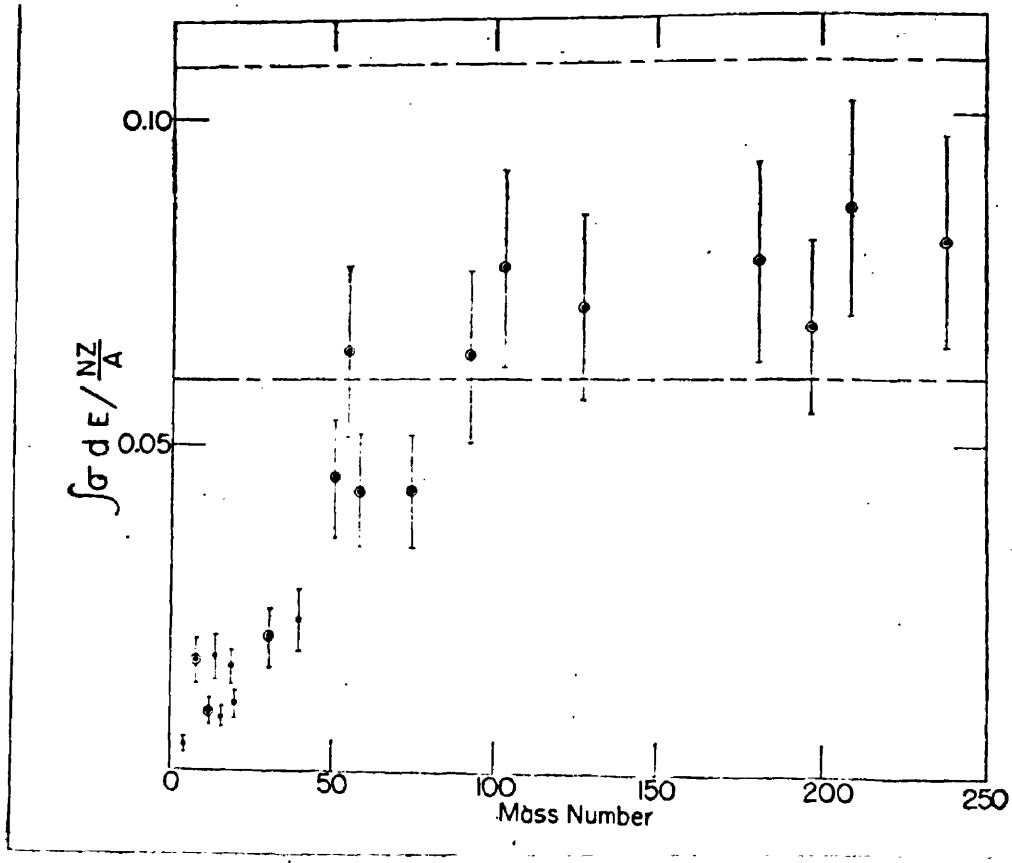
0.10
0.05
$\int \sigma \, d\epsilon / \frac{NZ}{A}$
0
50
100
150
200
250
Mass Number

Fig. I.4

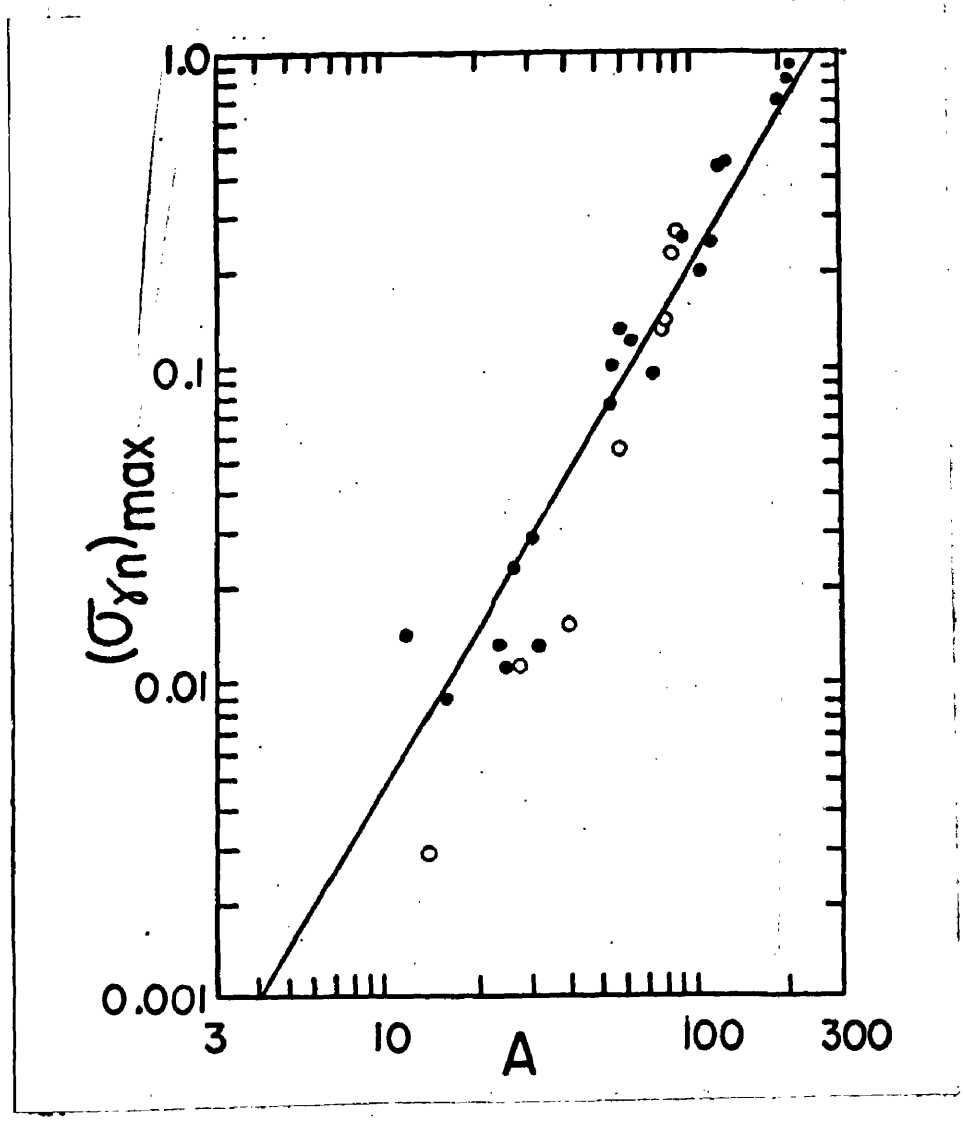
1.0
0.1
0.01
0.001
$(\sigma_{\gamma n})_{max}$
3
10
A
100
300

Fig. I.5

be explained by considering (γ,n) to be the dominant reaction for elements with high Atomic Numbers where the Coulomb potential barrier prevents the emission of charged particles, whereas the (γ,n) is only one of a number of photo-reactions for light elements.

7) The peak cross section, σ_m, is a smooth function of A (as would be expected from the A - dependence of E_m, Γ and $\int\sigma.dE$). This is shown in Fig. I.5.

8) The yield of neutrons from U and Th is anomalously large. This is due to the additional process of photo-fission occurring.

9) The cross section generally rises rapidly near the threshold to about 10% of the peak value. This is found especially with the heavy elements.

10) Above the giant resonance the cross section falls and then gradually rises due to interactions with the mesonic field. Perlman and Friedlander (1948) and Jones and Terwilliger (1953) found the cross section relatively small up to 100 MeV although the contribution of 30 - 100 MeV quanta to the integrated cross section is not negligible. There is some evidence, Sagane (1951), that in light elements the (γ,n) cross section only falls slowly above the giant resonance, but the absolute values are not reliable as the shape of the bremmstrahlung spectrum is not well known at high energies.

11) Byerly and Stephens (1951), measured the energy distribution of photoneutrons from Copper by observing the proton recoils in photographic plates. They found reasonable agreement with the predictions of the Compound Nucleus theory except for an excess of high energy neutrons.

12) Kerst and Price (1951) and Jones and Terwilliger (1953) made crude measurements of the yield of neutrons of all energies and found approximately isotropic angular distributions except perhaps with C and A.

Poss (1950) measured the angular distribution of neutrons of energy greater than 4.6 MeV and found an excess of neutrons at 90° to the beam direction while Geller, Halpern and Yergin (1954), using a fast neutron, lucite -ZnS detector found no significant anisotropy.

13) The $(\gamma,2n)$ and (γ,pn) cross sections have generally been found to be about 10 to 20% of the (γ,n) cross sections. This is more than expected from the Compound Nucleus theory.

I.4. Photoproton Reactions.

(a) Experimental Methods

In the majority of cases the residual nucleus formed after a (γ,p) reaction in a stable nucleus is also stable and for this reason very few experimental results have been obtained using the radioactive product method.

Photoproton yield measurements have been made by two methods, using ZnS scintillators and using photographic plates. With the former method the counting had to be done while the beam was passing and as a result it was found that the "pile-up" of electron pulses constituted a large background to the proton pulses. Energy and angular distributions have not been obtained using this method.

The great advantage of photographic plates is that energy and angular distributions can be obtained but only with reasonable accuracy when very large numbers (10^5) of tracks are measured. Due to the electron background the plates could not be placed in the beam with the result that the origin of the event was not seen and it was difficult to distinguish photoprotons from (n,p) reactions. Some doubtful results have been obtained using this method as is discussed in Section III.5.

(b) Results

The first experiments were performed by Hirzel and Wäffler (1947) who measured the (γ,n) and (γ,p) cross sections for 17.6 MeV gamma rays in neighbouring isotopes. They found the ratio of the cross sections was about unity for light elements but then the (γ,p) cross section fell to 0.02 of the (γ,n) cross section at Z = 50. This value of 0.02 was much larger than that predicted by the statistical model of Weisskopf and Ewing (1940). The experimental results may be summarised as follows.

1. It has been found e.g. Weinstock and Halpern (1954), that the giant resonance also occurs in all (γ,p) reactions. The energy, E_m, of the peak cross section and the width, Γ, of the giant resonance were found within the experimental error, to be the same as those for the (γ,n) reaction in neighbouring elements.

2. The integrated (γ,p) cross section has a maximum at Z = 28, i.e.

nickel, drops rapidly to Z = 50 and then falls slowly with increasing Atomic Number. The existence of a maximum was expected due to the effect of the Coulomb barrier.

3. The ratio of the (γ,p) to the (γ,n) cross sections is about unity for low values of Z and falls to 0.01 for large values of Z. These latter values, although small, are much larger than those calculated from the Compound Nucleus model by a factor of 10^2 to 10^3.

4. Considering the light elements in detail, the ratio of the (γ,p) to the (γ,n) cross sections fluctuates and with aluminium the (γ,p) cross section was found by Diven and Almy (1950) to be greater than the (γ,n).

5. Energy distributions of the photo-protons obtained for medium and heavy elements showed that on comparison with evaporation spectra, the main peak had the expected shape but there was an excess of high energgy protons. Also it was found that while the angular distribution was isotropic for the large number of low energy protons, the high energy protons were peaked at 90°. (Diven and Almy 1950, Byerly and Stephens 1951, Towns and Stephens 1954). Later Russian experiments (Leikin, Osokina and Ratner (1955)) in which very large numbers of tracks were measured, showed that with copper the energy distribution of protons emitted at 28° and 152° to the X-ray beam was consistent with the evaporation spectrum, while the tracks at 90° gave an energy distribution having an excess of fast particles. The angular distribution of the high energy protons was given by a $\mathrm{Sin}^2\theta$ law for copper, but was found

to be isotropic for nickel. This difference was partly explained by them on the basis of the shell model.

I.5. The (γ,γ) Reaction

Fuller and Hayward (1954) have measured the elastic photon scattering cross section. Using a large NaI crystal they measured only those photons in the upper 10% energy bin of the betatron spectrum, first in the beam (the output being greatly reduced) and then at 120° to the beam. They found that the plot of the (γ,γ) cross section against energy had two peaks. The fall-off of the first peak occurred at the (γ,n) threshold. The sum of the (γ,γ) and (γ,n) cross sections was a smooth function of the energy, suggesting that the fall-off was due to competition with the (γ,n) reaction while the total photon absorption cross section was a monotonic function near the (γ,n) threshold.

The second peak of the (γ,γ) cross section curve occurred at the same energy as the giant resonance as measured by the (γ,n) reaction. The ratio of the (γ,γ) to the (γ,n) cross sections varied from 0.087 for Carbon to 0.018 for Uranium. As the (γ,n) cross section is almost equal to the total photon absorption cross section for medium and heavy elements and is about half the total cross section for light elements, this result means that the (γ,γ) cross section is a constant fraction of the total cross section for all elements. These results support the model in which following photon absorption a compound nucleus is formed and then gamma-emission competes unfavourably with particle-emission.

Other experiments on the (γ,γ) reaction are very few in number and are generally consistent with the above results.

I.6. Photodeuteron Reactions

The little information that is known about this reaction has come from photographic plate work. Byerly and Stephens (1951) measured the range of tracks of charged particles from copper and on the assumption that they were all photoprotons obtained an energy distribution with two peaks at $2\frac{1}{2}$ and 4 MeV. They suspected the lower energy peak might be due to deuterons and on performing a grain count obtained a clear separation of alpha tracks and a more doubtful separation of deuterons. This gave an unexpectedly high ratio of one deuteron per 3.24 protons. It is possible that shrinkage of the emulsion near the surface would give the low energy proton tracks a higher grain count and lead to their identification as deuterons.

Toms and Stephens (1954) searched for photodeuterons from Cobalt by grain counting in a manner similar to Byerly and Stephens but could not find any evidence for deuterons. In view of the uncertainty of this type of work, e.g. that the origin of the event is not visible, no definite conclusion can be reached.

I.7. (γ,α) Reactions

Few measurements have been made of the (γ,α) reaction for a number of reasons:

(1) the product nucleus is generally stable so that the radio-active

product method cannot be used,

(2) due to the Coulomb barrier, the yield of alpha particles is very small so that counters cannot easily distinguish them from protons or the build-up of the electron background.

Hence the measurements have been made using photographic plates.

In the (γ,α) reactions produced in Cobalt, Copper and Bromine (Toms, Gerado and Stephens 1954; Byerly and Stephens, 1951; Nabholz, Stoll and Wäffler 1952, respectively) it was found that the alpha yield was about a tenth to a hundredth of the photoproton yield. The (γ,α) cross section was rather higher than that expected from the statistical theory but agreement could be obtained by using a larger nuclear radius. For copper, the alphas had an approximately isotopic distribution as would be expected from compound nucleus theory but the statistics were not good.

The $O^{16}(\gamma,\alpha)C^{12}$ reaction has been studied by Miller and Cameron (1953) and Nabholz et. al. 1952. The results were inconsistent. The former claim to be able to separate (γ,α) events in N^{14} from those in O^{16} but the range-energy relation they use is not in agreement with other workers, possibly due to the underdevelopment of their plates.

The (γ,α) reaction in C^{12} is observed as $C^{12}(\gamma,3\alpha)$ due to the instability of Be^{8} and is discussed below.

I.8. Other Photonuclear Reactions

The $C^{12}(\gamma,3\alpha)$ reaction has been extensively studied, especially

by Goward and Wilkins (1953). It has been shown that the reaction proceeds mainly through excited states of Be^8. The $C^{12}(\gamma,3\alpha)$ cross section has two asymetrical peaks at 18.3 and 29.4 MeV and possibly other maxima. The fall in cross section near 19 MeV is probably due to competition with the (γ,p) and (γ,n) reactions whose cross sections are consistent with this compound nucleus theory.

Wilkins and Goward (1953) found that when the energy of the incident photon was above 26 MeV, most of the reactions went through levels in Be^8 ~~and~~ or 16.8 and 17.6 MeV. This result and the existence of the second maxima of the $C^{12}(\gamma,3\alpha)$ cross section at 29.4 MeV can be explained as the operation of isotopic spin selection rules. This reaction is discussed in Section I.10.

The O^{16} $(\gamma,4\alpha)$ reaction which also produces easily distinguishable events in irradiated photographic plates, has been widely studied (e.g. see review by Titterton, 1953). The existence of resonances in O^{16} has been indicated and the reaction has been shown to proceed through excited states of C^{12}.

A few examples have been found in photographic plates of the following reactions in nitrogen, $N^{14}(\gamma,d)3\alpha$, $N^{14}(\gamma,2\alpha)Li^6$, $N^{14}(\gamma,np)3\alpha$, $N^{14}(\gamma,p\alpha)Be^9$ and $N^{14}(\gamma,2p)B^{12}$, but not all of these reactions are definitely established.

The $Li^7(\gamma,t)He^4$ has been studied by Titterton and Brinkley, 1953, who found evidence for the resonance absorption of the gamma rays.

I.9. Summary of the Main Experimental Results

The experimental data has been mainly obtained for the (γ,n) reaction and the generalised results are mainly for this reaction and to a lesser extent for the (γ,p) reaction.

There exists a giant resonance in all photonuclear reactions. The properties of the giant resonance can be expressed with few exceptions as a continuous function of the Atomic Weight. It is not known whether the giant resonance is in fact a simple resonance or whether it is composed of a group of energy levels whose individual character cannot be recognised due to the lack of accuracy of the present experimental methods.

For medium and heavy elements the photo-yield of charged particles is small relative to the neutron yield, due to the Coulomb barrier, but this yield is nevertheless much larger than that expected from compound nucleus theory.

For light elements the yield of charged particles is known to be as large and in some cases larger than the photoneutron yield but few experiments have been done on such reactions.

Few experimental measurements have been made of the energy and angular distributions, but those obtained indicate that in general, the compound nucleus model will explain most of the results except that there appears to be an excess of high energy particles which have an asymmetric angular distribution which would be expected on an Independent Particle Model.

In several of the reactions in Section I.8 and in some (γ,n) reactions, the photodisintegration has been shown to go through energy levels and these intermediate states could be the compound nuclei of that theory.

I.10 Photodisintegration Theories and Calculations

(a) Sum Rule Calculation

In addition to the two models of the nucleus described in Section 1.1, (i.e. the Collective Model and the Independent Particle Model), Levinger and Bethe (1950) have calculated the total integrated yield of photodisintegration reactions using the Sum Rules. They showed that photo-absorption was mainly by electric dipole transitions while magnetic dipole and quadrupole absorption was an order of magnitude less.

Levinger and Bethe translated the classical calculation of the electric dipole absorption of electromagnetic radiation by a charged simple harmonic oscillator, into quantum mechanics and found an integrated cross section of

$$\sigma_{int} = 0.06 \frac{NZ}{A} \doteq 0.015 \text{ A MeV barns}$$

As this calculation neglects the neutron-proton exchange forces, Levinger and Bethe (1950) later modified their calculation to the form

$$\sigma_{int} = 0.015 \text{ A}(1 + 0.8 \chi)$$

where χ is the ratio of exchange forces to the two-body neutron-proton force. This calculation is independent of a nuclear model except that a degenerate Fermi gas was assumed in calculating the exchange factor

of 0.8. These calculations neglected mesonic effects.

In Fig. I.4 the (γ,n) cross section integrated to 24 MeV, is divided by $\frac{NZ}{A}$ and plotted against the Mass Number. It can be seen that reasonable agreement is obtained for high mass numbers where the total photodisintegration cross section for all reactions is comprised almost entirely of the (γ,n) cross section. Agreement is not good at lower mass numbers as the (γ,p) and other reactions have appreciable cross sections. However, Halpern and Mann, (1951), showed that the sum of the integrated cross sections for the (γ,p) and (γ,n) reactions for eight elements from Mg to Zn was approximately proportional to $\frac{NZ}{A}$.

Attempts have been made to compare theory and experiment to evaluate the neutron-proton exchange factor, χ, but the difficulty is to decide the upper limit of the integration. The value of 24 MeV has been chosen as it was often the maximum energy experimentally available but it is almost certainly too low as it excludes part of the high energy "tail" of the giant resonance. On the other hand the value of 80 MeV which has also been used, is probably too high as mesonic effects, excluded in the theory, appreciably effect the cross section. In Fig. I.4 the two horizontal dotted lines correspond to χ values of nothing and one.

(b) Calculations Giving E_m.

Earlier theoretical calculations were directed to the prediction of a giant resonance, proving that the energy E_m, at the cross

section peak was proportional to $A^{-1/6}$, approximately, and then to obtaining quantitative agreement with the experimental relation,

$$E_m = 38. A^{-0.185}$$

In these quantitative calculations, the parameter r_o is involved and it is given by the expression:

$$R = r_o \times 10^{-12} A^{1/3} cm$$

for the nuclear radius, R. Earlier experiments gave $r_o = 1.5$ but later work has favoured $r_o = 1.2$.

Goldhaber and Teller (1948), were the first to use a Collective Model of the nucleus. They considered three cases of electric dipole absorption in which the centre of mass is fixed but the centre of charge oscillates:-

1). Each nucleon oscillates about its equilibrium position.

2). The protons and the neutrons oscillate against each other as two compressible fluids.

3). As 2). but the two fluids are incompressible.

They found that the energy, E_m, of the peak of the giant resonance varied as A, $A^{-1/3}$ and $A^{-1/6}$ respectively in these models. As the third case gave the closestagreement with the experimentally found index, it was developed to give numerical values of E_m in agreement with experiment, but it is difficult to believe this model.

Steinwedel and Jensen (1950) and Danos (1952) developed Goldhaber and Teller's second case and found $E_m = \frac{85}{r_o} A^{-1/3}$ MeV.

Reasonable agreement with experiment is obtained if $r_o = 1.2$ is taken (the authors actually assumed $r_o = 1.42$). The integrated cross section, σ_{int}, was calculated and found to be in agreement with the sum rule limit.

Ferentz, Gell-Mann and Pines (1953) assumed a plasma oscillation of the neutron and proton fluids and found $E_m = 80. A^{-1/3}$ MeV and obtained agreement with the sum rule limit for σ_{int}.

Thus all the above Collective Models obtained reasonable values of E_m although they neglected any damping force on the simple harmonic oscillator.

Two main calculations using the Independent Particle Model were made by Reifman (1953) who assumed an infinite square well and found $E_m = 83. A^{-1/3}$ MeV for $r_o = 1.2$ and Burkhardt, 1953, who assumed a finite square well which was adjusted to give the observed binding energy. He performed a detailed calculation for Cu^{63} and on finding $E_m = 9$ MeV, declared that I.P.M. was inconsistent with the experimental results. However, Levinger (1954) states that on using a smaller value of r_o and including the effect of exchange forces, Burkhardt's calculations can be brought into agreement with experiment.

Thus it is possible to fit both types of theories to the experimental results for E_m by a suitable choice of parameters.

Calculations of other parameters such as the harmonic mean energy, can also be made to agree with experiment but these experimental values are not well defined.

(c) Direct Photodisintegration

If it is assumed that following photo-absorption, a compound nucleus is formed and that statistical theory may be employed to calculate the modes of de-excitation of the nucleus, then the results obtained are not all in agreement with experiment. In particular the ratio of the number of protons to the number of neutrons from medium and heavy elements is larger than expected; the yield of high energy protons and neutrons is greater than predicted, and these particles do not have isotopic angular distributions as would be expected from the decay of a compound nucleus.

The statistical calculations were repeated using a different level density formula (Schiff, 1951) and different nuclear radii but it was not possible to obtain agreement with experiment.

Calculations by Courant, (1951), using an Independent Particle Model have been more successful. He assumed a square potential well and independent wave functions for each nucleon. After a nucleon has absorbed a photon it may be emitted directly or after a few collisions or secondly, it may make many collisions so that a compound nucleus is formed which then decays as in the manner given by the statistical model. The directly ejected particles would account for the excess of high energy particles with an anisotropic angular distribution. The ratio of photoprotons to

photoneutrons is higher with this model but is still less than that found experimentally. However, this ratio is increased if the square well is replaced by one having a wine bottle shape or if an alpha particle model is assumed or if a lower nuclear radius is used.

(d) Wilkinson's Shell Model Calculations

Wilkinson (1954, 1956) using the Shell Model, was able to calculate most of the parameters that have been measured experimentally.

He considered that the gamma quantum is absorbed by a nucleon which is raised to a single-particle state. He assumed that the momentum of the quantum is small so that the momentum of the final state is the same as that of the initial state. The interaction of the gamma-quantum with a nucleon is assumed to take place not only with the outer or "valence" nucleons but also with those in the core, so that there are a large number of single-particle states that can be produced. These states could be considered individually on the Shell Model but it is easier to consider their summed effect from which the major parameters of the giant resonance can be found. The fact that there are a large number of final states would mean that the giant resonance would have a "fine structure" as has been suggested experimentally (Montalbetti et. al., 1953 and Nathans and Halpern, 1954). Some of these excited states will lie in the ~~the~~ continuum so that they can emit excited nucleons and this could be used to explain the emission of an unexpectedly large number of high energy nucleons.

In considering the relative probabilities of the different transitions, Wilkinson found that in the absorption of the gamma-ray into closed shells, strong electric dipole transitions were obtained whose total cross section was about the same as that given by the Dipole Sum Rule. Further these strong transitions clustered about one energy and therefore may be expected to form the giant resonance.

As the giant resonance consists of a number of "resonances", it may be expected to be unsymmetrical in some cases. Such results have been found but the experimental errors were large.

The greatest difficulty in Wilkinson's theory is that unlike other theories, the peak energy, E_m, of the giant resonance is not in good agreement with experimental results. However, it is possible that by introducing a velocity-dependent potential and/or other devices, agreement could eventually be obtained.

The width of the resonances due to transitions from closed shells may be expected to be about 3 to 5 MeV but as the width of the weaker transitions involving valence nucleons is much greater, the total width of the giant resonance will normally be about 6 to 8 MeV. Howevever for those nuclei in which all the shells are closed, the width will have a minimum value of 3 to 5 MeV. This effect, which is clearly predicted by this model alone, had previously been noted experimentally (Nathans and Halpern, 1953).

To derive the energy distribution of the emitted nucleons it

is assumed that after the single-particle state has been formed, this nucleon may interact with the rest of the nucleus to form a compound nucleus whose mode of decay can be found from the statistical theory, or the nucleon may be emitted directly. To this latter process the name "resonance direct" has been given as it differs from the collective model "direct" process described in (c) above in that these "direct" nucleons would not be expected to display a giant resonance. The "resonance direct" process is preferred from the work of Ferrero et. al., 1956, who found by use of threshold detectors, that the fast photo-neutrons from Bi^{209} exhibited a giant resonance. The calculations of the energy distribution of the neutrons and protons and of the ratio of the yield of protons to neutrons in heavy elements were found to be in good agreement with experiment.

The angular distributions of the photo-neutrons and photo-protons will be anisotropic, of the form

$$1 + \frac{1}{2} \cdot \left(1 + \frac{2}{l}\right) \mathrm{Sin}^2 \theta$$

for transitions from the l orbit. Summing over all shells, then for heavy nuclei, the neutron angular distribution would be $1 + 0.7\ \mathrm{Sin}^2 \theta$ while the proton angular distribution would be $1 + 1.4\ \mathrm{Sin}^2 \theta$. Similar angular distributions have been found experimentally, e.g., Ferrero et. al. 1956, found $1 + 0.9\ \mathrm{Sin}^2 \theta + 0.2\ \mathrm{Cos}\ \theta$.

(e) Conclusion

A variety of calculations based on Collective Models and on

Independent Particle Models have been proposed. All can provide values in agreement with experiment for the integrated cross section and all except Wilkinson's Shell Model, for the peak energy, E_m. Thus, in general, the major parameters of the nuclear photo-effect can be described but the "secondary" ones such as the excess of high energy photonucleons, can only be explained on Wilkinson's theory.

It should be noted that these theories are mainly applicable to nuclei containing large numbers of nucleons and that little is known about the detailed behaviour of photo-reactions in light nuclei.

I. 11 Isotopic Spin Selection Rules

If it is assumed the forces between nucleons are independent of the charges of the nucleons, then it is possible to consider neutrons and protons as two possible "states" of the nucleon. These "states" are distinguished by introducing a further quantum number called the isotopic spin. The nucleon has an isotopic spin, T, of $\frac{1}{2}$ while the neutron and proton have in the direction of the z - axis, isotopic spins of $T_z = -1/2$ and $T_z = +1/2$ respectively. A nucleus will then have a T_z value of $\frac{Z - N}{2}$.

Radicati (1952) showed that for light nuclei, the total isotopic spin T is conserved in reactions involving particles: it is not necessarily conserved in reactions involving photons as the electromagnetic interaction is charge dependent. However, he deduced the following selection rules for the latter reactions:-

When $T_z = 0$, then the change in isotopic spin $\Delta T = 0, \pm 1$ for all multipolarities.

When $T_z = 0$, $\Delta T = \pm 1$ for electric dipole transitions.

Hence for nuclei with N = Z, i.e. $T_z = 0$, electric dipole transitions between states such that $\Delta T = 0$, are forbidden. As the ground state of such self-mirrored nuclei have T = 0, this means that E.D. absorption cannot occur unless the photon has sufficient energy to form T = 1 states of the nucleus. This is important as Levinger and Bethe, (1950), have shown that photon absorption is almost entirely through E.D. transitions so that the states formed in self-mirrored nuclei will be mainly T = 1. Deuteron and alpha particle emission from these states will be inhibited by the conservation of the total isotopic spin since the ground state of the product nucleus will also have T = 0. Thus the (γ,d) and (γ,α) reactions in self-mirrored nuclei will generally have a small cross section except when the photon has sufficient energy to excite T = 1 states of the product nucleus. A demonstration of this occurs in the $C^{12}(\gamma,3\alpha)$ reaction when the cross section suddenly rises above 26 MeV due to the fact that it is then energetically possible to form the T = 1 states of Be^8.

Gell-Mann and Telegdi (1953) discuss other theoretical examples of the operation of the isotopic spin selection rules. It should be noted that at higher energies and at higher atomic numbers, the energy levels are close together and overlap so that the states are not pure and the rules are not absolute.

I. 12 Discussion

From the experiments described above, it can be seen that a considerable amount of information has been obtained on the (γ,n) reaction in medium and heavy elements and a moderate amount on the (γ,p) reaction, mainly in medium elements. It is therefore clear that further experimental results are required on the (γ,p) reaction in light elements. Results obtained from such experiments would be of theoretical use as the theories up to now have tended to be mainly concerned with nuclei containing large numbers of nucleons and no detailed predictions have been made about photodisintegration in light elements. In addition to the (γ,p) reaction, further information is required on the emission of charged photo-particles as few such experiments have been performed.

The isotopic spin selection rules are expected to affect the yield of charged particles from light elements and hence a study of these reactions should allow the applicability and validity of these rules to be tested.

The cloud chamber technique is particularly suited to this type of study as it is possible to fill the chamber with a light element in gaseous form, pass a pulse of X-rays from a synchrotron through the chamber and then observe the tracks of the charged photo-particles produced. There will be a large number of light electron tracks but the heavy tracks of the charged photo-particles can be distinguished from

this background if the X-ray output is not too high. This is a distinct advantage over the counter method as a counter has difficulty distinguishing between single large pulses from a photoproton and the "pile-up" of large numbers of small pulses from electrons.

The feasibility of this cloud chamber technique was demonstrated by Gaerttner and Yeater, 1951, but they did not analyse their photographs fully, only counting the number of events in which the resultant momentum went forwards in the X-ray beam direction and the number in which it went backwards, thus obtaining an estimate of the proportion of reactions in which neutrons were involved.

It is interesting to compare the cloud chamber method with the use of photographic emulsions. The cloud chamber is placed directly in the X-ray beam so that the origin of the event can be seen and therefore all the charged particles emitted from that event can be observed. Also it is in general, possible to distinguish a photon-induced reaction from a neutron-induced one. The photographic emulsion is generally only placed in the beam when easily identifiable reactions such as the three-pronged stars from $C^{12}(\gamma,3\alpha)$ reactions are to be studied. In most experiments the photographic emulsions have been placed outside the beam, so that the origin of the event is not seen. Hence a photoproton cannot be easily distinguished from protons knocked on by neutrons and this has possibly led to serious errors (see Sec. III.5). Also as the photographic plate cannot measure simultaneity in time, it is not

possible to measure star events in elements such as neon which cannot be included in a photographic emulsion. A further advantage of the cloud chamber is that the target element in the chamber is almost pure so that there is little uncertainty as to which element the reaction occurred in, whereas in photographic emulsions there are several elements present.

Hence for these reasons it was decided to investigate the photodisintegration of light gases using a cloud chamber.

References

Baldwin and Kaliber 1948, Phys. Rev. 73, 1156.

Bothe and Gentner 1937, Z. Physik. 106, 236.

Burkhardt 1953, Phys. Rev. 91, 420.

Byerly and Stephens 1951, Phys. Rev. 83, 54.

Collie 1954, Proc. Of Glasgow Conf. On Nucl. Phys.

Courant 1951, Phys. Rev. 82, 703.

Danos 1952, Ann. Phys. 10, 265.

Diven and Almy 1950, Phys. Rev. 80, 407.

Ferentz, Gell-Mann and Pines 1953, Phys. Rev. 92, 836.

Ferguson, Halpern, Nathans and Yergin 1954, Phys. Rev. 95, 776.

Ferrero, Hansen, Malvano and Tribuno 1956, Physica 22, 1148.

Feshbach, Porter and Weisskopf 1953, Phys. Rev. 90, 166.

Feshback and Weisskopf 1949, Phys. Rev. 76, 1550.

Fuller and Hayward 1956, Phys. Rev. 101, 692.

Gaerttner and Yeater 1951, Phys. Rev. 83, 146,

Geller, Halpern and Yergin 1954, Phys. Rev. 95, 659.

Gell-Mann and Telegdi 1953, Phys. Rev. 91, 169.

Goldemberg and Katz 1954, Phys. Rev. 95, 471.

Goldhaber and Teller 1948, Phys. Rev. 74, 1046.

Goward and Wilkins 1953, Proc. Roy. Soc. A217, 357.

Halpern and Mann 1951, Phys. Rev. 82, 733.

Hirzel and Wäffler 1947, Helv. Phys. Acta. 20, 374.

Jones and Terwilliger 1953, Phys. Rev. 91, 699.

Katz and Cameron 1951, Can. J. of Phys. 29, 518

Katz, Haslam, Horsley, Cameron and Montalbetti 1954, Phys. Rev. 95, 464.

Kerst and Price 1951, Phys. Rev. 79, 725.

Leikin, Osokina and Ratner 1955, Proc. Acad. Sc. U.S.S.R. 102, 245.

Leikin, Osokina and Ratner 1955, Proc. Acad. Sc. U.S.S.R. 102, 493.

Levinger 1954, Ann. Rev. Nucl. Sc. 4.

Levinger and Bethe 1950, Phys. Rev. 78, 115.

Montalbetti, Katz and Goldemberg 1953, Phys. Rev. 91, 659.

Nathans and Halpern 1953, Phys. Rev. 92, 207.

Penfold and Spicer 1955, Phys. Rev. 100, 1377.

Perlmann and Friedlander 1948, Phys. Rev. 74, 442.

Poss 1950, Phys. Rev. 79, 539.

Price and Kerst 1950, Phys. Rev. 77, 806.

Radicatti 1952, Phys. Rev. 87, 521.

Reifman 1953, Naturforsch 8a, 505.

Steinwedel and Jensen 1950, Naturforsch 5a, 413.

Titterton 1955, Prog. In Nucl. Phys. 4.

Titterton and Brinkley 1953, Proc. Phys. Soc. A66, 579.

Toms and Stephens 1954, Phys. Rev. 95, 1209.

Weinstock and Halpern 1954, Phys. Rev. 94, 1651.

Weisskopf and Ewing 1940, Phys. Rev. 57, 472.

Wilkins and Foward 1953, Proc. Phys. Soc. A66, 661.

Wilkinson 1954, Proc. Of Glasgow Conference On Nuclear Physics.

Wilkinson 1956, Physica 22, 1039.

Wu 1951, Unpublished, Doctral Thesis, Univ. of Illinois.

CHAPTER II.

THE PHOTODISINTEGRATION OF HELIUM

Introduction.

In this chapter the basic method used in all experiments is given. The cloud chamber, its associated apparatus and the reprojection apparatus are briefly described. An account is given of an experiment on the photodisintegration of helium. It is shown that the identification of certain events as $He^4(\gamma,p)H^3$ reactions, can be checked in several ways so that the reaction may be considered to be definitely established. Photodisintegration events in heavier nuclei are described and identified.

II.1. Method and Apparatus

The collinated X-ray beam of the Glasgow University 23 MeV synchrotron was passed through a Wilson Cloud Chamber. The tracks were photographed and the negatives reprojected stereoscopically on to an adjustable table on which the images were aligned and measured.

The cloud chamber used was a volume-defined chamber of conventional design with a diaphragm of thin neoprene rubber. The gas to be irradiated was contained in a glass cylinder $2\frac{1}{2}$" high and of 12" diameter surmounted by/

by a $\frac{3}{4}$" thick triplex plate and resting on a perforated brass plate. To provide a good background for photography the bottom of the chamber was covered with black velvet. The expansion ratio was controlled by varying the pressure in the bottom section of the chamber (i.e. below the diaphragm) which was filled with nitrogen from a tank at constant pressure. The expansion valve consisted of a rubber-capped steel plunger which was held by the magnetic field of a solenoid against an orifice of one inch diameter in the bottom of the chamber. The expansion was effected by cutting off the current to the solenoid for a short time. The valve was reset by means of a second solenoid, which forced the plunger upwards where it was held by the first solenoid. Slow expansions, to clear the chamber between the fast expansions, were performed manually using a second valve with a smaller orifice.

The stopping power of the chamber gas was calculated from measurements of the range of alpha particles from a polonium source on the wall of the chamber and also from the composition and expanded pressure of the gas.

The output from the synchrotron was restricted to single bursts of X-rays and the cloud chamber was triggered by a pulse directed from the synchrotron timing pulses. The/

The delay between the opening of the cloud chamber expansion valve and the X-ray pulse was changed in five millisecond steps and the shortest delay that gave sharp tracks was used. If this delay were reduced, the tracks rapidly became vague due to the charged droplets diffusing before they had grown sufficiently. On the other hand, a longer delay resulted in an increase in the chamber background without appreciably increasing the sharpness of the tracks. The timing of the flash was similarly adjusted. The flash lamp consisted of a discharge tube filled with Xenon at about 10 cm. pressure. The electrodes were charged to 2 KV from a 1000μF bank of condensers. A wire from a motor car-type induction coil was wrapped round the flash-tube. The discharge from the coil induced a discharge between the electrodes which gave a flash lasting less than a millisecond.

Two 60 mm. cameras each holding 25 feet of high contrast film (Ilford 5G91) were used. One camera was directly above the centre of the chamber while the other was inclined at an angle of 20 degrees to the vertical and had its lens tilted to make the focal plane horizontal. To enable the films to be aligned during reprojection, five spikes were placed in a horizontal plane on the walls of the/

the cloud chamber.

The X-rays from the synchrotron were collimated by means of a lead block six inches thick. The centre and direction of the beam were located by placing two thin lead plates each with a pattern of holes drilled in it, over the ends of the hole in the collimator then irradiating an X-ray film fronted with lead sheeting, which was placed on the distant side of the collimator. The pattern of dots on the X-ray film produced by the holes then allowed the collimator to be accurately positioned. The X-ray beam was then replaced by a beam of light which passed through the central holes of the thin lead plates. The cloud chamber was positioned so that the beam of light passed through the centre of the sensitive region. The resulting X-ray beam through the cloud chamber was 10 cm. wide and $2\frac{1}{2}$ cm. high.

II.2. The Photodisintegration of Helium

In nuclear physics, the alpha particle has an unusual role. Although it is normally considered as the nucleus of the Helium atom, it is sometimes regarded as a fundamental particle and an "alpha-particle model" of the nucleus has been postulated. Thus a study of the interaction of/

of radiation with the helium nucleus is of especial interest.

The cloud chamber is particularly useful for studying disintegrations in which two charged particles are emitted. These events are called 'flags' since they usually consist of a short heavy track (the recoil) and a lighter and longer track (the fragment). Helium, where the recoil is a triton and the fragment a proton provides the simplest case. It should be noted that helium cannot be included in photographic emulsions and so its disintegration products cannot be observed directly.

There are practical advantages in studying helium as opposed to other gases, in a cloud chamber. The recoil is long and straight and thus its range is easily measured. A range-energy relationship is well established for the recoil, and can be employed to give accurate results as there is little range straggling. The angle, φ_{rf}, between the fragment and recoil which includes the forward directions of the X-ray beam, is a function of the momentum, M_γ, of the incident quantum, but in most cases M_γ is much less than the particle momentum so that the variation in φ_{rf} with M_γ is small and is insignificant compared with the errors/

errors due to multiple scattering and measurement. However, in the case of Helium the particles are light and the (γ,p) reaction threshold is high (19.8 MeV) so that in this case M_γ is comparable with the particle momenta. Thus for Helium, φ_{rf} may be expected to provide an accurate measurement of the momentum of the incident quantum.

II.3. Analysis - Apparatus and Method

The films were analysed by putting the developed negatives back in the cameras, placing an air-cooled lamp-house on top of each camera and projecting on to a movable table which could be adjusted until the two images of the track coincided, the films having been first aligned by means of the spikes in the chamber wall. Optical distortions in reprojection were avoided by the use of the same camera lenses as in photography and a glass plate equivalent to the top glass plate of the chamber. Geometrical distortions were avoided by placing the cameras on the stand which had been used in the track photography.

The reprojection table, which was 12 inches square, had five modes of motion. Below the table and attached to it at its centre, there was a steel hemisphere which rested in a steel cup. The final rotation of the table was made by/

by the movement of the hemisphere in the cup. When the desired position of the table had been found, a strong magnetic field was switched on, fixing the hemisphere in the cup. For most purposes the movement of the hemisphere was restricted so that the table had an axis of rotation about a horizontal line through its centre.

A useful feature of (γ,p) events was that the incident quantum, the proton and the recoil all lie in the one plane. This characteristic was exploited by placing the reprojection table relative to the cameras, so that its axis of rotation lay along the X-ray beam. The table was adjusted to make the images of the origin of the event come into coincidence on the axis of the table. If the fragment and recoil track lay in the same plane as the X-ray beam, then on tilting the table, the images of both tracks came into coincidence at the same inclination. This was a simple but sensitive test of the "coplanarity" of the event.

The following measurements were made:-

(1) The co-ordinates of each significant point (i.e. origin of the event, end points of the track, point of scattering),

(2) track lengths,

(3) the angles of each track to two fixed axis and the angles between tracks,

(4)/

(4) "coplanarity" of the event,

(5) the "appearance" of the track e.g. intensity, scattering.

II.4. Analysis and Results for Helium

From the ranges of alpha tracks from the Polonium radioactive source on the wall of the cloud chamber, the stopping power of the gas was calculated to be 0.4, corresponding to a gas pressure of two atmospheres of Helium. With diffusion of air through the thin rubber diaphragm, the gas contained helium, some nitrogen, a little oxygen and water which was used as the condensable vapour.

The events were first classified phenomenologically as -

Singles:- these were simply single tracks - the other agent involved left no visible track, e.g. a neutron or photon.

Flags:- two tracks originating at the same point. Usually one track was short and heavy (the recoil) and the other was long and light (the fragment).

Stars:- three or more tracks originating from the same point. The flags were sub-classified as coplanar and non-coplanar.

(a)/

(a) Coplanar Flags

It was found that the coplanar flags fell into three distinct classes by their "appearance" alone, but the distinction was given more precisely by the range distribution of the recoils, shown in Fig. II.1, where the events with a heavy recoil are shaded and the events with a light recoil are unshaded, (all the recoils except one were found to stop in the illuminated region of the chamber).

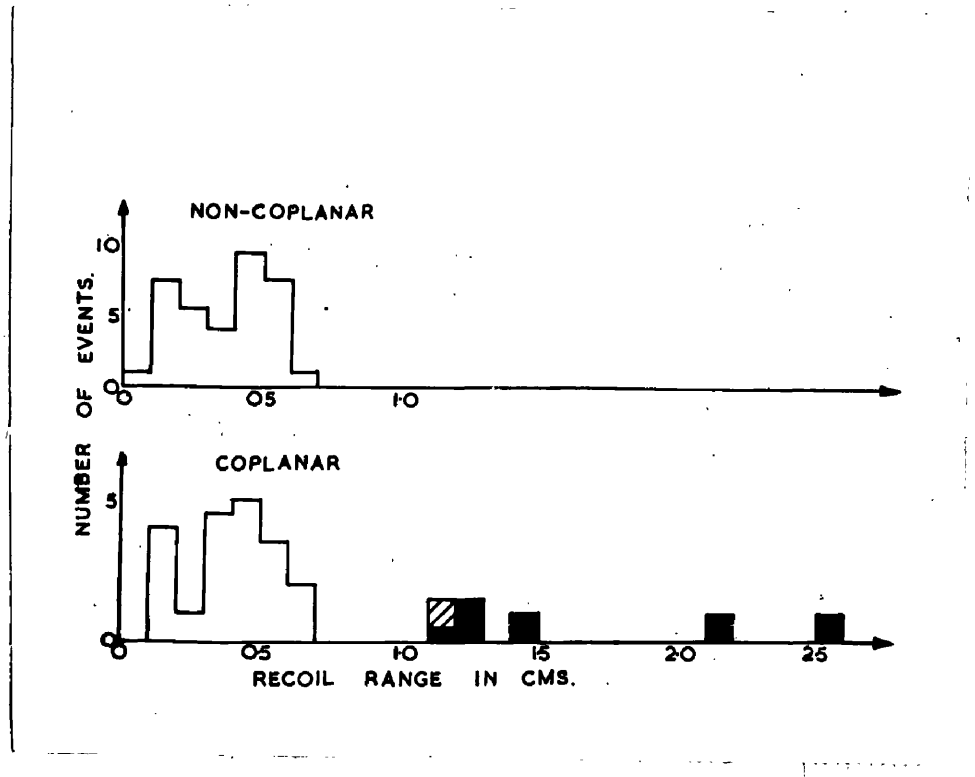

Fig.II.1.

Flags with a recoil range less than 0.7 cms. formed a separate group. Every member of the group had the/

the same appearance as the event shown in Plate III.1 i.e. it had a short heavily-ionising recoil and a long lightly-ionising fragment. This suggested that the event was a (γ,p), or possibly a (γ,d) reaction in a heavy nucleus i.e. nitrogen or oxygen. The angles φ_{rf}, between the recoil and fragment were between 165° and 185° confirming that as the momentum of the quantum was relatively small, the event had originated in a heavy nucleus.

In five of the six events with recoil length greater than 1.0 cm. the recoil and fragment were both lightly ionising, but in every case there was a slight but distinct difference in ionisation at the origin - a typical event is shown in Plate II.1. The only possible reaction in which two different particles were emitted from a light nucleus was $He^4(\gamma,p)H^3$. All these events had φ_{rf} values between 156° and 165° which was confirmation that it was a light nucleus which had been disintegrated.

The remaining event with a long recoil which is shown partly shaded in Fig. II.1, had both tracks heavily ionising but there was a slight difference in ionisation at the origin. It was identified as a (γ,α) event in nitrogen or oxygen - the φ_{rf} value of 175° added confirmation. It is shown in Plate II.2.

This/

This classification is given in Table II.1.

Table II.1.

Assumed Reaction	Ionisation			Recoil Range (cms.)	φ_{rf}	Coplanarity.
	Frag.	Recoil	Change at Origin			
$N^{14}(\gamma,p)C^{13}$ or $O^{16}(\gamma,p)N^{15}$	Light	Heavy	Large	0.7	$185^{o}-165^{o}$	Coplanar
$N^{14}(\gamma,pn)C^{12}$	Light	Heavy	Large	0.7	-	Non-Coplanar
$N^{14}(\gamma,\alpha)B^{10}$ or $O^{16}(\gamma,\alpha)C^{12}$	Heavy	Heavy	Small	0.7	$185^{o}-165^{o}$	Coplanar
$He^{4}(\gamma,p)H^{3}$	Light	Light	Small	0.7	$165^{o}-156^{o}$	Coplanar

It was shown above that an accurate measurement of angles gave the energies of the photon and of the particles for a (γ,p) reaction in helium, but not for reactions in nitrogen or oxygen. This was done for the suspected $He^{4}(\gamma,p)T$ events, the work being considerably simplified by the use of a momentum diagram which had been introduced by Mr. J.M. Reid.

The/

TABLE II.2.

Event No.	Are Tracks Coplanar?	Ionisation Change at Origin	E_t	E_p	$\frac{E_p}{E_t}$ Calc.	E_γ From Angles	E_γ From E_t	E_γ From E_p
1	Yes	Yes	0.33	1.08	2.89	21.0	21.1	21.2
2	Yes	Yes	0.30	0.96	4.84	22.0	21.6	
3	Yes	Yes	0.70	0.60	2.86	22.4	22.5	
4	Yes	Faïrly definite	0.60	1.21	2.62	21.9	21.9	
5	Yes	Yes	0.68	0.62	2.21	22.9	22.0	
6	Yes	Yes	0.60	0.92	2.12	22.9	21.7	
7	Yes	Faïrly definite	0.33	0.83	2.77	21.7	21.1	
8	Yes	Faïrly definite	0.48	1.30	2.37	21.6	21.4	21.6
9	Yes	Yes	0.48	1.42	4.80	22.8	22.6	
10	Yes	Probable	0.90	0.94	2.04	23.0	22.5	
11	Yes	Faïrly definite	0.81	1.02	2.39	22.6	22.6	
12	Yes	Yes	0.45	1.26	3.48	23.1	21.8	

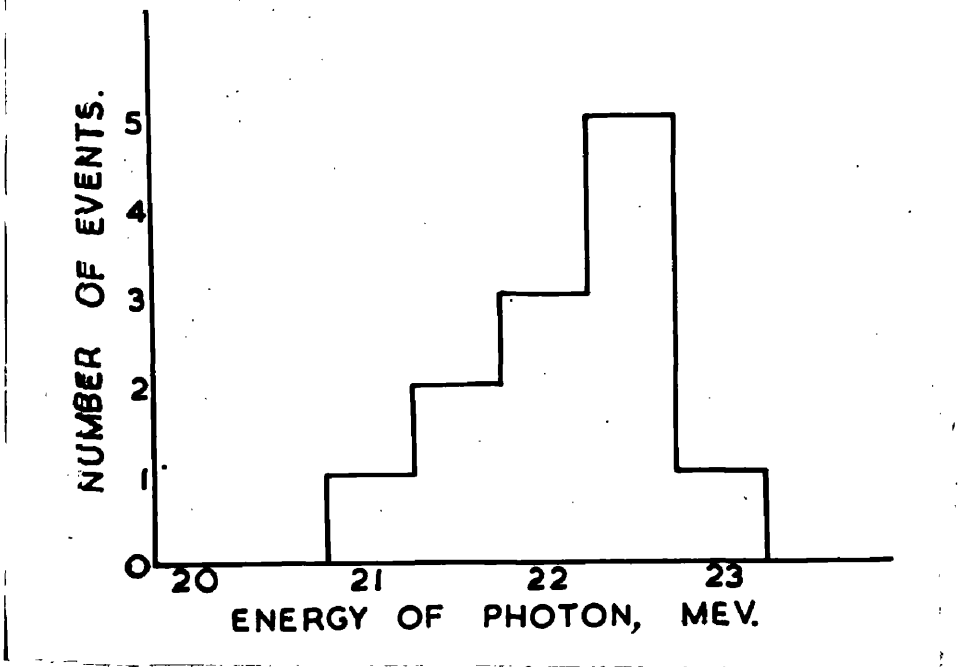

FIG. II.2

The most accurate values of the energies involved were obtained from range measurements of the triton or of the proton. This gave the particle energy and from the position of the event on the momentum diagram (only rough values of the angle measurements being required), the ratio of the proton energy to the triton energy was obtained. The energy, E_γ, of the incident photon was then found and compared with the values calculated from accurate angle measurements. In one case where the proton and the triton both stopped in the illuminated region of the chamber, three values of E_γ were obtained. In view of various improvements in analysis technique the $He^4(\gamma,p)H^3$ events found in a preliminary experiment on helium were re-analysed.

The complete results are shown in Table II.2. In view of the continued agreement, it may be concluded that the $He^4(\gamma,p)H^3$ reaction does occur.

The distribution of the photon energies producing the $He^4(\gamma,p)H^3$ events is shown in Fig.II.2.

With the (γ,p) events in nitrogen or oxygen, almost all the fragments left the visible region of the chamber, due to the low stopping power of the gas. The ranges of the recoils could not be measured accurately by reprojection but from the approximate values, it was found that in no case was the recoil range inconsistent with the assumption that the event was a (γ,p) reaction in nitrogen. The required range-energy relation for

C^{13}/

C^{13} ions was taken from Blackett and Lee's range velocity relation for nitrogen (corrected by 5% for the error in Brigg's range-velocity relation for alpha particles), using Blackett's relation.

$$R \propto M.Z^{-\frac{1}{2}} f(v)$$

This relation was later found to be of very limited application and more accurate values are given in the Appendix.

(b) Non-Coplanar Flags

Apart from one event which was identified as a proton which had been knocked on by a neutron and then scattered (there was no ionisation change at the "origin" and the angles were quite inconsistent with a $He^4(\gamma,p)H^3$ event - as well as being non-coplanar), all the events had a short heavy recoil and a light fragment, indicating that the event had originated in a heavy nucleus. From the lack of coplanarity, a neutron must have been involved in the reaction. (n,p) reactions produced by fast neutrons, would have appeared as non-coplanar flags but they were assumed to be few in number as no non-coplanar flags were observed in the portion of the cloud chamber outside the X-ray beam. As the (γ,pn) thresholds in nitrogen and oxygen are 12.5 and 23.0 MeV respectively, these non-coplanar flags were identified as $N^{14}(\gamma,np)C^{12}$ events.

(c) Singles

Due to the short range of the majority of singles and to the presence of an indeterminate number of tracks of helium nuclei knocked on by neutrons of moderate or high energy/

energy, no definite conclusions could be obtained from the measurement of single tracks.

(d) Stars

Two three-prong stars and one four-prong star were observed. By use of conservation of momentum, these were identified as $N^{14}(\gamma,2\alpha)Li^{6}$ and $O^{16}(\gamma,4\alpha)$ reactions.

II.5. Conclusions

Twelve events were identified as $He^{4}(\gamma,p)H^{3}$ reactions. In ten cases the triton range and in two cases the proton range could be measured. In every case good agreement was obtained with the angular measurements. Thus the $He^{4}(\gamma,p)H^{3}$ reaction may be considered to be definitely established.

It had been shown that the technique could be used to allow an investigation of the photodisintegration of heavier gases.

CHAPTER III.

THE PHOTODISINTEGRATION OF NITROGEN.

Introduction.

In this chapter the study of photodisintegration of nitrogen using a cloud chamber is described. The importance of this experiment is first demonstrated. The description of and modifications to the apparatus and method are given. The method of analysis is described. It is shown that background events can be identified and separated from photodisintegration events. The range distribution of low energy protons is shown to give an energy level structure which is in agreement with that found from the $C^{13}(p,\gamma)N^{14}$ reaction by detailed balancing. The accuracy of the microscopic measurements of recoil ranges is demonstrated and this technique is then employed to find the (γ,p) cross section at high energies. (γ,α) and $(\gamma,star)$ events are considered. The relative probabilities of the various reactions were studied by measuring the numbers of events at three different peak energies of the synchrotron. The results are discussed and it is shown that from a detailed study, general conclusions can be drawn.

III.1. The Photodisintegration of Nitrogen.

It has been shown in Chapter I that very little

was known of the photo-emission of charged particles from light elements although this was of interest as the (γ,p) cross section was expected to be comparable with the (γ,n) cross section.

The (γ,n) cross section in nitrogen was measured by Horseley et. al. (1952) who found that it was considerably lower than the (γ,n) cross section in Carbon and Oxygen. They also found the unusual result that the cross section was higher at 13 MeV than at 16 MeV. These results as shown in Fig. III.1.

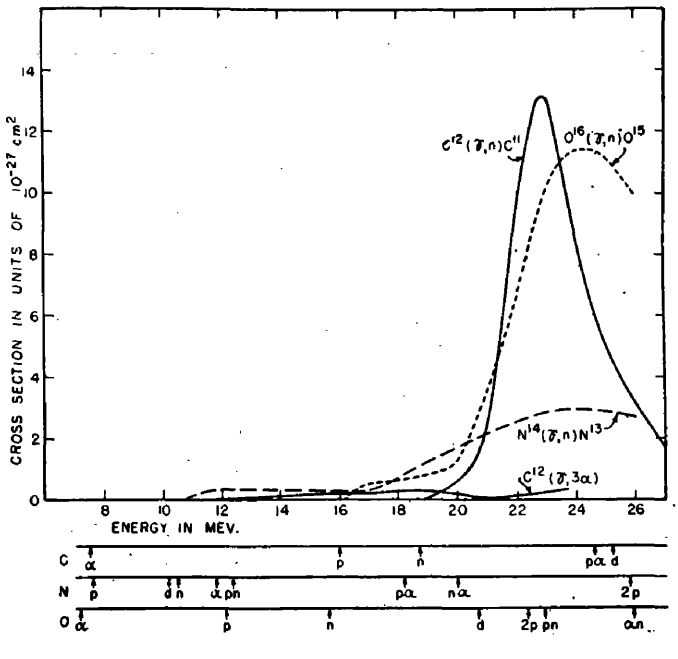

Fig.III.1.

The photodisintegration of nitrogen was particularly interesting/

interesting as the thresholds for the (γ,p), (γ,n), (γ,d), (γ,α) and (γ,pn) reactions are all well below the energy of the giant resonance and therefore it might be expected that a study of the photodisintegration of nitrogen using X-rays of up to 23 MeV energy would yield information about the change in the nature of the photonuclear process in going from energies below to energies in the vicinity of the giant resonance.

The cloud chamber technique which was described in Chapter II, had shown that (γ,p), (γ,α) and (γ,pn) events could be readily distinguished from the electron background and hence this technique was especially suited to the study of the photodisintegration of nitrogen. In addition, it was expected that (γ,d), $(\gamma,\alpha\alpha)$ and $(\gamma,\alpha p)$ events would be observed.

III.2. Method and Apparatus

The basic method employed was that described in Chapter II, but in this experiment it was necessary to make accurate measurements of the recoil tracks and for this a high standard of track quality was required. It was found possible to obtain this track quality if the cloud chamber expansion and the synchrotron pulses were correctly timed relative to one another and if the cloud chamber conditions were kept constant so that the X-rays always entered

the/

the chamber at the same supersaturation.

As the initial pulse from the main push-button was random in time, the cloud chamber was triggered with a pulse derived from the synchrotron timing pulses. The delay between the opening of the cloud chamber expansion valve and the synchrotron firing pulse was varied in 5 millisecond steps. The shortest delay that gave sharp tracks was employed. With shorter delays, the tracks became diffuse while with longer delays the background increased without any appreciable change in the sharpness of the tracks.

To keep the cloud chamber conditions constant, it was surrounded by a water-cooled aluminium cylinder. It was found that the expansion ratio did not require to be adjusted during 6-hour runs.

The background of electron tracks was reduced by thinning down the Perspex wall to 0.09 inches thick to form a window through which the X-ray beam entered the chamber.

To speed the cycle of operations, an electrostatic clearing field of 400 Volts was introduced across the chamber. However, it was found that the recoil tracks became diffuse due to the ions being dragged out by the clearing field and hence provision was made for the field to be switched/

switched off by the cloud chamber triggering pulse for the duration of the expansion.

As it was not always possible to estimate the energy of the photons responsible for the events observed, irradiations were made at three different values of the peak X-ray energy, these energies being approximately 19, 21 and 23 MeV.

It has been found previously that if a track lay in the vertical plane of the line joining the two cameras, then it was difficult to align its two images on the reprojection table. For this reason a third camera was introduced at right angles to the other two and according to the direction of the track, the appropriate pair of cameras were employed in reprojection. This third camera was found to be very useful as extra evidence e.g. with a recoil track which was scattered in such a manner that it appeared bent from one camera but a straight line from another.

The cloud chamber was filled with nitrogen to give an expanded pressure of 1.4 atmospheres. Water was used as the condensable vapour. The stopping power of the gas was calculated from its composition and the expanded pressure which was measured during each run. As a check the range of/

of alpha tracks from a polonium source on the wall was measured.

To obtain more uniform illumination of the chamber a second flash lamp was introduced. To enable the films to be aligned more accurately on reprojection, the pins round the side of the chamber were replaced by a grid of 0.002 inch thick nickel wire on the base of the chamber.

To monitor the output of the synchrotron, an ionisation chamber was mounted behind a 3 inch thick lead wall and placed in the X-ray beam behind the cloud chamber. The output of the individual pulses of X-rays were measured by observing the height of the pulse from the ionisation chamber on the screen of a cathode-ray oscillograph. The ionisation chamber was calibrated by comparing its pulse height with the activity induced in a copper disc irradiated in a standard position in front of the cloud chamber and counted in a standard geometry. The relative doses for the 19, 21 and 23 MeV runs were then calculated from the peak energies using the Cu^{62} activation curve measured by Katz and Cameron (1951). Absolute values were then obtained by comparing, at a peak energy of 23 MeV, the activity induced in the copper disc with the response of a Victoreen thimble/

thimble mounted at the centre of a Perspex cylinder of 8cm. outside diameter, this being a standard configuration. This comparison is estimated to be accurate to 20%.

III.3. Analysis.

Three cameras were used, one being mounted vertically above the chamber while the two side cameras were separated from this top camera by $25\frac{1}{2}^{o}$ in the vertical plane, and from each other by 90^{o} in the azimuthal plane. To make the focal plane of the lens in the side cameras horizontal with respect to the film, the film was tilted with respect to the axis of the lens and was at an angle of 30^{o} to the horizontal. High contrast film of 60mm. width was used.

The method of reprojecting the films on to a movable table and aligning the images was basically the same as that described in Chapter II, except that with the addition of a third camera each event was analysed using the top camera and the appropriate side camera so that the line joining the two cameras was approximately at right angles to the track direction. The third camera was used as a check. The three films were initially brought into register/

register using the images of the grid wires on the base of the chamber. This procedure had the advantage of automatically checking the accuracy of the reprojection system for each track measured. Very little distortion was found. In addition, artificial tracks were drawn, photographed and reprojected when it was found that the length measurements were accurate to $\frac{1}{2}$mm. for all lengths and the angles were accurate to 1^{o} for tracks within 60^{o} of the horizontal.

The reprojection system was used to measure all tracks of length greater than 3mm., but with shorter tracks it was difficult to secure accurate alignment. Thus, with (γ,p) events in which the fragment left the visible region of the chamber, the recoil was too short to be measured and hence the energy of the particles could not be found by reprojection. To solve this problem, the possibility of microscopic analysis was investigated. It was found that when the films were viewed directly with a low powered microscope, it was possible to measure the lengths of the recoil images. The microscope magnification was 40 and the chamber-film reduction ratio was 1/6 so that the final image viewed in the microscope was approximately seven times the original track size. It was demonstrated later that the energy of the recoil could be found from the

ranges/

ranges measured by this method.

Thus the analysis procedure was as follows:-

(1) The events were viewed with the microscope and classified phenomenologically. Each recoil length was measured with the eyepiece seale.

(2) The length, direction in space and co-ordinates of the origin and end points of each track were measured by stereographic reprojection.

The events were classified into Singles, Flags and Stars as in Chapter II, but due to the shortness of the recoil lengths, the reprojection method could not be used to classify the flags as coplanar or non-coplanar. Instead, the flags were examined by the microscope and if the recoil and fragment were very nearly in a straight line on all three films, the event was classified as a "collinear flag" while the other events were called "non-collinear flags". This group of collinear flags was intended to include all photo-events in which the recoil and the fragment were the only two products of the reaction for in these cases, the momentum of the incident photon was very small and only slightly affected the departure from collinearity (e.g. for a (γ,p) event the angle between the fragment and the recoil could only vary between 170° and 180° depending on the/

the angle of emission of the particles relative to the direction of the X-ray beam). As multiple scattering could cause slight bending of the recoil track, the criterion used was that events in which the recoil was within $\pm 10^{o}$ of its expected direction were counted as collinear.

The events were then classified as:-

(1) Collinear Flags.

(2) Non-collinear Flags.

(3) Unclassified Flags - events with a visible recoil whose direction was uncertain (e.g. because of its short length).

(4) Singles - events without a visible recoil.

(5) Stars - events with three or more prongs.

(6) Tracks coming from the chamber wall.

The thresholds for the photonuclear reactions possible in Nitrogen and also the neutron-induced "background" reactions, are given in Table III.1, together with the expected classification of the event.

Table III.1./

Table III.1. Reaction Thresholds and Classifications

Photonuclear Reactions			Threshold (MeV)
$N^{14} + \gamma \longrightarrow n + N^{13}$			10.54
$p + C^{13}$	Collinear	Flags	7.54
$d + C^{12}$	Collinear	Flags	10.26
$\alpha + B^{10}$	Collinear	Flags	11.6
$p + n + C^{12}$	Non-collinear	Flags	12.49
$\alpha + \alpha + Li^{6}$		Stars	16.07
$p + \alpha + Be^{9}$		Stars	18.2

Neutron Reactions		Threshold (MeV)
$N^{14} + n \longrightarrow p + C^{14}$	Non-collinear flags (except for slow neutron reactions).	- 0.63
$\alpha + B^{11}$	Non-collinear flags (except for slow neutron reactions).	0.15

III.4. Background Events

In addition to the large number of tracks of photodisintegration events observed in the cloud chamber, the reactions produced by the X-ray beam were expected to give a "background" of unwanted tracks.

(a) Background Due to Slow Neutrons

As the $N^{14}(n,p)C^{14}$ reaction is exothermic by 0.63 MeV, slow neutrons were expected to give tracks with a/

a characteristic total length in the chamber gas of 7½mm. (Bøggild, 1945) and also such events were expected to be uniformly distributed throughout the chamber. The energy distribution of tracks stopping in the visible region of the chamber shows such a group at the expected value of 0.63 MeV. That these events were due to slow neutrons, was confirmed by the fact that half of them had their origins outside the X-ray beam which was expected as the volume of the chamber outside the X-ray beam was approximately equal to that within the beam. Thus the background of events due to slow neutrons was easily identified and eliminated (also shown in Figs. III.2 and III.3 and in section III.5(A)).

(b) Fast Neutrons.

Fast neutrons were expected to produce (n,p) and (n,α) events which would appear as flags of length greater than one cm. and which would be non-collinear due to the relatively large momentum of the neutron. Knock-on collisions between fast neutrons and gas nuclei were not included as they would produce tracks of less than 3 mm. length which were not measured.

The/

The spatial distribution of fast neutrons was considered to have an isotropic part and an anisotropic part due to a possible flux of fast neutrons in the X-ray beam. The isotropic distribution was estimated from the number of non-collinear flags with origins outside the X-ray beam and both parts were estimated from the distribution of proton tracks from the chamber walls.

The number, 15, of non-collinear flags with origins outside the X-ray beam was less than 10% of the number inside the beam, and was only 2% of the total number of events, although the volumes inside and outside the beam were approximately equal.

The protons from the wall must either be knock-on protons from collision of fast neutrons with hydrogen nuclei or photoprotons from the C^{12} and O^{16} of the perspex wall. As the two (γ,p) thresholds are high and as the cross sections are low below 20 MeV, the number of photoprotons expected in the 19 and 21 MeV runs was small. Hence, the number, 7, of knock-on protons from that part of the wall in the beam is known with little error and may be compared with the number 17, of knock-on protons out of the beam. As the area of wall out of the beam is

three/

three times that in the beam, it can be seen that there is no appreciable flux of fast neutrons in the X-ray beam. A similar comparison cannot be made for the 23 MeV run as the number of photoprotons is appreciable, but it can be seen from Table III.2 that the numbers are not inconsistant with the assumption of an isotropic distribution of fast neutrons.

Table III.2..

Distribution of Protons Coming from the Perspex Wall

Run	19 and 21 MeV	23 MeV
Protons from the wall out of the beam.	17	13
Protons from the wall in the beam.	9	30
Estimated number of photoprotons.	1 - 3	15 - 40
Knock-on protons from the wall in the beam.	7	----

Hence corrections can be made for "background" events/

events due to slow and fast neutrons, and any errors are small compared with the statistical error.

III.5. Results

The results to be presented in this section fall naturally into two main divisions, low energy events ((γ,p) reaction) and high energy events (all reactions). The distinguishing feature was that the proton tracks of the former mainly stopped in the visible region of the chamber while the end-points of most of the tracks of the high energy events were not seen.

For the tracks which stop in the chamber, the ranges of the protons gave the energies accurately so that a detailed energy distribution was obtained in the region immediately above the (γ,p) threshold.

At high energies, the fragment range cannot as a rule be measured, so that a similar precise energy distribution cannot be obtained. However, two other methods were available. The relative activation cross sections of the different reactions were obtained from a count of the numbers of each type of event. The energy dependance was obtained from the numbers found for runs made at different peak energies of the synchrotron. A

new/

new technique, introduced by the author, was to measure the ranges of the recoils of collinear flags; this gave the momentum of the fragment. Although the recoils were too short to be measured on reprojection, being only about a mm. long, they could be clearly seen with a microscope. This method was shown to yield significant results by comparing for those events where the fragment stopped in the chamber, the measured recoil range with that calculated from the fragment range.

A. Energy Distribution of Low Energy (γ,p) Events.

(γ,p) events were expected to appear as collinear flags but if the proton were of low energy the recoil would be short and in some cases would not be visible e.g. for a 1 MeV proton the recoil length is about 1/3mm. Thus in this low energy region (γ,p) events may be expected to be recorded as unclassified flags or singles. For this reason collinear flags (with the (γ,α) events excluded, see Section D), unclassified flags and singles, were assumed to be (γ,p) events and from the fragment range measured,* the total energy of the event was calculated, using Bethe's (1950) range-energy curve.

---

* For the singles the total range was measured and from the C^{13} range energy relation a correction was applied for the recoil range. This procedure is experimentally justified in Section B.

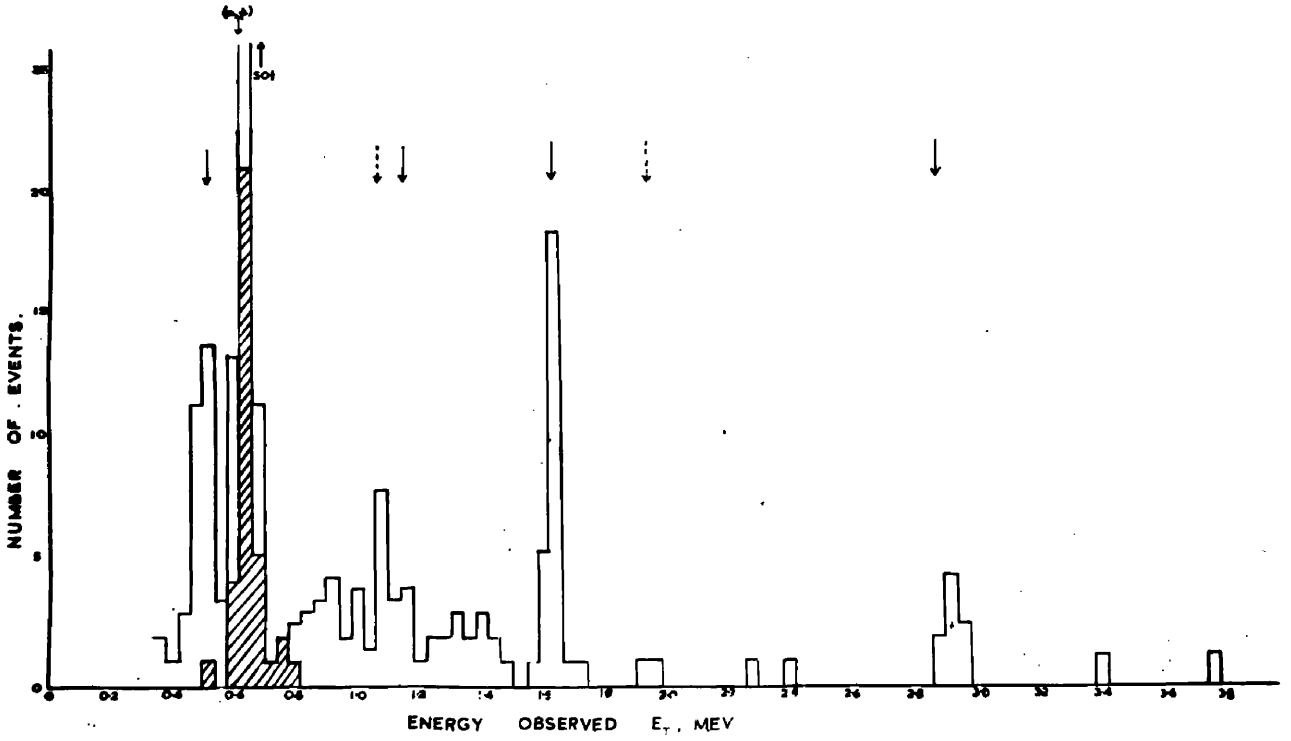

Fig.III.2.

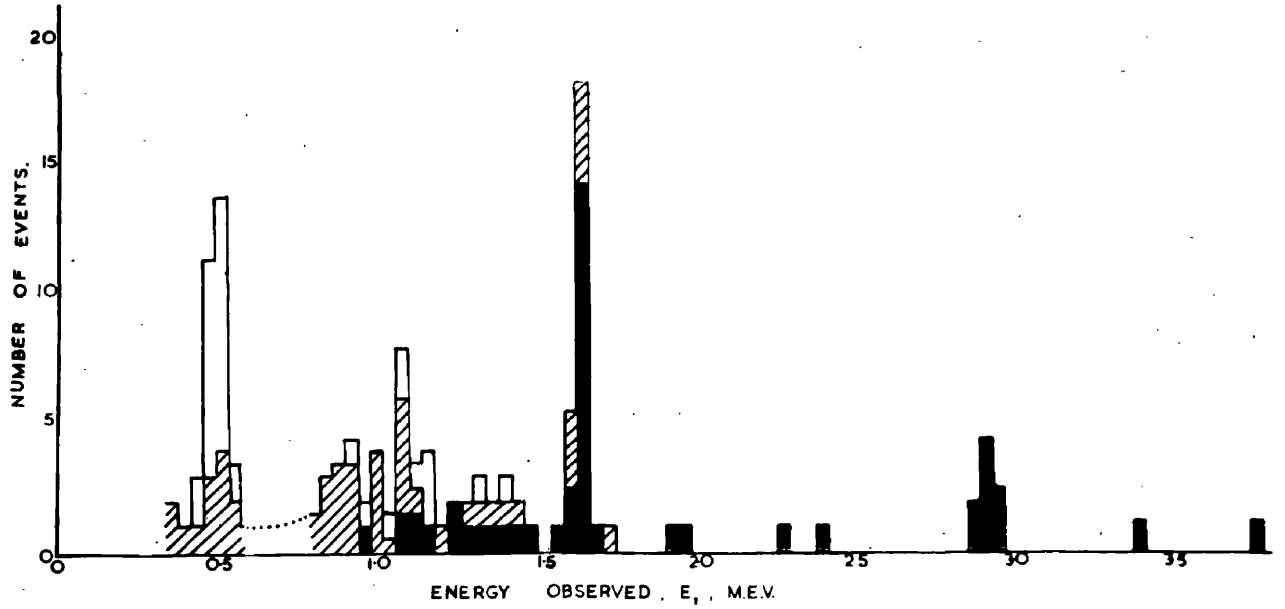

Fig.III.3.

The energy distribution obtained is shown in Fig.III.2. Events with their origins out of the beam are shown shaded. It is seen they group about 0.63 MeV and so may be identified as slow neutron (n,p) reactions. When these events and the corresponding number of events in the beam are subtracted as "background" the resulting energy distribution is shown in Fig.III.3. The classification of events is also shown in Fig.III.3. The higher energy events are all collinear flags while towards lower energies (and shorter recoil lengths) the numbers of unclassified flags and singles increase.

Unlike the energy distributions of photoprotons which had been previously reported, distinct groups were found. Narrow groups occurred at 0.51 ± 0.2, 1.63 ± 0.02 and 2.92 ± 0.03 MeV and a broad group at 1.15 ± 0.05 MeV. This energy distribution is experimental, no allowance having been made for the events in which the fragment left the chamber. Thus, the 2.92 MeV group is considerably larger than is indicated in Fig.III.3.

The $C^{13}(p,\gamma)\ N^{14}$ reaction has been investigated by Seagrave (1952) and by Woodbury et. al. (1953) who found/

found that for gamma-ray transitions to the ground state of N^{14}, narrow resources occur at centre of mass energies of 0.52 and 1.64 MeV while there is a broad resonance ($\frac{1}{2}$ MeV half-width) at 1.16 MeV. Also Dr. H.B. Willard has found (private communications) that there is a narrow resonance at 2.89 MeV. A comparison was made between the experimental results and the results for the inverse reaction (i.e. $C^{13}(p,\gamma)N^{14}$) using the principle of detailed balancing. From the integrated (p,γ) cross section, the integrated (γ,p) cross section was found, then on multiplying by the measured X-ray doses and by the fraction of tracks stopping in the chamber, the number of tracks expected to stop was calculated and this number was in good agreement with the number observed as is shown in Table III.3.

There is a further point of secondary importance. The 9.49 MeV level was reported to have no transitions to the ground state in the $C^{13}(p,\gamma)N^{14}$ reaction within the experimental error. If an upper limit of 5% ground state transitions is put on this error, then the calculated "number" of events is 2.4; in this experiment two possible events/

events were observed. Clearly this has no statistical significance but there is a possibility that a more detailed examination might yield a positive result.

Table III.3.

Comparison of the Observed Proton Groups with Predictions from the $C^{13}(p,\gamma)N^{14}$ reaction.

(1)	(2)	(3)	(4)	(5)	(6)	(7)
8.06	0.52	0.065	0.603	0.99	34	32
9.18	1.64	0.044	0.813	0.62	24	26
10.43	2.89	0.040	1.2	0.20	12	9

(1) N^{14} energy of excitation (MeV); (2) energy of proton + recoil (MeV); (3) $\sigma_{int.}(p,\gamma)$ (MeV mbn); (4) $\sigma_{int.}(\gamma,p)$ (MeV mbn); (5) fraction of events stopping in the chamber; (6) number of tracks calculated; (7) number of tracks observed.

What is believed to be the most accurate cross section is given in Fig.III.4. The cross section up to 1.8 MeV is calculated from the results of Seagrave (1952) and Woodbury et. al. (1953) for the (p,γ) reaction by detailed balancing. Above 1.8 MeV the results are taken from/

from the present experiment (the value of the integrated cross section for the 2.89 MeV level found by Willard is preliminary).

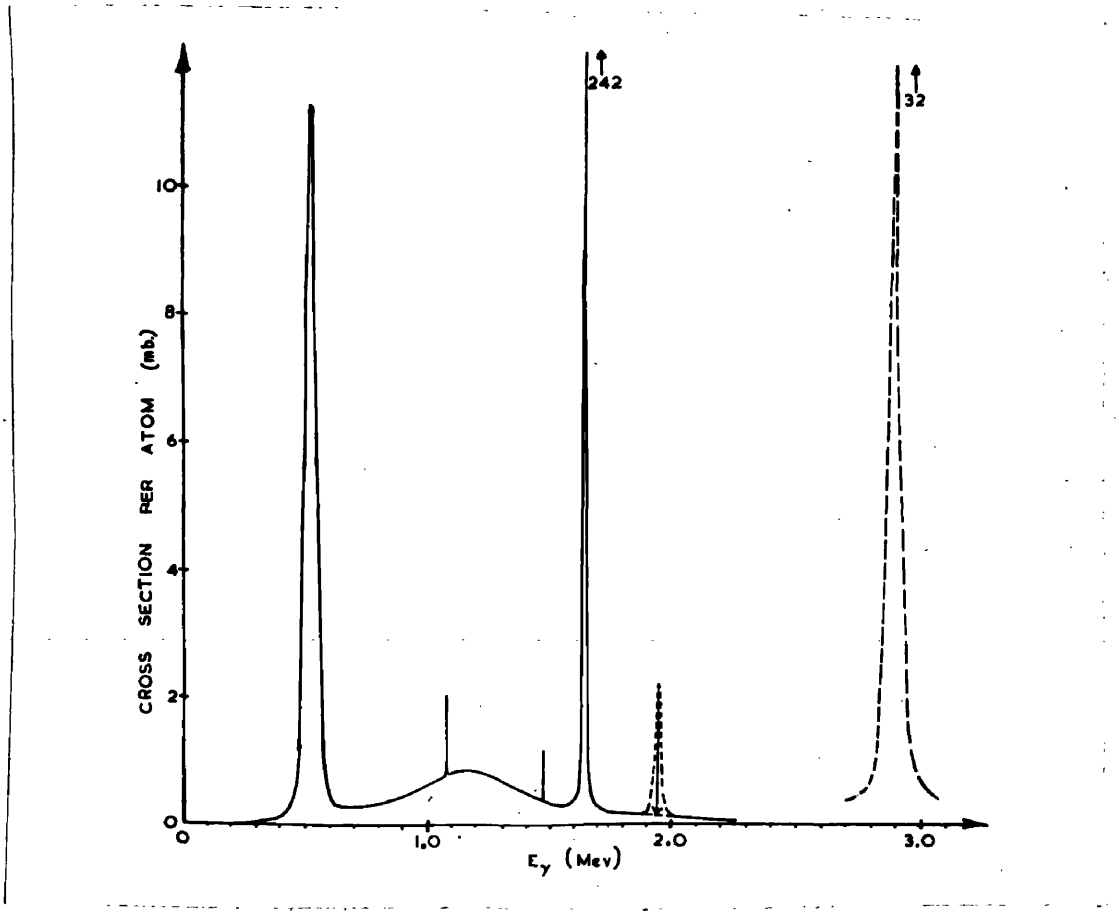

Fig.III.4.

In this experiment there is no direct way of deciding whether a photoproton is produced from the reaction $N^{14}(\gamma,p)C^{13}$ or the reaction $N^{14}(\gamma,p\gamma')C^{13}$, however/

however when it was assumed that all the events were $N^{14}(\gamma,p)C^{13}$ reactions, good agreement was found for the cross sections of the 0.52, 1.64 and 2.89 MeV groups by detailed balancing. It may be noticed that there were very few protons of energy between 1.7 and 2.8 MeV. It follows that not merely is the (γ,p) cross section low in this energy region, but also that there are few protons from $(\gamma,p\gamma')$ reactions with these energies. Thus the number of $(\gamma,p\gamma')$ reactions are probably small. It can be seen from the manner in which it was derived that Fig.III.4 is independant of any background of $(\gamma,p\gamma')$ reactions.

During the course of the present experiment a measurement of the low energy photoprotons from nitrogen was reported by B.M. Spicer (1953). The result obtained was irreconcilable with the present work. A narrow beam of X-rays of peak energy 11.5 MeV was passed through a gas target chamber. Nuclear emulsions were placed at the side of the chamber and the range of the protons was measured in them. After making corrections for (n,p) tracks and for the energy lost by the proton in the gas before reaching the emulsion, an energy distribution of the protons was obtained./

obtained. This distribution showed a rapid decrease in the number of protons from 165 protons in the energy range 2.0 to 2.2 MeV to 19 protons in the range 3.0 to 3.2 MeV. The distribution gave no indication of a peak at 2.9 MeV. As protons of less than 2.2 MeV might not reach the emulsion, the number in the interval 2.0 to 2.2 MeV was a lower limit; also the distribution fell very rapidly to zero at energies below 2.0 MeV. This energy distribution is in complete disagreement with Fig.III.3 where only two events are observed between 2.0 and 2.8 MeV. The cloud chamber experiment is preferred for the following reasons:-

(a) The entire event is observed, not just the end of the proton track. This allows (n,p) events to be eliminated as they produced non-collinear flags or are due to slow neutrons which give a track with a characteristic range of 7mms.

(b) The agreement of the present results with the various measurements of the inverse reaction.

In view of disagreement found here, results of similar nuclear emulsion experiments must be treated with some reserve.

B./

B. Accuracy of Recoil Measurement

High energy (γ,p) events, in which the fragment left, could be analysed by means of measurements of the recoil range. This new technique first required to be justified as regards the significance of such measurements and their accuracy. This was done by considering (γ,p) events in which the fragment stopped in the chamber.

For all collinear and unclassified flags of fragment ranges greater than 1cm. in the chamber, microscopic measurements were made of the lengths of the images of the recoil and fragment, l_r and l_f respectively. Since the flags are either observed to be collinear or are believed to be collinear, the recoil length, L_r is given by:-

$$L_r = \frac{l_r}{l_f} \times L_f \qquad \ldots\ldots(III.1).$$

where L_f is the fragment length measured by reprojection. Microscopic measurements were made on all three films and L_r calculated in each case. In calculating the weighted mean, the recoil track quality was considered and the film from the top camera had more weight than those of the side cameras.

A/

A precise calculation of the recoil length and direction could be obtained from microscope measurements of the three films but with the camera geometry used, such calculations were excessively time-consuming. The errors involved in the approximations used in equation III.1 are small compared with the unavoidable range straggling, and are partly compensated for by taking the weighted mean of three values of L_r.

Each of these 'observed' recoil ranges was compared with the recoil range calculated from the fragment range. The calculation consisted of assuming the fragment to be a proton, finding its energy from the range (Bethe 1950) calculating the recoil energy (see Appendix) and from an assumed C^{13} range energy relation obtaining the calculated recoil range. In general, the largest source of error was the assumed C^{13} range-energy curve. For this reason the subject of range-velocity relations for ions of $Z>3$ was studied in considerable detail and the following conclusions reached.

(a) For the ions from Boron to Neon the R.M.S. straggling for recoils of 0.5 to 2mm. range in air at S.T.P. is about 15%. This implies that recoil range/

range measurements are significant within these limits.

(b) For a given velocity, the ion range is proportional to the mass. Therefore, from the range-velocity relation for C^{12} the relation for C^{13} can be obtained.

(c) There appears on the basis of experimental evidence, to be a systematic behaviour of ions from Boron to Neon. Thus in conjunction with (b), the range-velocity relation assumed for C^{12} may be checked by comparison with the range-velocity relations of its neighbouring elements.

The basis for these conclusions is presented more fully in the Appendix.

The results of the above comparison are shown in Fig.III.5 where the directly measured recoil range is plotted against the calculated recoil range, each event being shown as a cross. Almost all the crosses group about the expected (γ,p) line. The R.M.S. deviations of the 1.64 and 2.9 MeV groups are 26% and 16% respectively. From (a) above, the expected range straggling is 15% so that the experimental error in the microscopic range measurements is about 0.2mm. (being mainly due to end-effects, it is approximately a constant),/

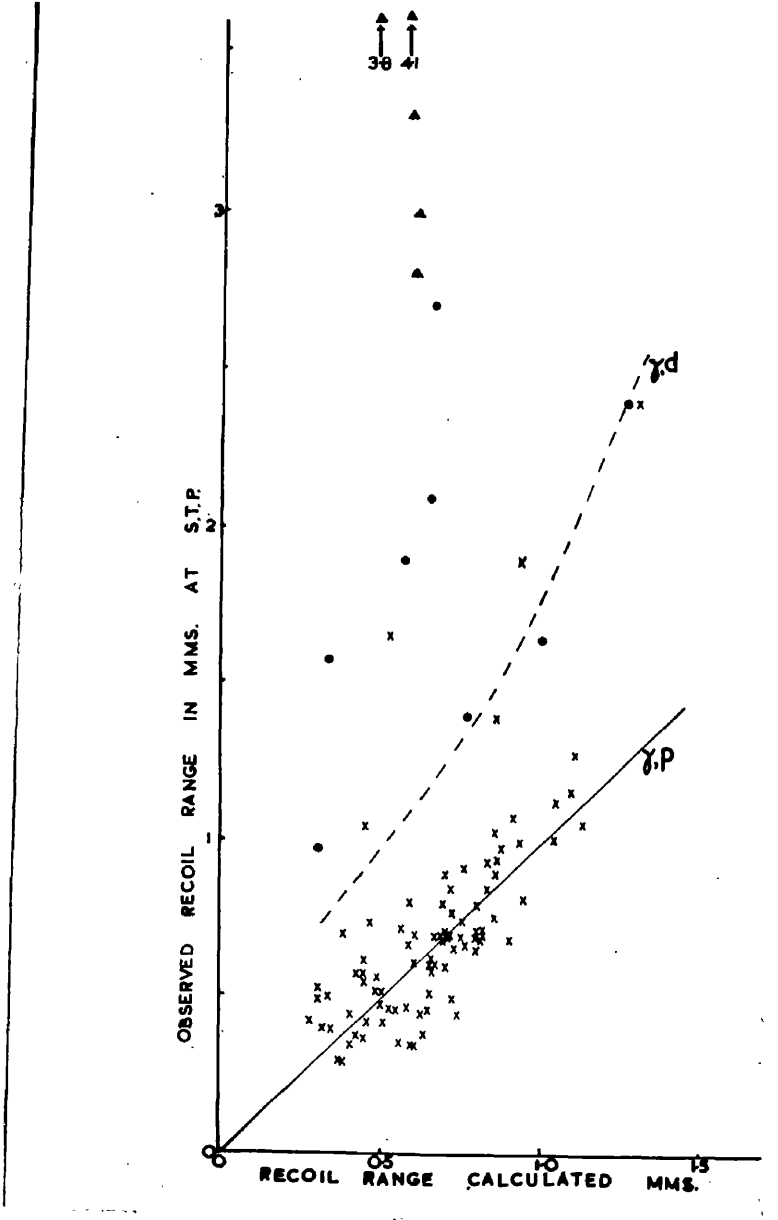

Fig. III.5.

constant), and at ranges corresponding to energies higher than 3 MeV, the spread in recoil range measurements is almost entirely due to unavoidable range straggling.

The assumption used in section A and here, that these events are (γ,p) reactions is justified by the grouping of events round the expected (γ,p) line and by their small deviations from it.

The possibility of identifying (γ,d) events by this method was investigated. In Fig.III.5 the dotted line/

line shows approximately the expected positions of such events. A few crosses are observed at higher ranges than the (γ,p) line. Some of these five events could be (γ,d) reactions, but they could also be (γ,pn) events where the neutron is emitted in approximately the same direction as the proton. The number of (γ,pn) events of this type cannot be directly estimated (due to unavoidable angle scattering) but for comparison some non-collinear events which were almost collinear (and where the proton stops) were assumed to be (γ,p) events and are plotted on Fig.III.4 as circles.

It can be seen from the figure that these events could be all (γ,pn) or mainly (γ,d). Hence no classification of these five crosses can be definitely made.* In general it may be said that this method is not suitable for detecting deuteron emitting reactions where p-n emission is also present.

(γ,α) events will be discussed later (Section III. 5.D.) but a similar technique can be applied to them. The measured recoil range was compared with the recoil range calculated from the range of the fragment on the assumption it was a (γ,p) reaction. The resulting points are plotted on Fig.III.5 as triangles. It can be seen that the/

* They were not included in Fig.III.1 or Fig.III.2.

the suspected (γ,α) events all have much larger recoil ranges and are well separated from the crosses representing other collinear events.

It is now possible to assess this new technique of recoil range measurements. This is best done by comparing it with magnetic curvature measurements.

(1) Both methods give a direct measurement of the fragment momentum.

(2) The unavoidable error in range straggling (~15%) is similar in origin to the equally unavoidable error in curvature due to multiple scattering and is also of the same magnitude. (For a magnetic field of 5000 gauss and a chamber filled with one atmosphere of nitrogen, the error in curvature for a 5 MeV proton, measured over a track length of 10cm. is approximately 15%).

(3) Recoil range measurements can be applied to practically all events whereas curvature measurements can only be applied to events which give long (10cm.) tracks in the chamber.

(4) At high energies, the recoil range becomes an accurate measurement as range straggling becomes very small while curvature measurements become difficult as the track approaches a straight line.

Thus/

Thus the method of recoil range measurements is equivalent to and in some ways better than magnetic curvature measurements.

C. Recoil Range Measurements

The accuracy of recoil range measurements and of the C^{13} range-velocity relation has been demonstrated for low energy events in which the fragment stopped in the chamber. It is now justifiable to apply this method to high energy (γ,p) events in which the fragment did not stop in the chamber. As the recoils were longer in this case, the measurements were more accurate.

For collinear flags, the recoil direction was assumed to be exactly opposite that of the fragment whose direction had been measured by reprojection. The error introduced by this assumption is small and less than the range straggling. The recoil range was then calculated from the microscopic measurement of the projected recoil image, a small correction being applied for the position of the track in the chamber. These measurements were only made on the film from the top camera as the geometrical calculations are excessively lengthy for the other two films. The data for the run with a peak energy of 23 MeV was obtained from just over half of the films since the

fragment/

fragment directions of tracks leaving were not measured for the remainder.

The assumption that the recoil and fragment are in the same straight line gives an insignificant error for horizontal tracks, but can give an appreciable error in steep tracks. For this reason the results were first analysed in three groups, more than 60° from the horizontal, between 45° and 60° from the horizontal, and within 45° of the horizontal. The steep tracks gave a few anomalous values, but the distribution of the tracks between 45° and 60° was consistant with the "horizontal" distribution. Hence by taking only tracks within 45° of the horizontal there will be no significant error in the distribution due to this assumption. If an isotopic distribution is assumed, 29% will be excluded; in fact 27% were excluded.

Unclassified flags were assumed to be collinear and their recoil ranges were similarly calculated from the projected images. In all cases the corresponding proton energies calculated were less than 3 MeV. Hence in the energy range from 10.54 MeV (the (γ,n) threshold and also 3 MeV above the (γ,p) threshold) to the peak energy of 23 MeV only collinear flags were considered.

The recoil range distributions found at the three peak/

peak energies of the synchrotron are shown in Fig.III.6.

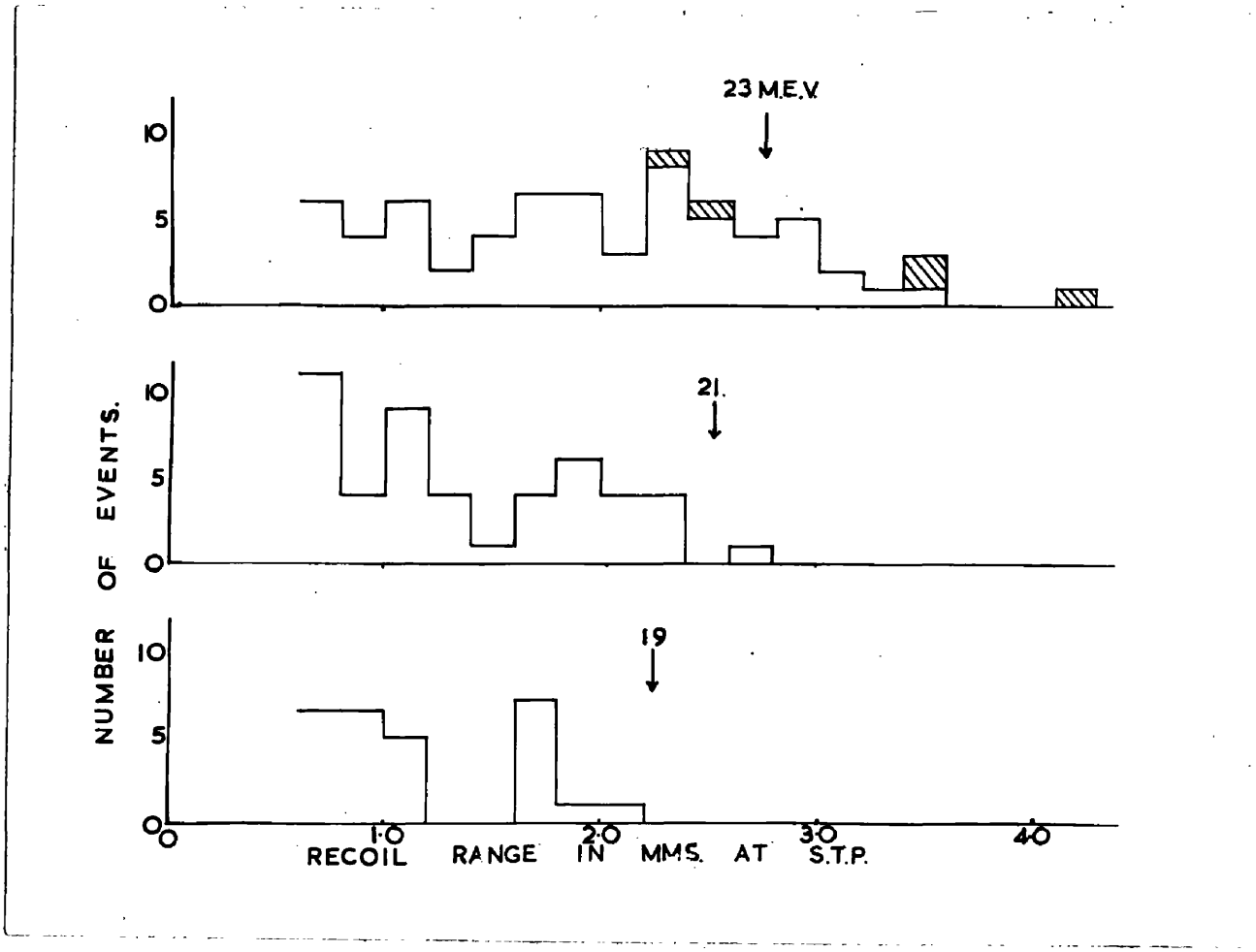

Fig.III.6.

For the purpose of comparison the recoil ranges have been corrected to the values they would have if the particles had been emitted at 90° in the centre of mass co-ordinates to the γ - ray direction. The shaded events are (γ, α) reactions (see section D). One important result can be simply seen from the fact that approximately equal numbers of events/

events occur in all range intervals. As the number of quanta in the synchrotron spectra decreases steeply with increasing energy, the (γ,p) cross section must rise as the energy increases. In order to deduce the (γ,p) cross section from these recoil range measurements, it is necessary to know the number and distribution of protons going to excited states of C^{13} and this information is not at present available. However, if it is assumed that in all cases the proton goes to the ground state of C^{13}, then the "cross section" deduced from the data for the 23 MeV run is as shown in Fig.III.7. If the residual C^{13} nucleus is left in an/

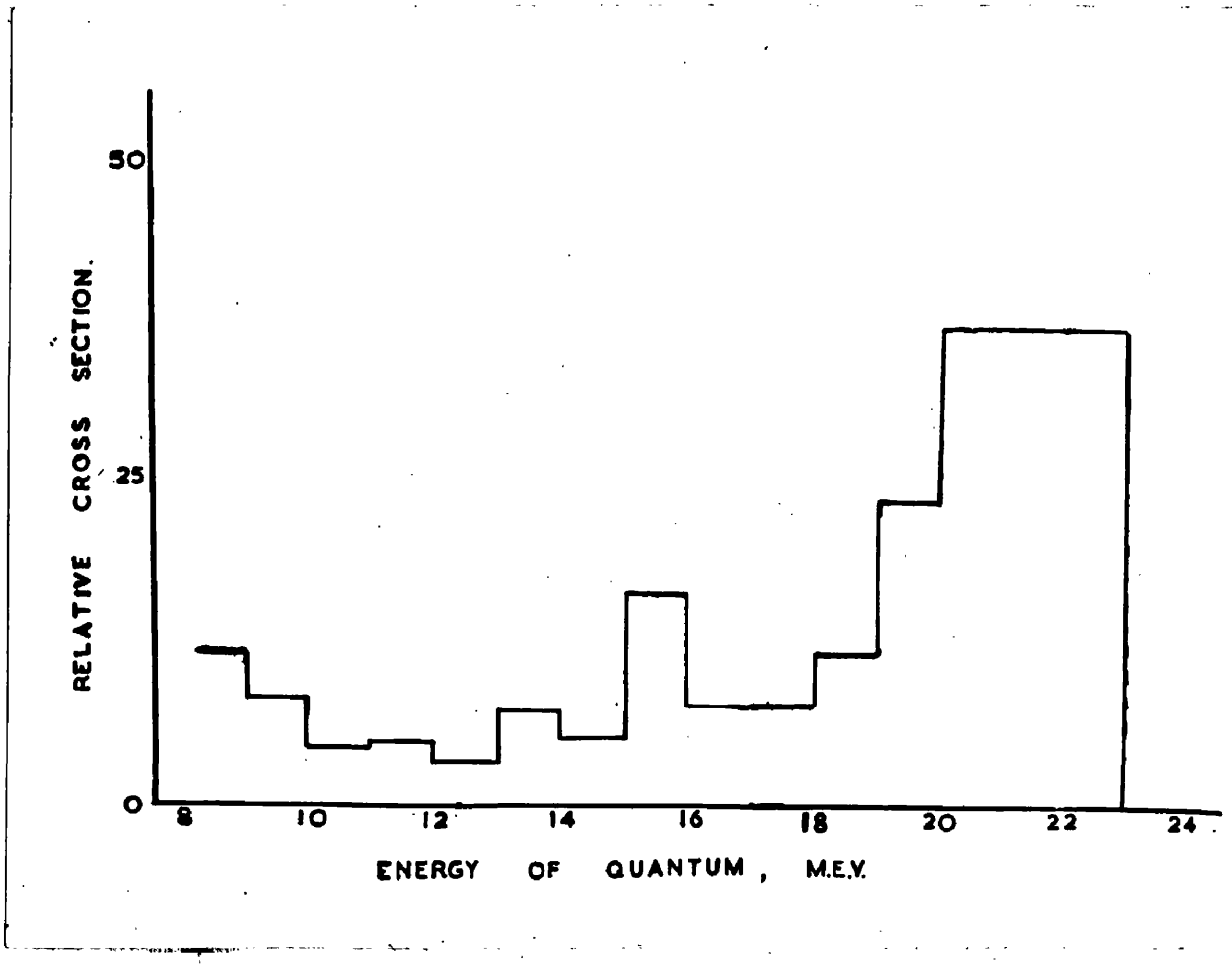

Fig.III.7.

an excited state, the value of the energy, E_γ of the photon calculated from the recoil range will be too low. The true E_γ will be higher by between 3 MeV (the lowest excited state of C^{13}) and 6 MeV (when neutron emission will produce (γ,pn) events which appear as non-collinear flags) - see Fig.III.9. It follows that the true (γ,p) cross section rises as steeply as or more steeply than the "cross section" of Fig.III.7.

A possible source of error is the presence of (γ,d) events. For incident photons of the same energy, they would have longer recoil ranges than would (γ,p) events, and so would produce an artificial rise in the (γ,p) cross-section near the peak energy. No experimental evidence is available for or against the presence of (γ,d) events, but on theoretical grounds, their number is expected to be small. The argument is:-

(a) From Sum Rule calculations the greater part of the gamma ray absorption is by electric dipole transitions. The Isotopic Spin Selection Rules state that for electric dipole transitions, a zero change of isotopic spin is forbidden. As the ground state of N^{14} has isotopic spin $T = 0$, almost all the gamma ray absorption will lead to excited states of N^{14} with $T = 1$ (states of higher isotopic spin do not occur in the/

the present energy region).

(b) The ground state of C^{12} has T = 0 (the first T = 1 state is at 16 MeV) and the deuteron has zero isotopic spin. Hence, by Conservation of Isotopic Spin, the excited state of N^{14} must have T = 0 to be able to emit deuterons.

Thus few (γ,d) reactions will take place, as if the excited state of N^{14} can be formed with any strength, it cannot emit deuterons while states which can emit deuterons, will seldom be formed.

D. (γ,α) Events.

(γ,α) events in which the fragment stops in the chamber can be identified since for a given fragment range the recoil from a (γ,α) reaction will be at least three times as long as those from other reactions producing collinear flags as shown in Fig.III.5. In addition (γ,α) events could be easily identified from their "appearance" — the heavy ionisation of the fragment, the small ionisation change at the origin and the multiple scattering at the end of the fragment track were all characteristic features (a typical event of this type is shown in Plate II.2). The identification of the suspected (γ,α) events was confirmed by comparing the measured recoil range with that calculated

from/

from the measured fragment range using the B^{10} range-energy relation derived in the Appendix. The comparison is made in Table III.4 and the agreement in the ranges is consistent with the expected range straggling of 10% to 15%.

Table III.4. (γ,α) Events

Recoil Range (cm.) Calculated	Observed	Appearance of Fragment Track	Total Observed Energy MeV $E_T = E_\alpha + E_{B10}$
0.30	0.32	α	4.43
0.28	0.33	α	4.66
0.33	0.35	α	5.54
0.41	0.36	α	5.63
0.38	0.365	α	7.13

In addition to the five events definitely identified, there are two other possible sources of (γ,α) events; (a) in which the fragments left the chamber and (b) in which the ionisation change at the origin was too small to be observed so that the event was classified as a single.

(a) In Fig.III.7, where the above five events are shown shaded, there are no collinear flags with recoil lengths greater than that of the highest energy (γ,α) event/

event which had a fragment range of $2\frac{1}{2}$cm. The probability of a track of this length leaving the chamber was less than 20% and for lower energy tracks the possibility is considerably less so that it is unlikely that there were any (γ,α) events in which the fragment left the chamber.

(b) The 16 singles of such a range that they could be (γ,α) events, were carefully re-examined and in every case the classification of the event as a 'single' was confirmed. The majority of these singles had the appearance of protons from their low track density and small multiple scattering but in three cases the tracks had a resemblance to alpha particles although this classification was doubtful. Hence the upper limit to the number of (γ,α) events was eight.

E. Relative Probabilities of the Various Reactions

The relative numbers of events found for the various reactions are listed in Table III.5 for the different peak energies of the synchrotron.

In order to facilitate comparison with the (γ,n) reaction only (γ,p) events which were initiated by photons of energy greater than that of the (γ,n) threshold (10.54 MeV) have been included in the table. The numbers of such (γ,p)/

(γ,p) events were obtained from the measured recoil ranges of collinear flags. It was assumed that the numbers of (γ,d) and of (γ,pγ) events were negligible.

The numbers of (γ,pn) events have been taken as the numbers of non-collinear flags. The possibility that some of the unclassified flags were (γ,pn) events requires investigation. There are two pieces of evidence:-

(a) The unclassified flags all have recoil lengths less than that corresponding to a three MeV proton and on the assumption that they are all (γ,p) events, with short or steep recoils, good agreement is obtained for the energy distribution of (γ,p) events with that found from the (p,γ), inverse reaction. Thus few, if any, unclassified flags will be (γ,pn) events.

(b) From the known energy distribution of protons from (γ,p) reactions of energy up to 3 MeV, whose tracks stopped in the chamber, and from the probability of a proton of a particular energy leaving the chamber, the number of protons of energy less than 3 MeV can be calculated. This estimated number is 58 ± 15 while the observed number of unclassified flags and collinear flags in this energy range whose fragment track left the chamber is 73, which is not inconsistant with the estimate. A maximum of 30 unclassified flags which may

have/

have been (γ,pn) events, was taken and the resulting upper limit to the numbers of (γ,pn) events is shown in Table III.5 in brackets. The number of unclassified flags added to the total for the 19 MeV run is probably abnormally high due to one of the films being of poorer quality due to an error in development.

Table III.5.
Relative Numbers of Events for the Various Reactions at Three Peak Energies of the Synchrotron.

Reaction	19 MeV.	21 MeV.	23 MeV.
(γ,p), with E > 10.54 MeV.	13	32	127
(γ,pn) probable.	4	22	132
" upper limit	(13)	(27)	(147)
(γ,α)	0	0	5 + (3?)
(γ,star)	0	0	8
(γ,n) calculated	8 ± 2	23 ± 5	75
No. of Roentgen at 1m.	0.014	0.024	0.050
No. of photographs.	304	265	333

The number of (γ,n) events was calculated from the induced activity measurements of Horseley et. al. (1952). An exact number of (γ,n) events is quoted for the 23 MeV run/

run in Table III.5 but to account for the uncertainties of the energy scale of the synchrotron and of the monitoring, errors have been given to the numbers of (γ,n) events calculated for the 19 and 21 MeV runs.

In Table III.5 the ratio of the numbers of (γ,p) events at the three peak energies is 0.10: 0.25: 1.00, while the ratio of the numbers of (γ,n) events, 0.11: 0.31: 1.00, is very similar. Hence the variation of the (γ,p) cross section with energy must be almost the same as the variation of the (γ,n) cross section with energy and the value of the (γ,p) cross section can then be obtained by multiplying the (γ,n) cross section by the ratio of the number of (γ,p) events to the number of (γ,n) events. Thus the (γ,p) cross section is small near 16 MeV and rises rapidly at about 20 MeV. As the ratio of the numbers of (γ,pn) events at the three peak energies are 0.03: 0.17: 1.00 (the upper limit values are 0.09; 0.18: 1.00), the (γ,pn) cross section must increase more rapidly with gamma-ray energy than does the (γ,n) cross section. This rise in the (γ,pn) cross section has also been established by the work of Ferguson et. al. (1954), who measured the sum of the (γ,pn) and (γ,n) cross sections by observing the total yield of neutrons. The (γ,pn) cross section which was then obtained by subtraction, had the same energy dependance as the (γ,n) cross section obtained by N^{13} activity/

activity measurements and was about three times as large.

The (γ,α) and (γ,star) cross sections similarly increase at about 20 MeV. The (γ,star) events were identified using the normal method of finding the smallest momentum unbalance. The "appearance" of the tracks confirmed the allocation of four of the events to the $(\gamma,\alpha p)$ reaction and three to the $(\gamma,\alpha\alpha)$ reaction. The tracks of the remaining event were too steeply inclined to permit exact measurement. Thus the (γ,α), $(\gamma,\alpha p)$ and $(\gamma,\alpha\alpha)$ reactions all have cross sections about 1 to 2.10^{-28} sq. cm.

III.6. Discussion of Results

With the results of this experiment and of the previous (γ,n) measurements it is possible to discuss all photonuclear reactions except (γ,d) and (γ,γ'), in N^{14} up to an energy of 23 MeV. The (γ,p) cross section up to the (γ,n) threshold (10.54 MeV), which is known in more detail than any other photonuclear cross section, will be considered first, then the higher energy region where several reactions can take place, will be discussed.

The range distribution of protons with energies below 3 MeV shown in Fig.III.3, gives the (γ,p) cross section below 10.5 MeV with an energy resolution of about 40 KeV. This may be compared with the energy resolution of $\frac{1}{2}$ MeV or more which is obtained with other methods of measuring photonuclear/

photonuclear cross sections. Although some earlier workers had obtained indications of a level structure in photonuclear reactions, the (γ,p) resonances found in the present experiment are the most convincing demonstration of such a level structure so far obtained. However, these levels could have been obtained in still greater detail by the application of detailed balancing to the inverse reaction, i.e. $C^{13}(p,\gamma)N^{14}$. It has been shown here that this procedure of using detailed balancing is justifiable. It follows that many more detailed photonuclear cross sections could be obtained from the inverse reaction using detailed balancing.

The nature of the $N^{14}(\gamma,n)N^{13}$ reaction cross section with its small maximum at 13 MeV and the giant resoance at 23 MeV (see Fig.III.1) led Blatt and Weisskopf (1952, p.651) to suggest that there were two different types of photon absorption involved. It was known (Levinger and Bethe, 1950) that the greater part of the absorption in the giant resonance region must be electric dipole. Blatt and Weisskopf postulated that below 15 MeV only electric quadrupole and magnetic dipole absorption were effective and that the sharp increase above this energy was due to the onset of electric dipole absorption. It is possible to test this hypothesis in the present experiment as in the range from 7.5 to 10.5 MeV the spins and parities of the levels involved are known; they are 1^-, 0^-, (2^-) and 2^- for the levels in N^{14} at

8.06/

8.06, 8.70 (broad level) 9.18 and 10.43 MeV (Ajzenberg and Lauritsen 1953, Willard 1955). As the ground state of N^{14} is 1^- the absorption in each case is by electric dipole transitions. These results are therefore in conflict with the above hypothesis and suggest that the giant resonance is due to a change in the probability of absorption rather than to a change in the character of the radiation absorbed.

We will now consider the energy region above 10.54 MeV. Only for the (γ,n) reaction has the energy dependance of the cross section been obtained, but as explained in Section III.5.E, the (γ,p) cross section has been found to be a constant multiple of the (γ,n) cross section and hence its variation with energy can be obtained. Similarly the (γ,pn) cross section which rises more steeply with energy, has been obtained. It is them possible to add all the cross sections and obtain the total integrated cross section. These established and inferred cross sections are shown in Fig.III.8 where it should be noted that while the cross section is known in detail below 10.54 MeV, the energy resolution was not sufficient to identify any levels at higher energies. The inferred (γ,p) cross section of Fig.III.8 is in rough agreement with the cross section, shown in Fig.III.7 obtained by measurement of recoil ranges.

It has been shown that the cross sections of all measured/

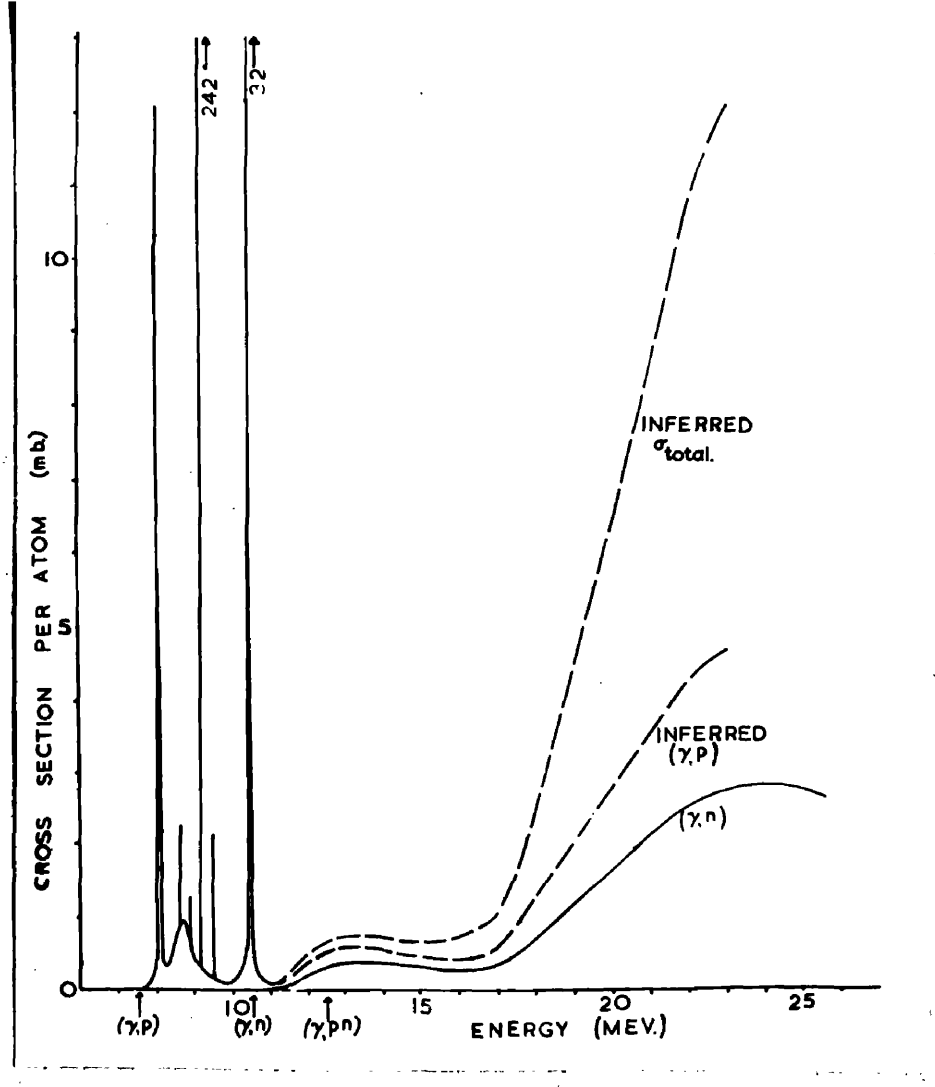

Fig.III.8

Fig.III.9.

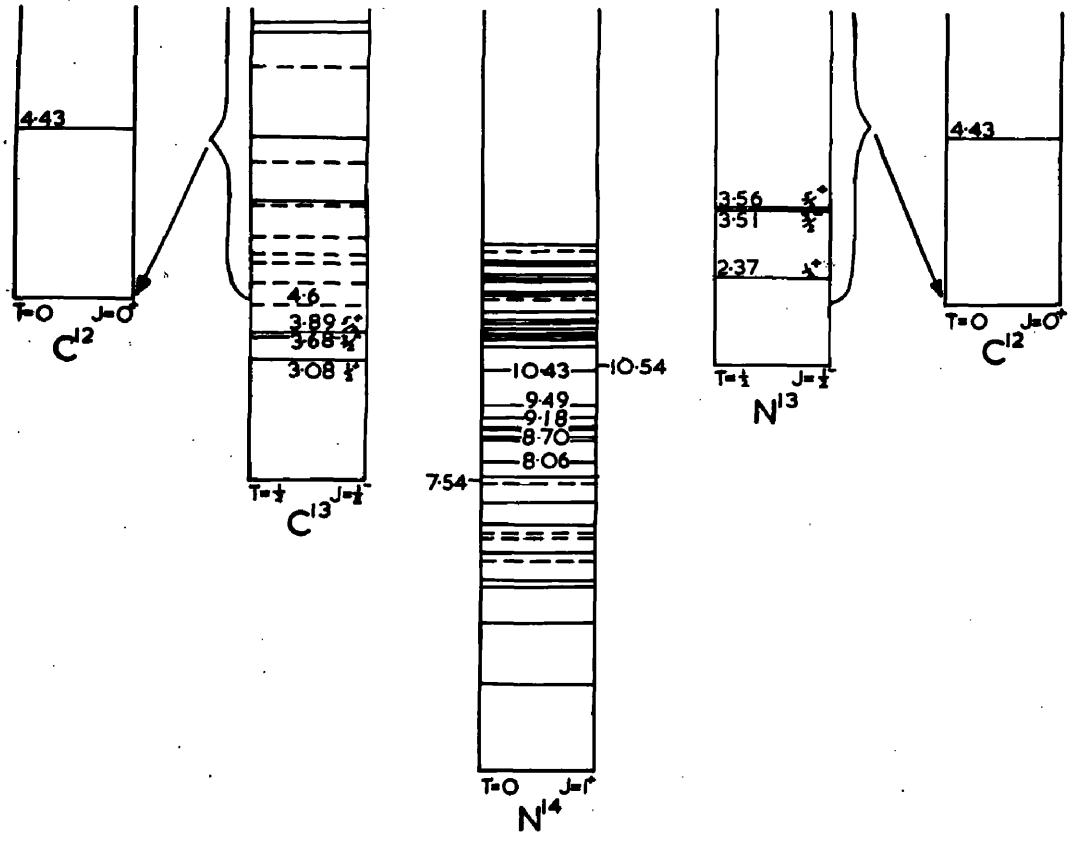

measured reactions in N^{14} have a pronounced increase at about 20 MeV which is taken to be the onset of the giant resonance. This confirms the view that the giant resonance is an increase in the nuclear photon absorption cross section and is not a resonance associated with only the (γ,n) reaction.

As was shown in Fig.III.1, the (γ,n) cross section in N^{14} is small compared with the (γ,n) cross sections in C^{12} and O^{16}. This result and the relative magnitudes of the (γ,n), (γ,p) and (γ,pn) cross sections may be explained by a detailed consideration of the energy level diagram, Fig.III.9.

The photo-emission of a neutron from N^{14} can leave the N^{13} nucleus in its ground state or in an excited state. If the N^{13} nucleus is formed in its ground state no further reaction can take place and the event will be a (γ,n) reaction. However, if the N^{13} nucleus is formed in any excited state, it can emit a proton to give the final reaction $N^{14}(\gamma,np)C^{12}$, and this is much more probable than the decay of the excited state by gamma emission to give an $(\gamma,n\gamma')$ event which would be recorded as a (γ,n) reaction. Similarly, following photoproton emission, if the C^{13} nucleus is left in its ground state or in any of the three excited states of energy less than 5 MeV, a (γ,p) reaction will be recorded, while if an excited state of higher energy is formed with an

energy/

energy greater than 5 MeV, neutron emission to give a $N^{14}(\gamma,pn)C^{12}$ reaction is much more probable than decay by gamma emission to give an $(\gamma,p\gamma')$ event which would be observed as a (γ,p) event. Thus, neglecting the decay of the excited states by gamma emission, the (γ,n) reaction can only occur if the residual nucleus is formed in its ground state while the (γ,p) reaction will occur if the residual nucleus is formed in the ground or first three excited states.

Assuming that, apart from small corrections due to coulomb forces and the neutron-proton mass difference, nuclear forces are charge independant (Burcham 1955) then the probability for the emission of a neutron which leaves N^{13} in a particular state differs only slightly from the probability for the emission of a proton which leaves C^{13} in the corresponding state. Hence the (γ,p) cross section is expected to be larger than the (γ,n) cross section by approximately the cross section for the formation of the first three excited states of C^{13}. Also the (γ,n) cross section is approximately the same as the cross section for the formation of the ground state of N^{13}.

As the (γ,p) cross section is almost twice the (γ,n) cross section, the probability that the emission of a proton (or neutron) will leave C^{13} (or N^{13}) in its ground state is equal to the total probability that the nucleus will be left in any one of the first three excited states.

As/

As the number of excited states of C^{13} and N^{13} which can be formed will increase as the photon energy increases, it may be expected that the (γ,pn) cross section will be initially small but will then increase more rapidly than the (γ,p) or (γ,n) cross sections and this is what has been found.

In C^{12} and O^{16} the thresholds for the (γ,pn) reactions are high (27 and 23 MeV respectively) so that following photoneutron emission, if the residual nucleus is formed in an excited state, it can only decay by gamma emission to give an event which would be recorded as a (γ,n) reaction. Thus the (γ,n) cross sections in C^{12} and O^{16} are expected to be larger than the (γ,n) cross section in N^{14}.

Thus it may be concluded that anomalous photodisintegration results may be understood by a detailed consideration of the energy levels involved and their relation to reaction thresholds.

The basic assumption of the above arguments is that the reactions proceed through levels in C^{13} and N^{13}, i.e. compound nuclei are formed. Thus the experimental results have been explained by use of a Compound Nucleus theory.

References.

Ajzenberg, F., and Lauritsen, T., 1955, Rev. Mod. Phys. 27, 77.

Bethe, H.A., 1950, Rev. Mod. Phys., 21, 213.

Blatt,/

Blatt, J.M., and Weisskopf, V.F., 1952, "Theoretical Nuclear Physics" (New York, John Wiley and Sons).

Boggild, J.K., 1945, Danske, Vidensk, Selskab, 23, No.4.

Burcham, W.E., 1955, Progr. Nucl, Phys. 4, 171.

Ferguson, G.A., et. al., 1954, Phys. Rev. 95, 776.

Horsley, R.J., et. al., 1952, Canad., J. Phys., 30, 159.

Katz, L., and Cameron, A.G.W., 1951, Canad. J. Phys., 29, 518.

Levinger, J.S., and Bethe, H.A., 1950, Phys. Rev., 78, 115.

Seagrave, J'D., 1952, Phys. Rev., 85, 197.

Spicer, B.M., 1953, Aust. J. Phys., 6, 391.

Willard, H.B., et. al., 1955, Bull. Amer. Phys. Soc., 30, No.1, p.45, (also private communication from Dr. H.B. Willard)

Woodbury, H.H., et. al., 1953, Phys. Rev., 92, 1199.

CHAPTER IV.

THE PHOTODISINTEGRATION OF NEON

Introduction

In this chapter the photodisintegration of neon using a cloud chamber is described. The importance of this experiment is first discussed. Improvements and modifications of the experimental method and apparatus are described and the method of analysis is given. The experimental results for the different reactions are then described in turn. The (γ,p) reaction was studied by measurement of the recoil range. Results for the (γ,α) and $(\gamma,star)$ reactions are given and the energy of possible compound nucleus states are calculated. Finally, the results are discussed firstly in groups according to the energy of the photon producing the event, and secondly with reference to the operation of isotopic spin selection rules.

IV. 1. The Photodisintegration of Neon

The photodisintegration of neon was next studied as it was of considerable theoretical interest and as the cloud chamber technique which had been developed was considered to be particularly suitable for such an investigation.

On/

On the assumption of the charge independance of nuclear forces, a number of Isotopic Selection Rules have been proposed (e.g. Radicati, 1952). If these rules were strictly applicable and if the reaction proceeds through Compound Nucleus states, then the (γ,star) events which would be formed in the photodisintegration of neon, were expected to have an unusual character and in particular an appreciable number of (γ,αp) stars having a low energy proton might occur. If the ranges of the tracks in these stars were measured it should be possible to decide whether the 12.51 MeV or the 12.95 MeV level in O^{16} had an isotopic spin of one. (These points are discussed more fully in Section IV.5). Such low energy (γ,star) events could be studied relatively easily by the cloud chamber method as the origin of the event and the range of all particles could be found. This is not easily possible using any other method e.g. neon being an inert gas, cannot be included in photographic emulsions.

The (γ,p) cross section in lightelements is expected to be large and of the same order as the (γ,n) cross section, but few measurements of (γ,p) reactions have been made. It was intended to measure the (γ,p) cross section and as the (γ,n) cross section has been measured by Ferguson et.al. (1954) the ratio of the two cross sections could be found.

As/

As the Ne^{20} nucleus can be split into an integral number of alpha particles, its photodisintegration is of interest in connection with the alpha-particle theory of nuclear structure. Also the yield of alpha particles from neon may be exceptionally large.

IV.2. Method and Apparatus.

The basic method and apparatus were the same as those described for the nitrogen experiment in Chapter III, that is, the X-ray beam from a synchrotron of 23.5 MeV peak energy was collimated and passed through a Wilson Cloud Chamber as shown in Fig. IV.1. The chamber was shielded

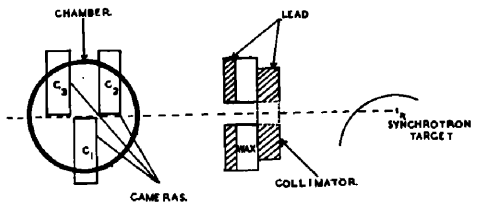

Fig. IV.1.

from neutrons by paraffin blocks four inches thick. The measurement of the synchrotron output was improved by recording it on a 100-channel kick-sorter, as well as noting it on an oscilloscope as before. The total X-ray dose was 0.1 Röntgen.

The stopping power of the gas was chosen to be

0.7/

0.7 which was sufficiently high to stop nearly all 4 MeV alphas or 1½ MeV protons but still gave long recoils which could be easily measured. The gas pressure was 1.25 atmospheres with the chamber expanded and this allowed easy operation of the chamber. Water was used as the condensable vapour.

With the success of the measurements of recoil tracks in the nitrogen experiment, it was decided to redesign the camera system to assist these measurements. Previously only the film from the top camera could be used for recoil measurements as the lenses and the films in the side cameras were not horizontal (they were inclined to make the focal plane horizontal) and complete calculations with this camera arrangement were impractically tedious. The three cameras were altered so that the film and the lenses were horizontal and this allowed calculation of the lengths and angles of the tracks.

To simplify the calculations, two 3 - 4 - 5 triangles were used, no camera being directly above the chamber, as shown in Fig. IV.1. Lens distortion, which becomes appreciable at large distances from the axis of the lens, was avoided by using the two cameras nearest the event.

In the previous experiment, the chamber had to be refilled at intervals with nitrogen due to leakage through the/

the thin neoprene diaphragm. This was not serious for nitrogen, but with its higher cost, was important for neon, hence the leakage was greatly reduced by using a thick diaphragm of butyl rubber. The compositions of the chamber gas, before and after the photographs were taken, were analysed by Dr. Reed of the Glasgow University Chemistry Department. The air contamination at the end of the run was less than 2% and therefore negligible. The presence of nitrogen could also be estimated by the appearance of (γ,pn) flags, since these are energetically impossible in neon but large numbers of them are found from nitrogen; only two (γ,pn) flags were found, confirming that the nitrogen content was unimportant. The stopping power of the gas was calculated from its composition and the expanded pressure. This value was confirmed by measurement of the ranges of alpha particles from the polonium source on the chamber wall.

To ensure that once good track quality had been achieved, it could be maintained for long periods, the operation of the chamber was made fully automatic.

The basic component of the electronic unit was a uniselector mechanism which consisted of a switch of eight banks each containing 25 contacts and these were 'selected' by a wiper arm which was moved round from one contact to the next by energising the coil of a control solenoid. The wiper arm/

arm had a contact for each of the eight banks. The coil was placed in the cathode circuit of a thyratron whose conduction was controlled by a variable R-C network in the anode circuit. The first bank of contacts was used to select the appropriate register which together with the 30μF condenser, provided the required delay before moving to the next position. The other banks of contacts were used to perform the following operations:

(a) open the camera shutters

(b) initiate the fast expansion of the chamber

(c) send a signal to the synchrotron controls which produced a pulse of X-rays after the appropriate delay

(d) flash the lamps

(e) close the camera shutters

(f) operate the reset solenoid

(g) perform the required number of clearing expansions.

(h) provide a delay of 35 secs. to allow the gas in the chamber to achieve equilibrium conditions

(i) operate a warning buzzer which indicated that the chamber was ready for the next fast expansion.

The slow expansions were performed by means of a magnetic valve which connected the chamber alternately to a compressed nitrogen reservoir and to the atmosphere, the timing used being 5 seconds to expand and 8 seconds to contract. The whole cycle of operations took 2 minutes.

IV.3./

IV.3. Analysis.

The films were first scanned with a low powered microscope and the events were classified as singles, collinear flags, non-collinear flags, unclassified flags and stars, using the definitions given in Section III.3. The thresholds of the reactions and the expected classifications of the events are given in Table IV.1.

As the (γ,pn) threshold was almost the same as the peak energy of the synchrotron, no non-collinear flags of measureable length could have been produced by this reaction. The two non-collinear flags with lightly ionising fragments that were found were assumed to have been $Ne^{20}(\gamma,p)$ events in which the recoil was scattered very close to the origin or were (γ,pn) reactions in nitrogen which may have leaked into the chamber. Unclassified flags with lightly ionising fragments were accordingly assumed to be all collinear flags.

The initial method of analysing the events was to clamp the negatives of each of the three films to the table of a microscope and then measure:

(a) the co-ordinates of each significant point (e.g. the origin of the event)

(b) the angle of the track relative to the central grid wire which was placed in the direction of the X-ray beam

(c) the length of the track image.

The/

Table IV.1.

Photonuclear Reactions in Neon^{20}.

			Threshold MeV.
$Ne^{20} + \gamma \longrightarrow$	$n + Ne^{19}$	Single	16.91
	$p + F^{19}$	Collinear	12.87
	$d + F^{18}$	Collinear	21.05
	$\alpha + O^{16}$	Collinear	4.746
	$p + n + F^{18}$	Non-collinear	23.28
	$\alpha + n + O^{15}$	Non-collinear	20.34
	$\alpha + \alpha + C^{12}$	3-prong stars.	11.895
	$\alpha + p + N^{15}$	3-prong stars.	16.856
	$p + p + O^{18}$	3-prong stars.	20.82
	5α	5-prong star.	19.07

Flags

The co-ordinates of the point in the chamber and the angle of the track to the direction of the X-ray beam were then calculated from the geometry of the camera system.

This measuring technique was found to be accurate, but slow, as in the complete analysis of a star some 200 steps were involved in the calculation. Miss M.B. McClements developed a device, shown in Fig. IV.2, which performed some of these calculations mechanically. It consisted of a straight steel needle, 6" long, mounted in a brass ball which could move/

move in a cup in a brass plate. To this plate were attached two protractors, one in a horizontal plane and one in a vertical plane, both being concentric with the ball, and the

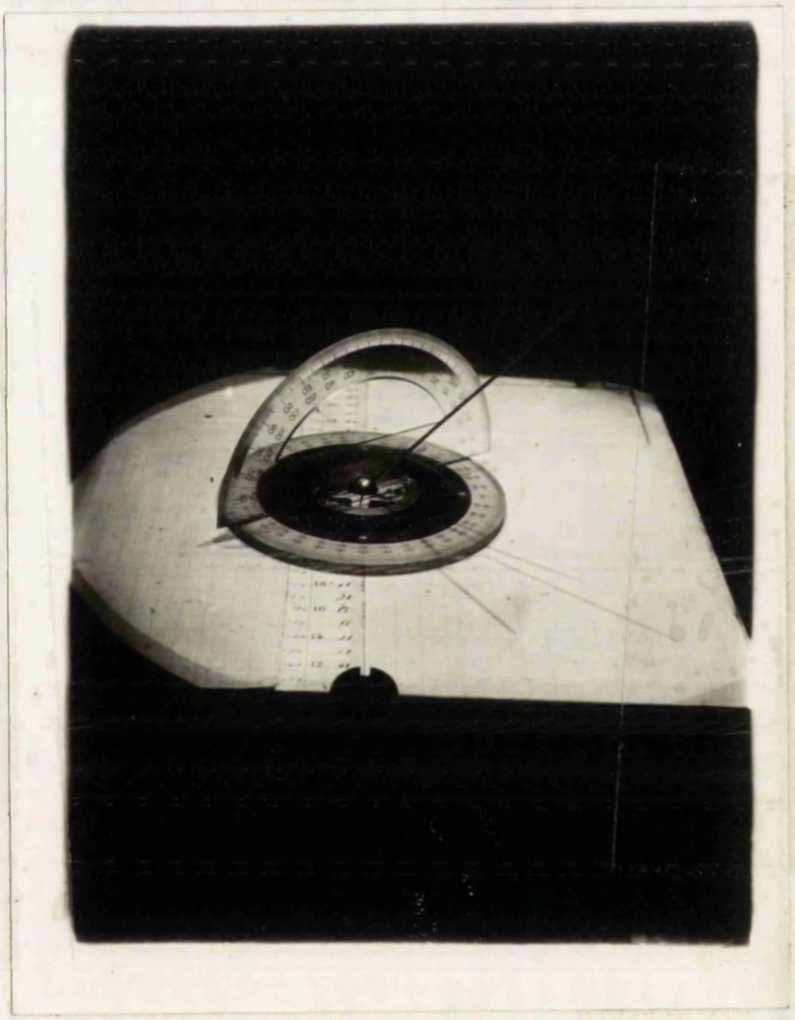

Fig.IV.2.

latter being able to rotate about the vertical axis through the ball. The three images of a track were measured using the microscopes as above and the position of the origin of the event in the chamber was calculated. Using the reprojection table, the centre of the brass ball was placed in the same position relative to the cameras as the origin of the event./

event. Lights were shone through the camera lenses to produce shadows of the needle on the table. For each track the needle was then adjusted until the shadows had the same set of three angles on the horizontal plane as those measured on the films. The needle was then lying in the same direction as the track and hence its angles with the horizontal and vertical planes could be measured. Then from the length of the shadow of the needle and from the length of the track image in the film, the true length of the track could be calculated. This was done for all three films and the mean of the lengths was adopted.

For straight tracks the accuracy of the method was found to be:-

1^{o} in the angle in a horizontal plane

2^{o} in the angle with the vertical

0.05cm. in length measurements.

As very few events were observed out of the beam, it was concluded that the background was negligible.

IV.4. Results.

The neon gas used in the experiment was that commercially available and which consisted of 90% Ne^{20}, ¼% of Ne^{21} and 9¾% of Ne^{22}. In the analysis of the results it was assumed that the neon was all of mass number 20, it being impossible to distinguish between the isotopes.

The/

The threshold of the $Ne^{22}(\gamma,p)F^{21}$ reaction was calculated to be about 17 to 18 MeV, for although F^{21} is not known, it is probably stable and its mass can be estimated.

Comparing the thresholds of the principal photo-disintegration reactions in Ne^{22} with those in Ne^{20}, it is found that the (γ,n) threshold of 10.36 MeV is much lower (by $6\frac{1}{2}$ MeV); the (γ,α) threshold of 9.66 MeV is higher by 5 MeV; the (γ,p) threshold is 4 to 5 MeV higher; the $(\gamma,\alpha\alpha)$ threshold of 15.90 MeV is 4 MeV higher and the $(\gamma,\alpha p)$ threshold is much higher at 27.4 MeV. Thus the yield of photo-neutrons from Ne^{22} may be higher than from Ne^{20}, while the yield of charged particles may be expected to be rather less. As the percentage of Ne^{22} is only 10%, then the assumption in the analysis that the gas consists entirely of Ne^{20}, will probably not lead to serious error.

The results have been divided into three sections according to the classification of the reaction, the sections being, (γ,p), (γ,α), and $(\gamma,$ star).

(a) <u>(γ,p) Events</u>.

The most apparent difference between the (γ,p) reactions in nitrogen and neon, was that in neon the fragment was observed to stop in the chamber in only three events. Thus, it was not possible to obtain a detailed energy distribution from the fragment ranges, but an approximate energy distribution was found from the recoil ranges.

As/

As the energies of the (γ,p) events were generally high and as the stopping power of the gas was low (0.7), the recoils were longer than in the nitrogen experiment and were easily measured. The very few singles and unclassified flags which occurred were assumed to be (γ,p) events as the fragments were lightly ionising.

As only three events were observed to stop in the chamber, then, taking into account the fraction of tracks of a given length which would be observed to stop, it must be concluded that there are very few protons of energy less than 1.6 MeV and few protons of energies between 1.6 and 2.0 MeV. Thus the (γ,p) cross section from the threshold of 12.87 MeV to 14.5 MeV is very small (about 0.1mb.) and is low in the energy region from 14.5 to 14.9 MeV.

In the inverse reaction, $F^{19}(p,\gamma)Ne^{20}$, it has been found (Sinclair, 1954) that there are no gamma ray transitions direct to the ground state of Ne^{20} for excited states in neon from 12.87 MeV to 14.23 MeV. From detailed balancing, this is in agreement with the result obtained for the $Ne^{20}(\gamma,p)F^{19}$ reaction.

From the measurement of the recoil range the energy of the recoil was found using the range-energy for F^{19} given in the Appendix. The energy of the photon producing the reaction was then calculated assuming that the F^{19} nucleus was formed in its ground state. From the resulting/

resulting energy distribution and the bremsstrahlung spectrum*, the (γ,p) cross section was obtained and is shown in Fig. IV.3.

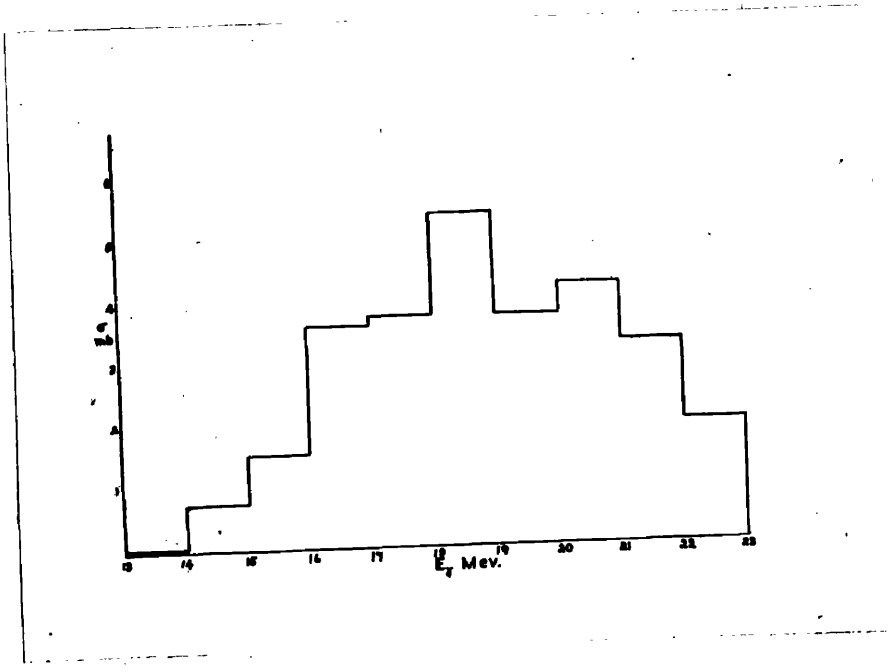

Fig.IV.3.

It was not possible to distinguish events in which F^{19} was formed in an excited state which decayed by gamma-emission, hence in Fig. IV.3 $(\gamma,p\gamma')$ events will have been considered as (γ,p) events. In this connection it has been found by Arthur et. al.(1952) that in the $F^{19}(p,p)F^{19}$ reaction with 8 MeV protons, the residual F^{19} nucleus could be formed in any one of 11 excited states with energies between 0 and 4.5 MeV. If in the $Ne^{20}(\gamma,p)F^{19}$ reaction, the same states of Ne^{20} are formed, then, on compound nucleus theory, excited states of F^{19} will occur. Accordingly, in analysing the (γ,p)/

* Assumed to be the same as that given by Katz and Cameron (1951)

(γ,p) events, it was assumed that in the proton emitting reactions produced by quantum of 19 to 23 MeV, $\frac{1}{3}$ of the reactions formed F^{19} in its ground state, $\frac{1}{3}$ formed levels of 0 to 2 MeV excitation and $\frac{1}{3}$ formed levels of 2 to 4.5 MeV excitation. The resulting cross section for the (γ,p) reaction which is given in Fig.IV.4, is similar to the (γ,n) cross section, shown dotted, obtained by Ferguson et.al (1954) and the integrated cross sections to 23.5 MeV are both approximately 0.04 MeV barns.

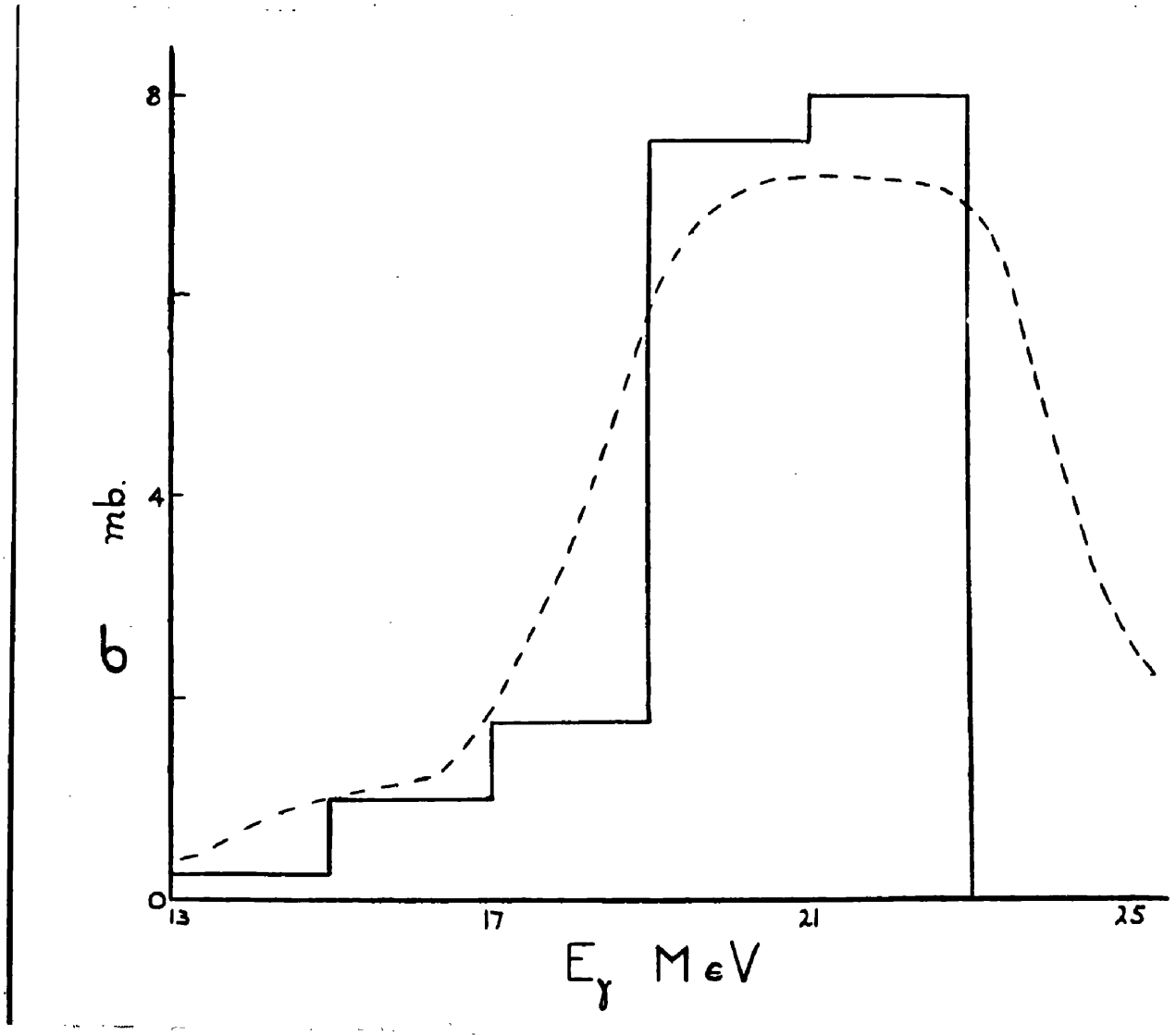

Fig. IV.4.

The/

The (γ,p) cross section shown in Fig.lV.4 is not exact and may require to be modified due to transitions to levels in F^{19} with energies greater than 4.5 MeV but as F^{19} is unstable to alpha particle emission above 4 MeV, these levels have a higher probability of decay by alpha emission giving $(\gamma,p\alpha)$ events, than by gamma emission.

The observed distribution of the angle, γ, between the proton and X-ray beam directions, is shown in Fig.lV.5.

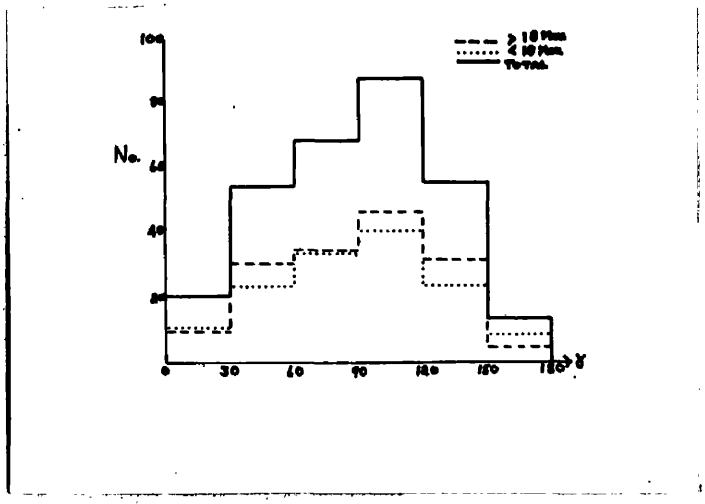

Fig. lV.5.

On the Compound Nucleus theory an isotropic distribution is expected and this would be observed as a $\sin\gamma$ distribution on Fig. lV.5 on allowing for the differing solid angles. With the Independent Particle Model, proposed by Wilkinson (1954), the experimental angular distribution would be of the form $\sin\gamma\,(1+\frac{3}{2}\sin^2\gamma)$ on L-S coupling or $\sin\gamma\,(1+\sin^2\gamma)$ on j-j coupling. Fig. lV.5 was compared with the relation

Sin/

$\sin\gamma(1 + \ell \sin^2\gamma)$ where a value for ℓ of $\frac{1}{8}$ was found. This favours the Compound Nucleus theory but the result is not statistically significant at the 5% level.

(γ,d) reactions cannot be distinguished from (γ,p) events. However, the $Ne^{20}(\gamma,d)$ threshold is so high (21.05 MeV) that the deuteron track would have had a high probability of stopping in the visible portion of the chamber. As such events WITH A LONG RECOIL were not found it must be concluded that the (γ,d) cross section is small below 23 MeV.

(b) <u>(γ,α) Events</u>

(γ,α) events were identified as collinear flags in which the recoil was exceptionally long and in which the fragment was heavily ionising so that the ionisation change at the origin is small. A (γ,α) event is shown in Plate IV.1. Nineteen events were thus identified. In addition in eleven other events, the track was heavily ionising and had the appearance of an alpha particle but the origin of the event could not be distinguished, possibly due to the small change in ionisation at the origin of (γ,α) events.

Assuming that the O^{16} nucleus was formed in its ground state, the energy of the quantum producing the event was calculated from the measured recoil range or in case of the six events in which the fragment stopped in the chamber, from the fragment range. The resulting energy distribution/

distribution is shown in Fig. IV.6.

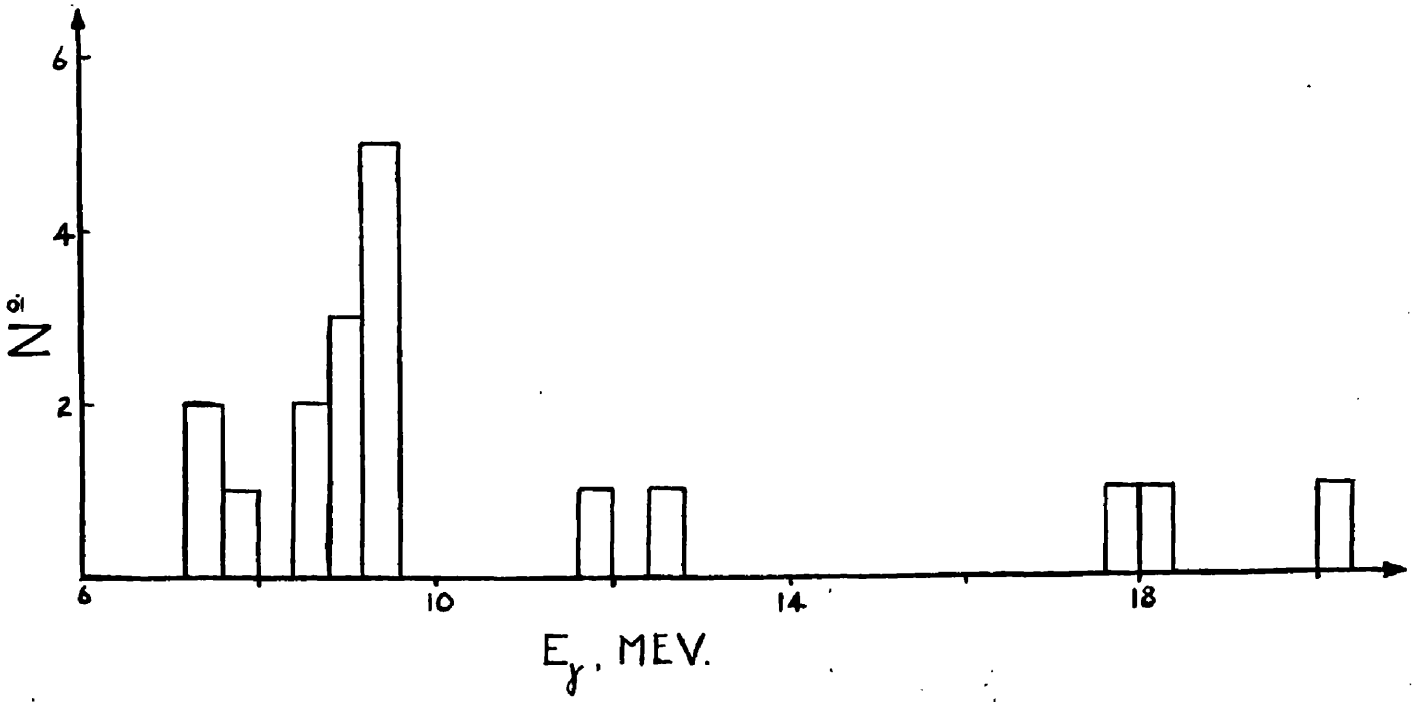

Fig. IV.6.

It has been found by Erdman (1953) that on bombarding neon with 17.6 MeV gamma rays from the $Li^7(p,\gamma)$ reaction that $Ne^{20}(\gamma,\alpha)O^{16}$ reactions which formed O^{16} in excited states of 6 to 7 MeV energy were several times more probable than ground state transitions. Hence the values of E_γ in Fig. IV.6 may require to be increased by 6 to 7 MeV except for the three events of energy greater than 18 MeV which must be ground state transitions. The form of Fig. IV.6 is discussed in Section IV.5.

(c) <u>(γ,Star) Events</u>

A total of 60 three-prong stars were observed. From the "appearance" of the star, (i.e. ionisation of the fragments relative/

relative to one another, multiple scattering and angles between the tracks) it was possible to classify the events as $(\gamma,\alpha p)$ or $(\gamma,\alpha\alpha)$ reactions. On Plates IV.2, IV.3 and IV.4 $(\gamma,\alpha\alpha)$ events are shown while on Plate IV.5 there is a $(\gamma,\alpha p)$ event in which the proton was of low energy.

This method of classifying the $(\gamma,$star$)$ events was checked for those events in which all three tracks stopped in the chamber. The event was classified by its "appearance" and from the measured ranges and angles the momentum unbalance was calculated, the momentum unbalance being defined as the vector sum of the momenta of the three particles and of the initial quantum. This momentum unbalance was always found to be less than 50 MeV/C. The next most probable assignment was given to be event and the momentum unbalance was calculated when it was found to be always greater than 80 MeV/C. This result is shown in Fig. IV.7 where the second assignments are shown shaded and where, for comparison purposes, the distribution of the momentum unbalances obtained by Goward and Wilkins (1953) with the $C^{12}(\gamma,3\alpha)$ reaction using photographic emulsions is shown dotted.

No (γ,pp) events were found.

Of the 20 events which were identified as $(\gamma,\alpha\alpha)$ stars, complete measurements could be made on 11 events in which all three tracks stopped in the chamber. The C^{12} range-energy relation/

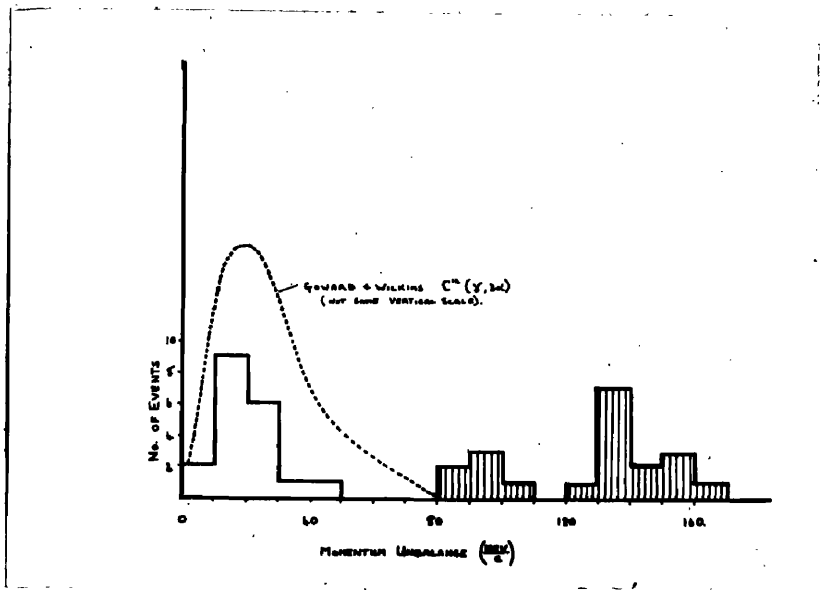

Fig. IV.7.

relation was checked by comparing the observed recoil range with the energy obtained by calculation from the ranges of the two fragments. Good agreement with the experimental points and the proposed relation was obtained as shown in Fig. IV.8 except that the ranges were slightly too long — this may be due to the stopping power of neon for C^{12} ions being different than that of air. Measurements were made on a further six $(\gamma,\alpha\alpha)$ stars in which only one fragment stopped, the energy of the remaining fragment being found from the angles and the ranges of the other two tracks. In the remaining three $(\gamma,\alpha\alpha)$ stars no fragment stopped or one or more of the tracks was too steep to be measured sufficiently accurately.

On the basis of the Compound Nucleus theory, it was assumed that in $(\gamma,\alpha\alpha)$ reactions, one alpha was emitted first forming/

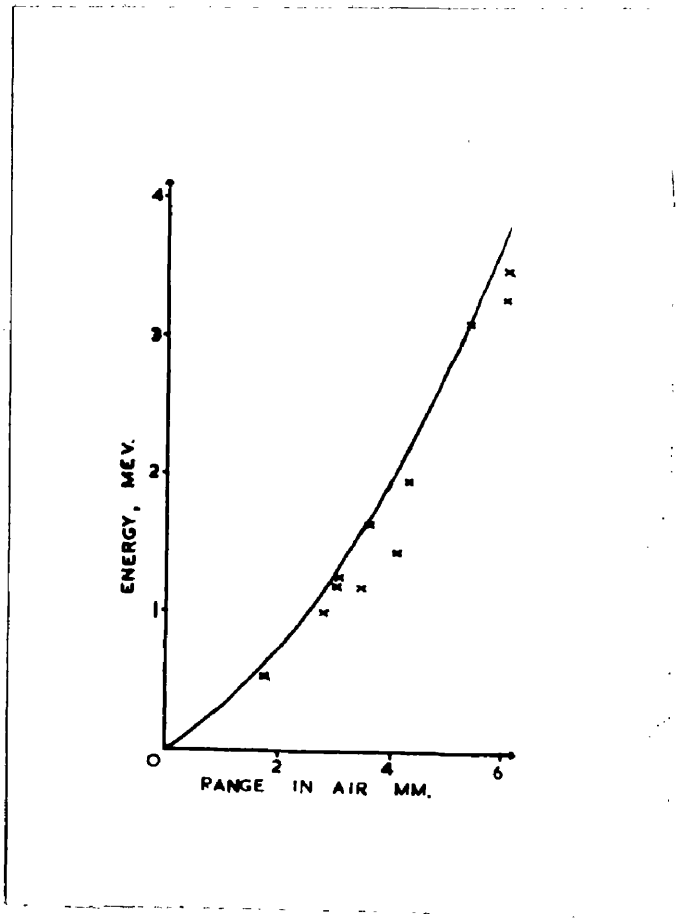

Fig. IV.8.

forming O^{16} in an excited state which then decayed by emitting a second alpha particle. As there was no means of deciding which alpha particle was emitted first, two values of the excitation energy of O^{16} were calculated for each event, it being assumed that C^{12} nucleus was formed in its ground state. In Fig. IV.9 where the values for the excitation energies of O^{16} are shown, the arrows indicate the position of the energy levels of O^{16} from which alpha emission had been observed (Ajzenberg and Lauritsen, 1955). Due to the impossibility of deciding which energy value is the correct one, it cannot be stated that agreement with the observed energy levels has been/

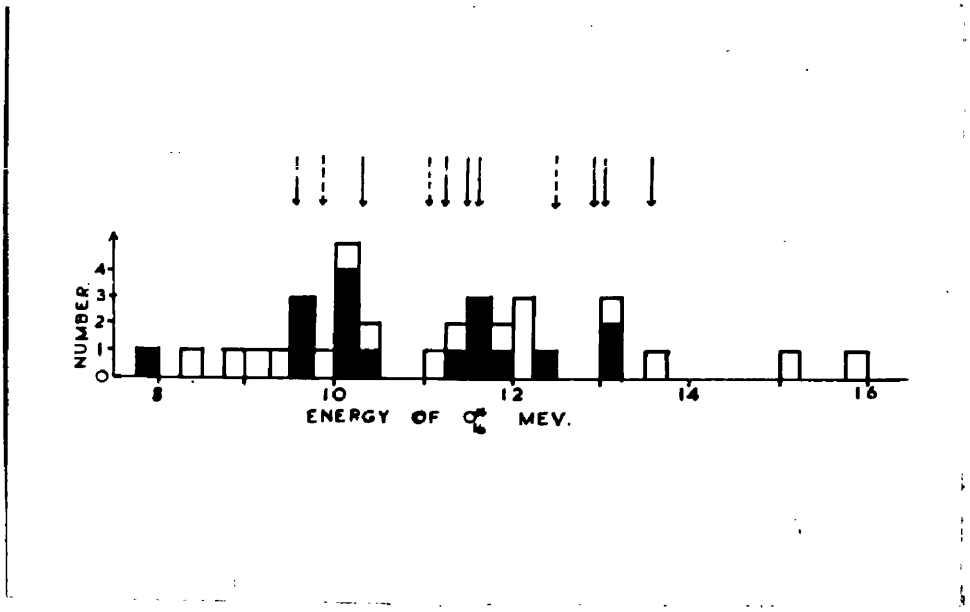

Fig. IV.9.

been positively obtained, but it was found that by selection of one of the two energy values for each event, it was possible to construct an energy distribution which was not inconsistent with the observed energy levels. The selected values of the excitation energies are shown shaded in Fig. IV.9.

For excited states of O^{16} of energy greater than 11.7 MeV it is possible for the C^{12} nucleus to be formed in its first excited state of 4.43 MeV but it has been reported by Nabholz, Stoll and Wäffler (1952) that in the $O^{16}(\gamma,\alpha)C^{12}$ reaction produced by 17.6 MeV gamma rays, less than 10% of transitions led to the 4.43 MeV state of C^{12}.

Forty $(\gamma,\alpha p)$ events were identified. In nine cases all three tracks stopped in the chamber and measurements were

also/

also made on seven events in which one fragment left the chamber. In the remaining 24 events the recoils which were much shorter than those from (γ,αp) events, could not be measured with sufficient accuracy*.

For each (γ,αp) event, the energy of the excited state of O^{16} was calculated on the assumption that the alpha particle was emitted first and also the energy of the excited state of F^{19} was calculated on the assumption that the proton was emitted first, there being no way of distinguishing between the two cases. The resulting energy distributions are shown in Fig. IV.10; the known levels in O^{16} are indicated by arrows. N^{15} was formed in the ground state in every case as the first level at 5.28 MeV, was not accessible.

The energy distribution of the quanta producing the stars is shown in Fig. IV.11 where the (γ,$\alpha\alpha$) events are shaded. It was assumed that C^{12} was formed in the ground state. It was noted in Fig. IV.11 that all the events occur in the giant resonance region except for three (γ,$\alpha\alpha$) events at E = 16 MeV.

Discussion./

---

* It may be noted that for the analysis of (γ,star) events in which one fragment left the chamber, an accurate energy value had to be obtained from one recoil range measurement and for this a fairly long straight track was required while for (γ,p) analysis the errors due to range straggling and measurement were not important for any one event as the results were based on a statistical interpretation of a large number of events.

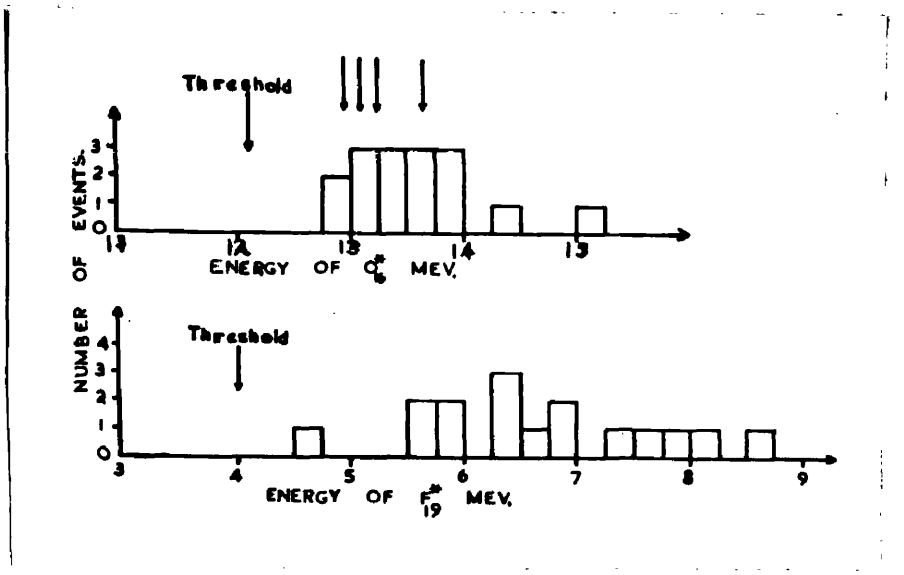

Fig. IV.10.

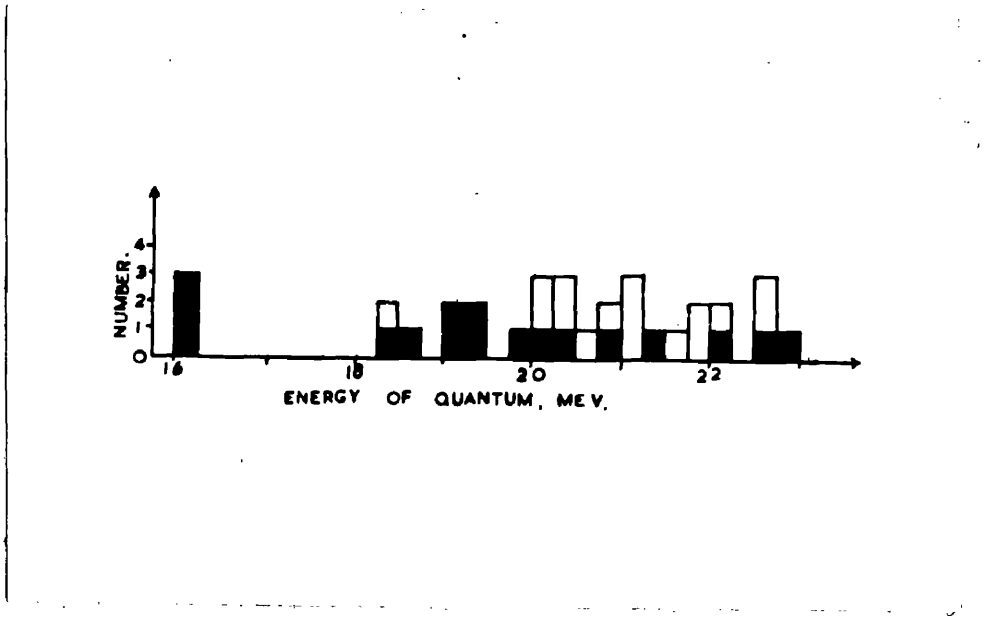

Fig. IV.11.

IV.5. Discussion

It will be shown that the results obtained above for the photodisintegration of neon are consistent with the picture of/

of photodisintegration processes which was developed in Chapter III.

A compound nucleus theory is used; the cross section for any reaction is assumed to be the product of two factors, the cross section for absorption of the incident photon and the probability of emission of the required particle, this probability being affected by the spins, angular momenta, parities and isotopic spins involved and by the character of the competing reactions. Some of the conclusions are summarised in Fig. IV.12.

(a) Photon Absorption

It is convenient to divide the photon absorption cross section up to 23 MeV into two parts. Firstly, there is the 'giant resonance' which is found in all nuclei and which occurs at about 20 MeV in neon. The large values of the photon absorption cross section near this energy result in correspondingly large yields of all reaction products. Thus in Ne^{20} the (γ,n), (γ,p) and $(\gamma,star)$ cross sections exhibit a rise near 20 MeV. Secondly, at quantum energies lower than those of the giant resonance, it is postulated on the basis of the study of the photodisintegration of nitrogen that photon absorption is by individual levels and that reaction cross sections are controlled by the nature of the levels involved. Recently there has been some evidence that the giant/

giant resonance is not continuous in nature, but is also composed of discrete levels.

Thus while photodisintegration cross sections show a general trend throughout the Periodic Table, the actual cross section of any reaction can only be found by a detailed consideration of reaction thresholds and of the character and number of the available energy levels. Anomalous results may sometimes be explained by such detailed work. For elements with a high Z, energy levels are numerous and statistical methods may be employed, but for elements with a low Z, the energy levels are widely spaced and such detailed consideration is necessary.

(b) E_γ below the (γ,p) Threshold

From the Sum Rules it has been shown that photon absorption is mainly by electric dipole transitions. The ground state of Ne^{20} has an isotopic spin $T = 0$ and as the isotopic spin selection rules forbid electric dipole transitions to higher energy states with $T = 0$, the photon absorption cross section is expected to be small below the energy of the first $T = 1$ state which is close to the (γ,p) threshold, that is, the photon absorption cross section is expected to be small at quantum energies below the (γ,p) threshold of 12.87 MeV.

There are only two competing reactions (γ,α) and (γ,γ) below the (γ,p) threshold and as the probability of particle/

particle emission is much greater than that of gamma emission, the total photon absorption cross section will be only slightly greater than the (γ,α) cross section which has been found in this experiment to be small. Thus the total photon absorption cross section below 12.87 MeV is small ($\sim 10^{-28}$ cm.^{2}).

(c) 12.87 MeV < E_γ < 15 MeV.

In this energy region, excited neon nuclei can decay by the emission of quanta, alpha particles or low energy protons. An upper limit of three proton tracks from (γ,p) events were observed to stop in the visible region of the chamber and it is possible that some or all of them could have been produced in reactions in which quanta of higher energy left the F^{19} nucleus in an excited state. This result is in striking contrast to the $N^{14}(\gamma,p)C^{13}$ reaction in which large numbers of protons of 0.5 to 2.0 MeV were observed to stop. Thus the (γ,p) cross section below 15 MeV is very small and this is in agreement with the inverse reaction, $F^{19}(p,\gamma)Ne^{20}$ in which no gamma rays giving ground state transitions have been observed. (Ajzenberg and Lauritsen, 1955).

Very few if any (γ,α) events could be identified as due to X-rays in this energy interval. It was concluded that the total photon absorption cross section is small up to 15 MeV.

(d) E_γ above 15 MeV

Above/

Above X-ray energies of 15 MeV, the yields of proton - and alpha - emitting reactions in neon were found to be very large corresponding to the giant resonance of the photon absorption cross section. The relative numbers of events in which protons, neutrons and alpha particles were the first particle to be emitted from neon are given in Table 1V.2, where it was assumed that in half the $(\gamma,\alpha p)$ stars the proton was the primary fragment.

Table 1V.2.

Primary Particle	Reaction	Number of Events	Total
Proton	(γ,p)	300	320
	$(\gamma,p\alpha)$	20	
Neutron	(γ,n) ✱	-	300
Alpha	(γ,α) ⊖	5	
	$(\gamma,\alpha p)$	20	55
	$(\gamma,\alpha\alpha)$	30	

✱ Calculated from Ferguson et. al. (1954).

⊖ Estimated number of (γ,p) events in which E_γ was above the (γ,p) threshold.

It was noted that the numbers of protons and neutrons emitted were almost identical. It is believed that basically proton and neutrons have equal probabilities of emissions, but that Coulomb barrier considerations, the availability/

availability of energy levels, etc. affect the actual yields, but for Ne^{20} such factors are not important and hence equal yields of protons and neutrons are expected up to quantum energies of 23 MeV, at which energy the (γ,pn) reaction will start to contribute and so will not permit a definite separation of primary proton-emitting and primary neutron-emitting reactions.

An important feature of the results is the relatively large number of events in which an alpha particle is the first fragment to be emitted. Table IV.2 shows that the yield of primary alpha particles was about a sixth of the yield of protons or of neutrons. This probability of emission is relatively high considering the effects of the Coulomb barrier and of the isotopic spin selection rules. The explanation may lie in the fact that it is possible to consider the Ne^{20} nucleus as being composed of an integral number of alpha particles.

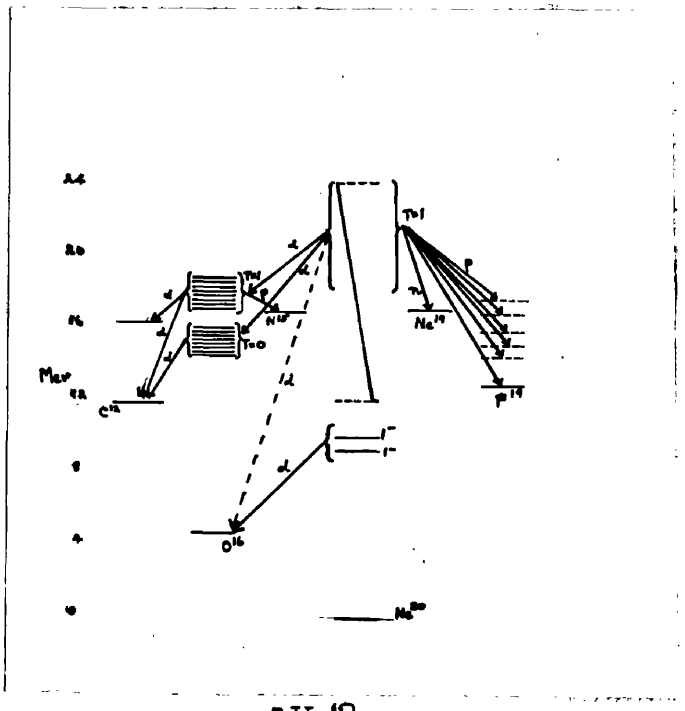

Fig.IV.12.

(e) Isotopic Spin

One of the major aims of this experiment was to test the applicability of the isotopic spin selection rules for if these rules are absolute, then the character of the (γ,star) yield is as expected to have an unusual but definite form which could easily be determined by an experiment using a cloud chamber.

Considering only the giant resonance region, then as the greater part of the photon absorption is by electric dipole transitions, the excited states of neon resulting will have isotopic spins of T = 1. The emission of alpha particles from T = 1 states is "inhibited" by the conservation of isotopic spin unless the resultant state of O^{16} has an isotopic spin of one. The first T = 1 level in O^{16} is known to be at about 12 to 13 MeV and to have a spin of 2^-. There are two levels, at 12.51 and 12.95 MeV which have a spin of 2^- and so could be the first T = 1 level in O^{16}. In O^{16} the thresholds for proton and alpha emission are 7.15 and 12.11 MeV respectively. Thus if the excited state of oxygen has an energy between 7.15 and 12.11 MeV, alpha particle emission, giving a (γ,$\alpha\alpha$) event, is the most likely mode of decay, but as the isotopic spin of the states is T = 0, the selection rules will inhibit their formation and hence the yield of (γ,$\alpha\alpha$) events was expected to be small. However, the cross section for the formation of T = 1 states with energies above/

above 12.5 to 13 MeV will be much larger as they will suffer no inhibition. When these T = 1 states of O^{16} have been formed, their decay by alpha-emission to give T = 0 states of C^{12} will be inhibited by Isotopic Spin Selection Rules, but they can decay by proton emission to T = $\frac{1}{2}$ states of N^{15} without violation of the Selection Rules. Thus, the most likely mode of decay of such states was expected to be by proton emission to give $(\gamma,\alpha p)$ stars which would be easily identifiable and measurable, due to the low energy of the proton.

Experimentally, a large number of such $(\gamma,\alpha p)$ stars were found one being shown in Plate IV.5, and from the calculated excitation energy of O^{16}, the first T = 1 state was identified as the 12.95 MeV level. The same conclusion was reached by D.H. Wilkinson (1956). There would appear to be a number of T = 1 states between 13 and 14 MeV but the statistics are not sufficient to identify them.

The yield of $(\gamma,\alpha\alpha)$ was surprisingly large and in some events both the values for the excitation energy of O^{16} lay above 13 MeV showing that "inhibited" alpha emission could compete with the "uninhibited" proton emission.

From these results it must be concluded that the rules/

rules derived from the conception of isotopic spin are not absolute. These results may be explained by assuming that at these high atomic numbers and energies, the states are not "pure" but have an admixture of other isotopic spins so that reactions which would otherwise be forbidden, do have a finite probability.

References.

Ajzenberg and Lauritsen, 1955, Rev. Mod. Phys., 27, 77.

Arthur, Allen, Bender, Hausman and McDole, 1952, Phys. Rev. 88, 1291.

Erdman and Barnes, 1953, Proc. Roy. Soc. (Canada), 47, 131.

Ferguson, Halpern, Nathans and Yergin, 1954, Phys. Rev. 95, 776.

Goward and Wilkins, 1953, Proc. Roy. Soc., 217A, 357.

Katz and Cameron, 1951, Canad. J. of Phys., 29, 518.

Nabholz, Stoll and Wäffler, 1952, Helv. Phys. Acta., 25, 701.

Radicati, 1952, Phys. Rev., 87, 521.

Sinclair, 1954, Phys. Rev., 93, 1082.

Wilkinson, 1954, Glasgow Nuclear Physics Conference.

Wilkinson, 1956, Phil. Mag., 1, 379

APPENDIX.

RANGE-ENERGY RELATIONS OF HEAVY IONS.

Introduction

During the course of the experiment on the photo-disintegration of nitrogen, it was found possible to measure the range of tracks of recoil nuclei. It was hoped that from these range measurements it would be possible to determine the energy of the particle and hence, with angle measurements, the energy of the incident photon, but this required a knowledge of the range-energy relations for the ions which in this case were of carbon, boron and lithium nuclei. However, it was found that little information was generally available about the range-energy relations of heavy ions apart from cloud chamber experiments on the collisions of alpha particles and gas nuclei from which Prof. P.M.S. Blackett (1925) had deduced the relation,

$$R \propto M.Z^{-\frac{1}{2}}.\ f(v) \quad \text{where} \quad f(v) \fallingdotseq V^{1.1} \qquad \ldots\ldots\ldots\ldots (A1)$$

where R is the range of an ion of mass M, atomic number Z and velocity V. A few more recent experiments yielded results inconsistent with this relation, also the original results required corrections as the range-energy relation for alpha particles which had been used, has since been determined more accurately. It was accordingly decided to undertake a review of the range-energy data available in order to obtain a satisfactory/

satisfactory range-energy relation to employ in the photodisintegration experiments.

For range-energy data obtained from cloud chamber experiments, it was found that a consistent relation was obtained between the range-energy relation and the Atomic Number of the ion.

Thus the accuracy of the particular range-energy relation employed in the photodisintegration experiments could be tested by its relation to the range-energy relations found for ions of approximately the same Atomic Number. This work was extended to include range-energy relations in solids (particularly photographic emulsions) and energy loss problems, but here only range-energy relations measured in cloud chamber gases will be considered.

In this Appendix, a brief theoretical discussion is first given to assist in the interpretation of the experimental results. The experimental methods which have been employed, are then discussed and possible sources of error are noted. Each element is then considered in turn and experimental measurements of range-velocity relations for its ions are discussed and from these the most probable range-velocity relation is deduced. The derived relations for each element are collected and considered as a function of Atomic Number when it is found that a consistent trend is obtained. It is suggested that the range-velocity relations exhibit a periodicity/

periodicity similar to that of the Atomic Table of Elements. The values of the range straggling found in the various experiments are discussed.

The validity and applicability of various theoretical range-velocity relations are considered. It is shown that there is no adequate theory available at present and that where possible, experimental results should be used. A method of extending the experimental results to high energies is described.

Mechanism of Energy Loss of a Charged Particle passing through Matter.

When a charged particle passes through a gas, or matter generally, it loses energy mainly by ionisation and excitation of the electrons of the gas. The rate of energy loss, $\frac{dE}{dR}$ for an ion of Atomic Number Z, and velocity v is given by

$$\frac{dE}{dR} \propto Z_1^2 \frac{1}{v^2} \qquad \ldots\ldots\ldots\ldots \text{(A2)}.$$

for the non-relativistic velocities considered here. At high energies the ion is completely stripped of its electrons, but as energy is lost, its velocity approaches that of its orbital electrons and it can then capture electrons into these states. There is also a probability of losing these electrons so that the ion is continually capturing and losing electrons. The cross section for capture is proportional to $\frac{1}{v^6}$ where v is the/

the velocity of the ion, while the cross section for loss of electrons is proportional to $\frac{1}{v}$. Thus as the ion is slowed down this process of capture and loss of electrons, gradually reduces the effective charge on the ion until eventually at very low velocities ($v \sim \frac{1}{2} \frac{c}{137} = 1.1 \times 10^8$ cm./sec.) it is neutral most of the time. As the ionisation is proportional to the square of the effective charge on the ion, this 'pick-up' of electrons reduces the rate of energy loss very appreciably. For protons and alpha particles, the velocities of the orbital electrons are small and therefore electron pick-up is only important at low velocities and since their mass is small, it is only important at very low energies, about 0.4 MeV for protons and about 2 MeV for alpha particles. For heavier particles, electron pick-up becomes important at high velocities and very high energies, e.g., about 20 MeV for Carbon and of the order of 1000 MeV for fission fragments. In the experiments described here, the most important factor is the effect of electron pick-up in reducing the ionising power of the ion and as electron pick-up is dependent on the velocity of the ion but not on its mass, we will consider range-velocity relations rather than range-energy relations.

When the ion has slowed until it has captured most of its orbital electrons, it begins to lose an appreciable proportion of its energy due to collisions between its nucleus and the nuclei of the gas.

These/

These collisions can be considered to be of two kinds, a few 'near collisions' in which there is a large energy loss (i.e. single scattering events which can be observed in a cloud chamber as branches from the main track and which are measured individually) and secondly, a large number of 'distant collisions' each giving a small energy loss whose effect is observed as a bending of the track due to the multiple scattering. The nuclear stopping effect has been treated as a statistical process by Bohr (1948), who found the energy loss, $\frac{dE}{dR}$, of a particle of Atomic Number Z, and velocity v passing through a gas with atomic number Z_2 and mass number M_2 to be given by the formula

$$\frac{dE}{dR} = \frac{Z_1 Z_2}{M_2} \cdot \frac{1}{v^2} L \quad \ldots\ldots\ldots\ldots\ldots\ldots \text{(A3)}.$$

where L is approximately a constant.

For protons, nuclear stopping is negligible and for alpha particles it is small but its effect can be observed by the characteristic slight bending of the track near the end of range. For heavier nuclei, nuclear stopping is important up to fairly high velocities, thus fission fragments are severely scattered and have fragment branches e.g. see Bøgglid (1948). Also the ranges of fission fragments in hydrogen and in deuterium are different being $6\frac{1}{2}\%$ longer in deuterium. If the energy were lost only by ionisation the mass of the gas atom would be unimportant but from equation (A2) the/

the energy loss due to nuclear stopping is greater in hydrogen than in deuterium.

At very low velocities less than $\frac{1}{2}\frac{c}{137}$ when the particle is mainly neutral, energy is lost in 'hard' collisions between the neutral particle and atoms of the gas. Hard collisions are generally unimportant but they have been used to explain the low values found for the total energy of fission fragments in ionisation experiments - called the Ionisation Defect. The fission fragments produce a large number of low energy gas atoms by nuclear stopping and these gas atoms lose their energy by hard collisions. This energy loss is not observed in ionisation measurements though it is found in calorimetric measurements.

These energy loss processes can be tabulated as various collision or interaction processes.

1.	Ionisation and Excitation	Collision between ion and electron
2.	Nuclear Stopping	Collision between nucleus and nucleus
3.	Hard collisions	Collision between atom and atom.

That the various processes are important for ions of different masses can be seen from Fig. A.1 (reproduced from Bøggild, 1948).

For the fission fragment the initial decrease in the rate of energy loss is due to the capture of electrons which reduces the effective charge on the ion and therefore its ionisation/

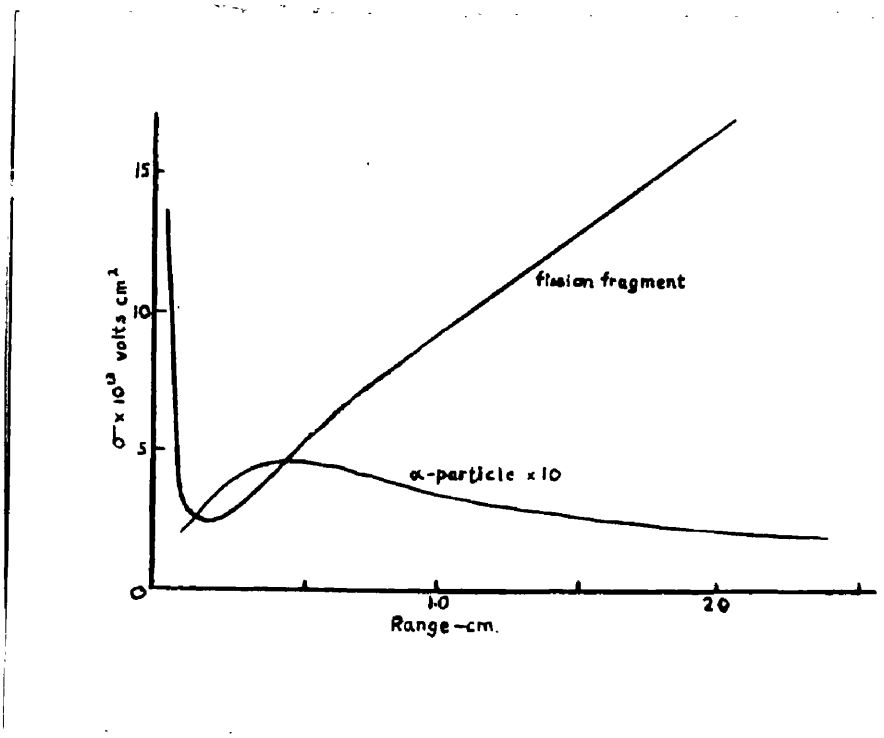

Fig. A.1.

ionisation cross section. At low velocities nuclear stopping becomes the dominant process and results in a rapid rise in the rate of energy loss. For the alpha particle a maxima is observed instead of a minima. This maxima is due to the onset of electron capture. Such a maxima which is observed at one MeV with the alpha particle, is also expected to occur with fission fragments but at a very much higher energy (about 130 MeV). The minima observed with the fission fragments may also occur with the alpha particle but as nuclear stopping is unimportant it will only be found at very low energies.

Thus all ions are subject to the same processes of energy loss but the relative rates of energy loss vary greatly with the Atomic Number of the ion.

The/

The question of the amount of range straggling is important for if the straggling is small, one range measurement gives the energy of the particle, but if the straggling is large, the energy is uncertain for any one event and a large number of measurements are required. Where the energy loss is mainly by ionisation and excitation there are a very large number of collisions, so that the total spread of energy loss is small. Similarly the process of electron capture and loss is repeated a very large number of times so that the straggling due to it is small.

In nuclear stopping, energy is lost not only in a large number of "distant" collisions with small energy losses, but also in a few "close" collisions where large energy losses occur. Hence, with nuclear stopping, the range straggling is large. Thus, protons, whose range is controlled mainly by ionisation and electron pick-up have a small, (1%), straggling of ranges but with fission fragments where nuclear stopping is important, the range straggling is large.

Experimental Methods

The experimental methods of obtaining range-velocity relations for ions in gases will be described in order, being classified according to the method of obtaining energetic ions.

1. Radio-active Sources

Radio-active elements can be placed in a cloud chamber and the range of the alpha particles measured. If the/

the energy of the alpha particles has been measured with a magnetic spectrometer, this gives a fixed point on the helium range-velocity curve. Similarly, fissionable material can be placed on a thin plate in a cloud chamber and the range measured.

2. Collisions with Radio-Active Alpha Particles

In this method, from which the greater part of the data has been obtained, the element to be investigated was inserted in a cloud chamber in gaseous form and the collisions of alpha particles from a radio-active source at the side of the chamber were observed. If the residual range of the alpha particle or the distance of the collision from the source was measured then the velocity of the gas ion was found while its range was measured directly.

As the chamber gas must contain a condensable vapour there were frequently other ions in the gas and therefore it was necessary to distinguish which ion was involved in the collision. The ratio of the mass of the ion to that of the alpha particle can be obtained from the angles alone, but when the mass of the ion was considerably greater than that of the alpha particle, the angle measurements became insensitive. Thus in a gas containing hydrogen, carbon and fluorine, the hydrogen collisions could be easily identified from the angle measurements but the distinction between C^{12} and F^{19} was not so certain due to the insensitivity of angle measurements/

measurements and to the difficulty of making precise angle measurements when there was some multiple scattering.

This method yielded values for the range-velocity relation at different velocities, but as the collision cross section is inversely proportional to the velocity squared, a large number of values were obtained at low velocities but only a few were obtained at high velocities.

In obtaining the range-velocity relation for the ion, a range-velocity relation for the alpha particle was employed. As more accurate experiments were performed, new relations were obtained for the alpha particle so that the range-velocity relation for the ion also needed correction.

In most of the early experiments the alpha range-velocity relation employed was that found by Briggs (1927) which gives velocities up to 12% too high compared with the most recent values quoted by Bethe (1950). Later experiments employed the Livingston and Bethe relation (1937) which is now thought to be in error by up to 8%. All the experimental range-velocity relations for ions given in this appendix have been corrected for the changes in the alpha range-velocity relations.

In some of the earliest experiments the curve through the experimental points was drawn to be in accordance with the current theories which did not consider nuclear stopping. These curves were re-drawn to give the best possible fit with the/

the experimental points; this resulted in slight changes in the values and bigger changes in the gradient.

3. Collisions with Fast Neutrons

Mills (1952) has reported an experiment in which 14 MeV neutrons were directed into a cloud chamber filled with oxygen. A large number of single heavily ionising tracks were observed which were assumed to be due to elastic collisions of fast neutrons with oxygen nuclei. It was further assumed that the neutrons had not been scattered and so were of 14 MeV energy. This experiment was liable to error as it was difficult to correct for the effect of collisions with neutrons which had been previously scattered.

4. Fast Neutron Reactions

Experiments have been performed by Lillie(1952) in which 14 MeV neutrons were passed through a cloud chamber containing first nitrogen and then oxygen and the $N^{14}(n,\alpha)B^{11}$ and $O^{16}(n,\alpha)C^{13}$ reactions were studied. They appeared as non-collinear flags with both tracks fairly short and the origin clearly visible so that they were easily measured. As a check that the neutron had not been scattered, the two tracks were required to be coplanar with the direction of the neutrons from the target. As the (n,α) reactions proceeded by a number of different energy levels in the product nucleus, a considerable range of energies of B^{11} and C^{13} were obtained.

The stopping power of the gas was first calculated

from/

from the composition of the gas and was then corrected by bringing the ground level groups to zero excitation.

Thus this is an excellent experimental method since it gives easily measurable events, good statistical accuracy up to fairly high energies and since the stopping power can be checked.

5. Slow Neutron Reactions

Slow neutrons enter a cloud chamber in which they can react exothermically with an element in the chamber gas, e.g. if the gas contains nitrogen the reaction $N^{14}(n,p)C^{14}$ occurs. The energies of the particles are generally known from other nuclear data and hence from measurement of the ranges, a "fixed point" can be obtained on the range-velocity relation for the ions.

If one of the residual nuclei is formed in an excited state then a further "fixed point" will be obtained e.g. in the $B^{10}(n,\alpha)Li^{7}$ reaction, lithium is formed in the ground state and in an excited state of 0.477 MeV so that two values are obtained for the lithium range-energy relation.

As the incoming particle has negligible momentum, the two particles produced lie in a straight line, and if they are of different masses the origin of the event will be marked by a pronounced change in ionisation and hence the ranges can be easily measured. Thus in the $N^{14}(n,p)C^{14}$ reaction accurate range measurements are possible for the proton and

for/

for the C^{14} ion.

If the two particles have approximately the same charge and mass, the change in ionisation at the origin will be small and the ranges difficult to distinguish, although the total range can be measured. This occurs with the B^{10} $(n,\alpha)Li^{7}$ reaction. The solution of this difficulty is discussed below.

Thus this method can be employed to yield one or more "fixed points" on the graph of range against velocity for ions but it is not capable of widespread application.

6. Statistical Analysis

When an ion track is recorded in a cloud chamber it is observed that branch tracks occur due to collisions of the ion with gas nuclei. The statistical distribution of these branch tracks with respect to the residual range of the ion can be used to calculate a range-velocity relation for the ion. This has been used by Blackett (1922) for protons and by Bøggild (1948) for fission fragments, when good agreement was obtained with later, and more accurate, results.

This method is little used as it is generally possible to employ simpler and more accurate methods.

Stopping Power of the Medium

In all the measurements of the range of an ion in

a/

a gas other than air it was then required to calculate the range the ion would have had in air. This was normally done by measuring the stopping power of the gas for alpha particles and assuming that the same stopping power could be applied to the ion. That this could lead to appreciable error has been widely recognised. For instance, a proton will start to capture electrons at approximately the same velocity in all gases, but a heavy ion will start to capture electrons at a lower velocity in hydrogen than in a heavy gas where the electrons have higher orbital velocity. Thus as the effective charge on an ion is less in a heavy gas its range may be expected to be slightly greater. A further point is that for alpha particles nuclear stopping is unimportant but with heavy ions nuclear collisions constitute a major source of energy loss and hence as the nuclear stopping cross section is dependent on the gas (see equation (A2)) the stopping power for heavy ions will vary in a different manner to that of alpha particles. Also the change of stopping power with velocity will be different for alpha particles and for heavy ions.

This question was treated experimentally by Wrenshall(1940) who observed the collisions of radio-active alpha particles with carbon atoms in two different gases. One gas contained only light atoms (Carbon, Hydrogen and Oxygen) while the other contained a high percentage of heavier Chlorine atoms. He observed a significant difference in the/

the value and in the gradient of the range-velocity relations.

Experimental Results

The experimental range-velocity curves obtained for each element will be considered in order and then the results will be combined to present an overall picture.

Hydrogen and Helium

The range-velocity for these two light elements are well established and the principle results on which they are based are summarised by Bethe (1950). A considerable number of exact measurements were possible from radio-active alpha particles and from nuclear reactions. A small correction to the alpha particle range-energy relation is suggested in the section on Lithium.

Lithium

No experiment has been performed to obtain a continuous range-velocity relation for Lithium ions in gas but the $B^{10}(n,\alpha)Li^{7}$ has provided two "fixed points" as when B^{10} captures slow neutrons it either decays by emitting an alpha particle and leaving Li^{7} in an excited state of 0.477 MeV energy or, more rarely, it decays by emitting a long range alpha particle and leaving Li^{7} in its ground state.

A number of early experiments were performed with moderate accuracy, which are summarised by O'Ceallaigh and Davis (1938). It was possible to observe the total range of short and long range groups but the origin was generally indistinct. J.C. Bower, E. Bretscher and

C.W. Gilbert (1938) analysed 20 short range tracks photometrically and found a mean partition ratio for the ranges of the ions of

$$\frac{R_{He}}{R_{Li}} = 1.62 \pm 0.3$$

while the total track length was 11.3 mm. This value of the range was later corrected by Gilbert (1948) for errors in the stopping power calculations to 12.5 mm while on the basis of an experiment by Wilson (1942) he deduced a range of 14.9 mm for the long range tracks (i.e. ground state transition) but as the chamber gas contained mainly Helium in the earlier experiment and mainly Argon in the later, this value may not be accurate. The corrections employed by Gilbert for the variation of stopping power with velocity are extreme and therefore the total range of 12.5 mm is an upper limit.

Bøgglid found total ranges of 11.35mm and 13.3mm for the short and long range groups but he did not correct for the variation of stopping power with velocity and hence his values are probably low. He evaporated Boron on to a thin gold foil which was placed across the chamber and measured the ranges of pairs of tracks from the foil. From 5 events he found a mean partition ratio of 1.60, but the method was not very accurate.

These experiments were performed partly to find the energy of the excited state of Li^7 but this energy is now well established from other experiments and hence the initial velocities of the alpha and lithium ions are known. It is thus possible to find the range of the

alpha particle and from the partition ratio, deduce the range of the lithium ion. Adding these two together, the total range is found and from the ratio of the ranges of the short to the long groups, the total range of the long group can be calculated. From the known energy of the long range alpha particle, its range can be obtained from range-energy data and hence by subtraction the range of the Li^7 ion is obtained.

In deducing the range of the low energy alpha particle, Bethe (1950) re-calculated Gilbert's correction to obtain 0.735cm took O'Ceallaigh and Davis's value of 0.715cm and Bøggild's value of 0.709cm and then assumed an average value of 0.720cm. However, he failed to correct Bøggild's value for the change in stopping power with velocity. Making this correction of 3%, the average value of the ranges becomes 0.727cm.

Assuming a partition ratio of 1.62,

$$\text{Range of } Li^7 \text{ ion} = \frac{0.727}{1.62} = 0.449\text{cm}$$

Assuming the reaction threshold to be 2.792 MeV and the excited state of Li^7 to be at 0.477 MeV, the velocity of the Li^7 ion is 4.82×10^8cm/sec. The total range of the short group is then 0.727 + 0.449 = 1.176cm. Using the ratio of the total ranges, the total range of the ground state group = $1.176 \times \frac{13.3}{11.35} = 1.378$cm. From Bethe (1950), the range of an alpha particle of energy $\frac{7}{11} \times 2.792 = 1.777$ MeV is 0.875cm. Hence the range of the lithium ion is 0.503cm and its velocity is 5.27×10^8cm/sec. The partition ratio for the long range group is then 1.66

whereas if Bethe's original alpha range of 0.720 cm had been used this partition ratio would have been 1.80.

Boron

Lille (1952) obtained a range-velocity relation for B^{11} ions from the $N^{14}(n,\alpha)B^{11}$ reaction by bombarding nitrogen in a cloud chamber with 14.1 MeV neutrons. An accurate relation was obtained.

Carbon

A number of experiments have been performed with carbon ions. Feather (1933) observed the collision of radio-active alpha particles with carbon and fluorine nuclei in a cloud chamber containing CF_4. Of the 63 collisions observed, 8 were assumed to be with carbon nuclei from the angle measurements. The range-velocity relation derived by Feather has been corrected for the error in the alpha particle range-velocity relation which was used. The result obtained for Carbon is not considered to be very reliable. G.A. Wrenshall (1940) in a careful experiment, observed the collisions of radioactive alpha particles with carbon nuclei in a gas containing carbon atoms as the only heavy atoms (apart from the oxygen atoms of the condensable vapour). He then repeated the experiments with a chamber gas containing 52% of CH_3Cl to discover whether the presence of heavier atoms would affect the carbon range-velocity relation. In the high velocity region where the greatest divergence was observed, only a few results were obtained, but even so there would appear to be a positive effect. The corrections required for the error in the Livingston

and Bethe (1937) range-energy for alpha particles used, were made.

The most accurate range-velocity relation was obtained by Lilla (1952) who observed $C^{16}(n,\alpha)C^{13}$ events in a cloud chamber containing oxygen which was bombarded with 14.1 MeV neutrons.

A fixed point was obtained from the slow neutron reaction $N^{14}(n,p)C^{14}$ which has been observed in a cloud chamber by Bøggild (1945) and by Hughes and Eggler (1948).

They obtained ranges for the C^{14} ion of 0.30 and 0.25mm respectively.

Energy release in Reaction = 0.627 MeV

$\therefore$ Energy of $C^{14} = \frac{1}{15}\ 0.627 = 0.0418$ MeV

Velocity of $C^{14} = 0.757 \times 10^8$ cm/sec.

It is then taken that a C^{14} ion of velocity 0.76×10^8 cm/sec. has a range of 0.275mm.

The range-velocity relation for carbon which was deduced from the above results was tested twice in the present experiment and found to be satisfactory as shown in Fig. III.5 and Fig. IV.10.

Nitrogen

Blackett and Lees (1931-32) found a range-velocity relation for nitrogen ions which were produced by collisions with radioactive alpha particles. The line through the experimental points was re-drawn and then corrected for the more recent values of the range-velocity relation of the alpha particle. Few experimental points were obtained at high velocities.

Oxygen

Blackett and Lees (1931-32) have measured two range-velocity relations for oxygen. In the first the cloud chamber gas contained 50% Argon and 10% oxygen, hence the reduction of the resulting ranges to the range they would have had in air is uncertain. The second relation was for O^{17} produced in the reaction $N^{14}(\alpha,p)O^{17}$. Both relations were altered corresponding to the corrections for Brigg's range-velocity relation for alpha particles.

Fluorine

Feather (1953) observed collisions of radio-active alpha particles with fluorine and carbon nuclei in a gas containing CF_4. Brigg's range-velocity relation for alpha particles was used originally.

Neon

The collisions of radio-active alphas with neon were observed first by Eaton (1935) and then by McCarthy (1938). Very similar results were obtained. The alpha range-velocity relation used was from Blackett and Lees (1931-32) for low velocities and Mano (1934) for higher velocities.

Sulphur

Alpha particle collisions with sulphur nuclei were measured by Anthony (1936). Blackett and Lees' range-velocity relation for alpha particles appears to have been used.

Chlorine

Hansen and Wrenshall (1940) measured the collisions

of radioactive alpha particles with chlorine nuclei. Livingston and Bethe's range-velocity relation for alphas was employed.

Argon

Blackett and Lees (1931-32) observed collisions of alpha particles with argon nuclei. Corrections were made for the alpha range-velocity relation used.

Fission Fragments

Range-velocity relations for fission fragments were measured by Bøggild, Arroe, and Sigureirsson (1941) and the ranges of the fragments in different gases were also measured (Bøggild, Bromstrom and Lauritsen, 1940, and Bøggild, Minnhagen and Neilsen, 1949).

Radio-Active Recoils

Joliot (1934) included radium and throium emanations in a cloud chamber gas at very low pressures and observed the tracks of recoil nuclei after radioactive alpha particle emission. The range straggling was very large due to the large number of nuclear collisions. Wood (1913), measured the ranges of recoil nuclei by moving a collecting plate away from a radioactive source.

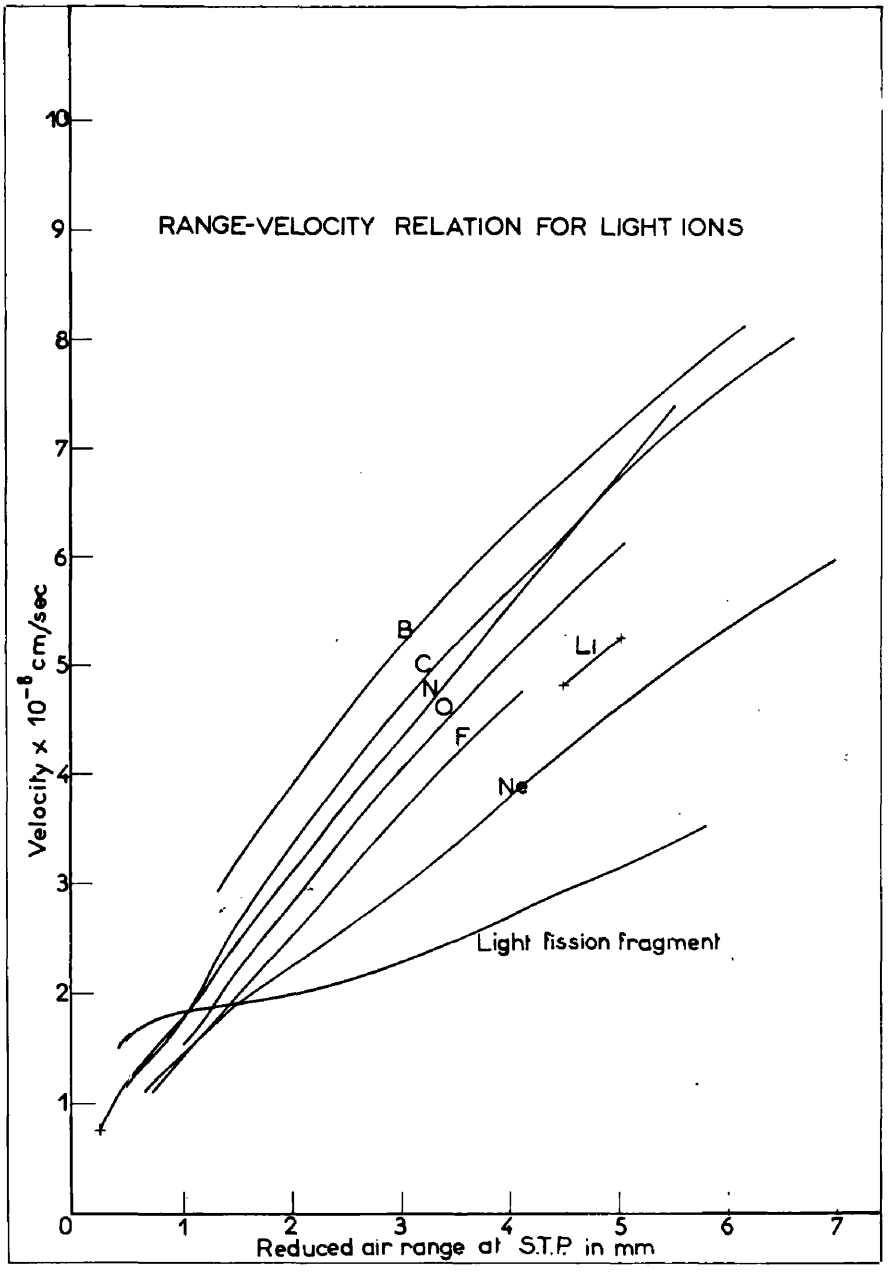
RANGE-VELOCITY RELATION FOR LIGHT IONS
Velocity x 10^{-8} cm/sec
Reduced air range at S.T.P. in mm
B
C
N
O
F
Ne
Li
Light fission fragment
0
1
2
3
4
5
6
7
8
9
10

Fig. A.2.

Combination of Results

To correlate the results obtained for different isotopes the range-velocity relation for each element was corrected to that of an ion whose Atomic Mass was chosen to be twice its Atomic Number. As it has been found that the rate of energy loss is proportional to the charge on the ion and is independent of its mass (e.g. protons and deuterons of the same velocity lose energy at the same rate), the ranges for a given velocity were calculated to be proportional to the mass. For example Li^7 ions of velocity 4.82×10^8 and 5.27×10^8 cm/sec. have ranges of 4.49 and 5.03mm respectively. Then Li^6 ions of velocity 4.82×10^8 and 5.27×10^8 cm/sec. have ranges of $\frac{6}{7} \times 4.49 = 3.85$ and $\frac{6}{7} \times 5.03 = 4.31$mm respectively.

The resultant range-velocity relations for the elements with Z = 3 to Z = 10 are shown in Fig.A.2. To illustrate the trend of the results the range-velocity relation for a (light) fission fragment is shown. At low velocities, the range of the fission fragment is much less than those of the lighter ions due to the high rate of energy loss caused by nuclear stopping. At higher velocities the effective charge on the fission fragment is comparable with that on the lighter ions and therefore its rate of energy loss is of the same order, but, as its mass is greater, the range is longer.

The most significant feature of Fig.A.2. is the consistency of the form of the range-velocity relations from Boron

to/

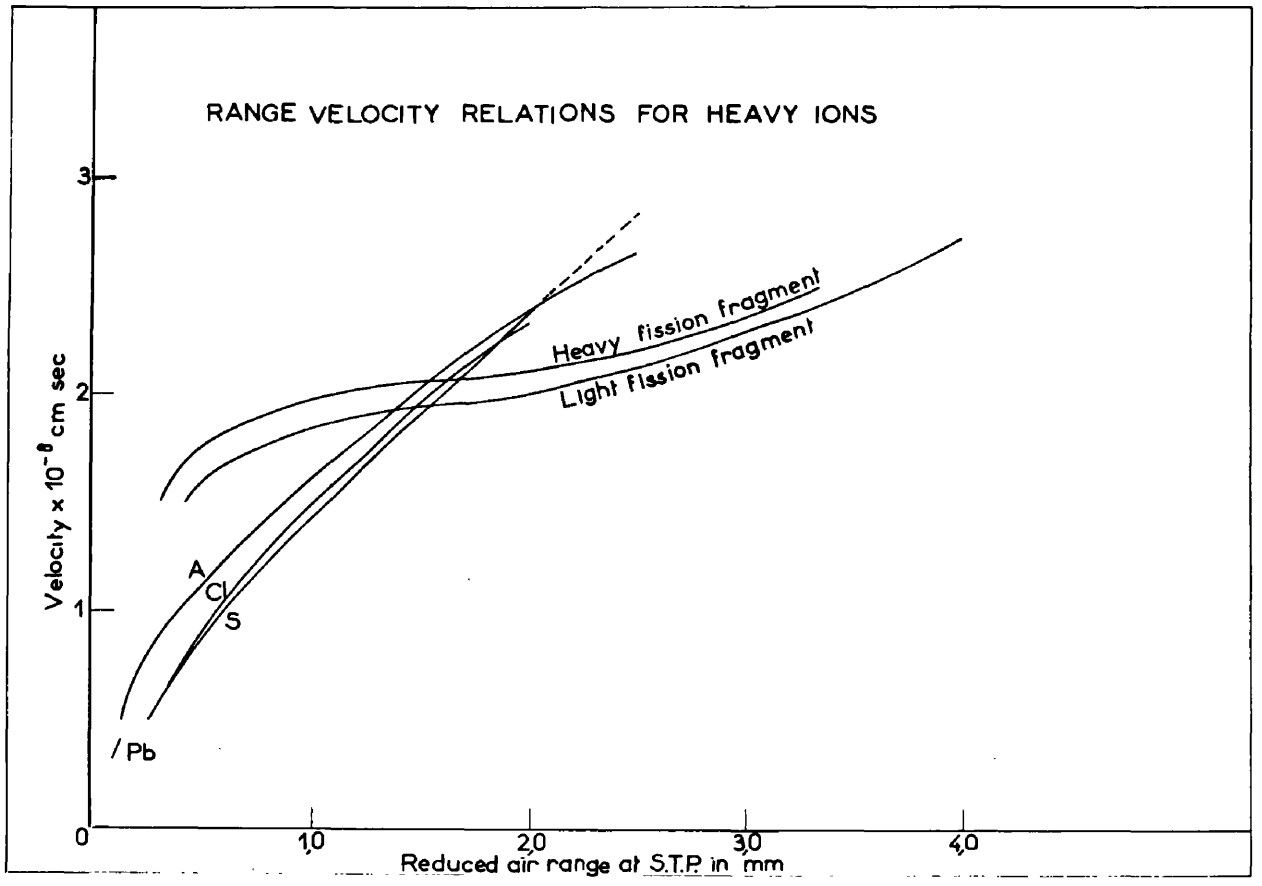
RANGE VELOCITY RELATIONS FOR HEAVY IONS
Velocity x 10⁻⁹ cm sec
3
2
1
0
1,0
2,0
3,0
4,0
Reduced air range at S.T.P. in mm
Heavy fission fragment
Light fission fragment
A
Cl
S
/Pb

Fig. A.3.

to Neon. This suggests that the accuracy of any one relation may be checked by the values found for its neighbours. The range-velocity relation drawn for nitrogen ions is inconsistent with those of its neighbours and it is accordingly suggested that at high velocities, above 6×10^8 cm/sec., the ranges be increased. In the experimental determination of the nitrogen range-velocity relation very few events were observed at these high velocities.

The other noticeable feature of Fig.A.2 is that the two "fixed points" for Lithium are not consistent with the other range-velocity relations.

The range-velocity relations derived for the heavier ions are shown in Fig.A.3., where the fission fragments were assumed to be Y_{39}^{78} and I_{53}^{106}. At the higher velocities, above 2.5×10^8 cm/sec., the range of the sulphur ions appeared to be inconsistently low and it is proposed that they be increased to bring them into agreement with their neighbours; the experimental range-velocity relation at these velocities was based on very few determinations.

The form of Figs. A.2 and A.3 suggested that the range-velocity relation could be expressed as a function of the Atomic Number of the ion. This idea was tested by plotting the range for a constant velocity, as a function of the Atomic Number. In Fig.A.4 this plot has been made for three different velocities. It/

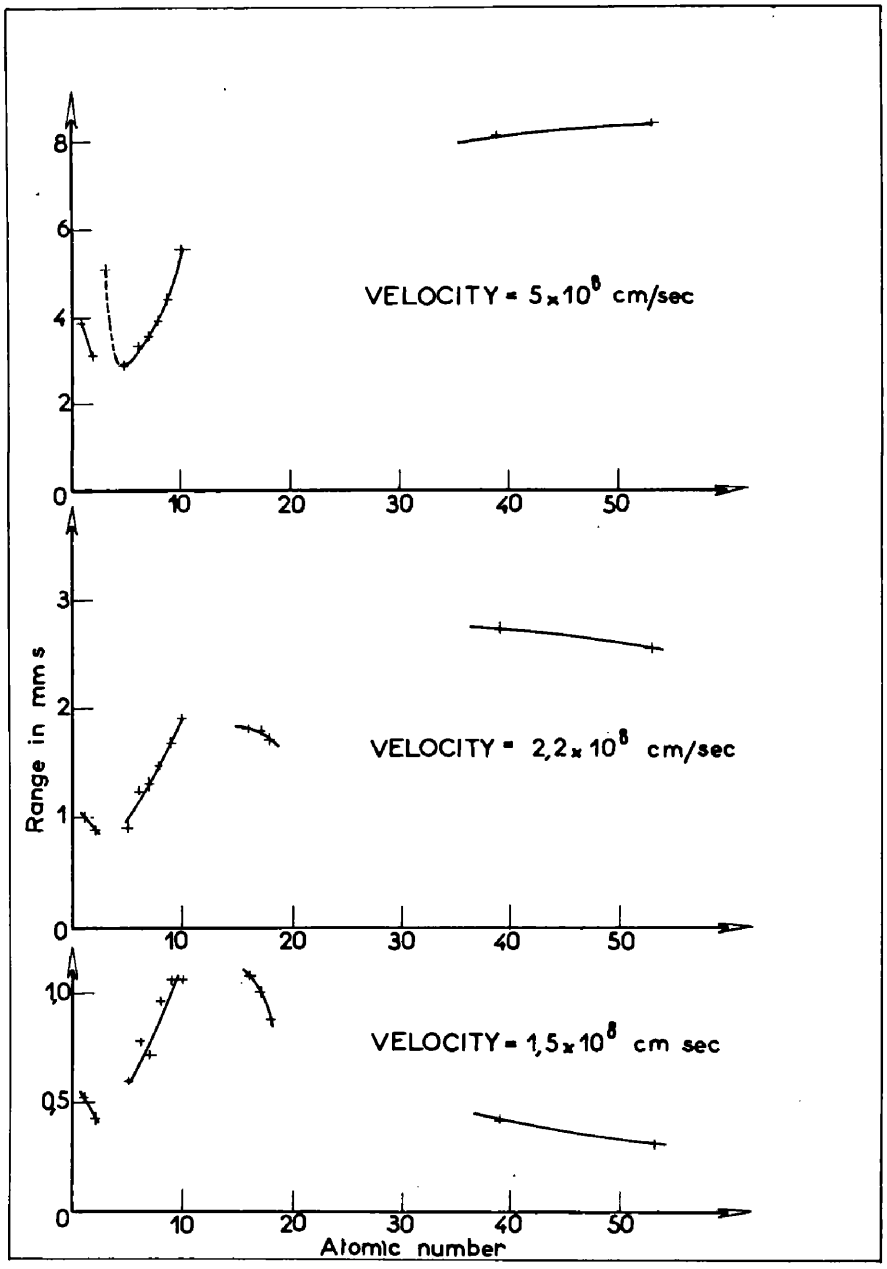
VELOCITY = 5x10⁸ cm/sec
VELOCITY = 2,2x10⁸ cm/sec
VELOCITY = 1,5x10⁸ cm sec
Range in mm s
Atomic number
0
2
4
6
8
1
3
0,5
1,0
10
20
30
40
50

Fig. A.4.

It was found that the ranges were approximately a function of the Atomic Number, but superimposed on this relation there was another factor. Thus for a velocity of 5×10^8 cm/sec. the trend of the ranges was to decrease as the Atomic Number decreases, but Lithium gave a longer range than boron, and hydrogen (actually H_2^1) gave a longer range than helium. It is suggested, that for the light elements at least, this other factor is a periodicity the same as that of the Periodic Table.

The explanation of this periodicity may lie in the fact that the first electron of a shell may be captured more easily than any subsequent electron. Thus the effective charge on an element which is the first in its period, will be reduced more easily than with other elements, so that the range will be longer as the rate of energy loss is proportional to the square of the effective charge.

Range Straggling

Very little is known about the range straggling of heavy ions of low velocity as the errors in measurement are usually of the same order as the range straggling so that authors are reluctant to publish results. However, for ions with ranges between 0.5 and 2.0mm the values of the R.M.S. range straggling expressed as a % of the total range, have been found and are given in Table A.1. In agreement with theory, (e.g. Bohr, 1948) the range straggling increases as the Atomic Weight increases.

TABLE A.1./

TABLE A.1.

Ion	% Straggling	Ion	% Straggling
He	6.5 ± 2	Ne	17.2 ± 2.5
C_1	11.7 ± 2.5	S	18.5 ± 2.5
C_2	14.5 ± 3	Cl	17.0 ± 3
F	13.5 ± 2.5	A	17.0 ± 3

C_1 is for carbon ions in a gas containing chlorine nuclei while C_2 is for carbon ions in a gas containing only light nuclei.

In addition, values of 17% and 12% range straggling have been obtained for nitrogen and oxygen ions respectively but due to the small number of events, the statistical significance is not great. In Chapter III, a range straggling of 15% was found for C^{13} ions from the (γ,p) reaction proceeding through the 9.18 MeV level of N^{14}, but this value includes the errors of measurement which are of the order of 10%.

The % straggling of C^{12} with longer ranges was found from the measurements of $Ne^{20}(\gamma,\alpha\alpha)C^{12}$ stars. In Fig. IV.10, the experimental points appear to lie on a line parallel to the expected range-energy relation (this may be due to the stopping power of neon for C^{12} ions being different from that for alpha particles): accordingly, the range straggling was measured from this experimental line when a R.M.S. straggling of 7% was found for/

for the 10 events with ranges between 2.7 and 6.1mm. Errors of measurement may be appreciable as the calculation of the energy of the C^{12} ion was complex.

These figures for the range straggling can only serve as an indication but not as absolute values.

Previous Theoretical Range-Velocity Relations

Two methods of calculating range-velocity relations have been used. One is a purely emperical relation proposed by Blackett in 1925 and the other is a semi-emperical calculation by Knipp and Teller (1941). A detailed account of the theory of the interaction of charged particles with matter has been given by Bohr (1948) but this was purely qualitative and emphasized the difficulties and uncertainties of the calculations rather than produced applicable formulae.

(a) Blackett's Relation

As a result of his experiments on the range-velocity relations of ions of N^{14}, O^{16} and O^{17}, Blackett (1925) derived an emperical relation for the range R, of an ion of Atomic Number Z, Mass Number M and velocity v, which is:-

$$R \propto M.Z^{-\frac{1}{2}}. f(v) \quad \ldots\ldots\ldots\ldots\ldots\ldots\ldots\ldots (A.1)$$

where the function f(v) was approximately $v^{1.1}$, that is, almost a straight line. This relation was intended to apply to velocities greater than 2×10^{-8} cm/sec. as the range-velocity relation was not linear below that velocity.

Blackett's/

Blackett's formula may be checked from the results of experiments performed since 1925. The main conclusions were:-

1) The range-velocity relations did not have straight line portions as can be seen from Figs. A.2 and A.3, that is, $f(v)$ does not have the form $v^{1.1}$.

2) If we assume

$$R \propto M.Z^{-n}. f(v) \quad \ldots\ldots\ldots\ldots\ldots\ldots (A.4)$$

then as can be seen in Fig. A.4, the index n, is not a constant but varies with the velocity v. Thus it is not justifiable to express the variables v and Z as separate functions.

3) Blackett's relation would be expected to be obeyed most closely at higher velocities where nuclear scattering is not so important. In Table A.2 the experimental ranges of ions with Atomic Numbers between 3 and 10, are given for a fixed velocity of 5.10^8 cm/sec. These experimental ranges are compared with the ranges calculated from Blackett's formula with $n = \frac{1}{2}$, using the experimentally measured range of the nitrogen ion as standard. Table A.2 shows that the value $n = \frac{1}{2}$ does not give agreement.

4) As shown in Fig. A.4 and Table A.2, the range-velocity relations exhibit a periodicity which is not included in equation A.1.

It is concluded that it is not possible to express

the/

the range as a product of a power of the Atomic Number and a function of the velocity, that is, no simple relation of the form of equation A4 exists.

TABLE A.2.

Ion	Li_3	B_5	C_6	N_7	O_8	F_9	Ne_{10}
Experimental Range	3.9	2.82	3.4	3.57	3.9	4.3	5.53
Calculated Range	2.34	3.02	3.31	Std.	3.82	4.05	4.27

(b) Knipp and Teller's Theory

A semi-experienced theory was devised by Knipp and Teller (1941).

On the basis of equation A.2 for the rate of loss of energy, $\frac{dE}{dR}$, due to ionisation and excitation, they assumed the formula,

$$\frac{dE}{dR} \propto i^2 . \sigma_e \qquad \text{.....(A.5)}$$

where i is the "effective charge" on the ion and σ_e is the specific electronic stopping cross section which is assumed to be the same for all ions. Thus σ_e is the stopping cross section for a particle of unit charge. The effective charge is taken instead of the Atomic Number as a correction for electron pick-up From measurements of the distribution of charges on alpha particles, the root mean square charge was calculated and this was taken as the effective charge, i. From measurements of

$\frac{dE}{dR}$ /

$\frac{dE}{dR}$ for alpha particles, σ_e was then calculated.

To find the effective charge i, Knipp and Teller assumed that the filling of the electronic states of the ion could be considered one at a time and then introduced the parameter γ, defined by,

$$\gamma = \frac{V}{V_e} \qquad \text{.....(A.6)}$$

where V is the ion velocity and V_e is the characteristic velocity at which the probabilities for capture and loss of electrons become equal for an orbital state. V_e was calculated using the Fermi-Thomas model for the ion. Assuming a constant value of γ for all velocities, the effective charge, i, was calculated.

After making a correction for nuclear stopping, range-velocity relations were then derived for a variety of values of γ which was so chosen as to give agreement with the experimental data, although the data only covered a small portion of the range.

The characteristic velocity, V_e, was calculated on two different bases:-

1. V_e was taken as the root mean square velocity of the energetically most easily removable electron where it was assumed that the electron's energy is determined by the average potential of the other charges.

2. V_e was the root mean square velocity of the outermost electron calculated on the assumption that collisions between

electrons/

electrons are very frequent so that states of a definite energy have little meaning for an individual electron.

On assumption 1, γ was found to increase with Atomic Number, from 1.2 to 1.3 for C^{12} to 1.8 for the heavy fission fragment. With calculation 2, γ decreased with Atomic Number, from 0.6 with C^{12} to 0.35 for heavy fission fragments.

More recent experiments allow the theory to be tested:-

1) For carbon ions, ranges have been measured at higher and at lower velocities when appreciable discrepancies were found. Thus at $v = 7.5 \times 10^8$ cm/sec. the experimental range is 6.0mm in air whereas the predicted ranges are between 4.0 and 5.0mm and the difference was increasing with increasing velocity. At $v = 0.76 \times 10^8$ cm/sec., a C^{12} ion has a range of 0.24mm while the predicted range is 0.13mm and this suggests that Knipp and Teller assumed too high a rate of energy loss due to nuclear stopping.

2) Walker and Fremlin (1943) measured the distribution of the charges on N^{14} ions of 15 MeV energy and deduced a value for γ of 0.6 which favours Knipp and Teller's second method of calculating V_e.

3) In assuming a constant value for γ, this theory does not take into account the effects of the periodicity of the atomic electrons which are demonstrated in Fig. A.4.

The assumption that γ is a constant for all velocities

is/

is not a reliable one. For example in helium it is found that the first electron is captured more easily than the second one, the values being

$$He^{+} \rightleftharpoons He^{++} \text{ occurs at } \gamma = 1.6$$

while $$He \rightleftharpoons He^{+} \text{ occurs at } \gamma = 0.8$$

Thus it is concluded that Knipp and Teller's semi-emperical theory is unreliable as it has been found to give inaccurate values and as it is based on doubtful assumptions, particularly the constancy of γ for all velocities.

(c) Overall Conclusion

The overall conclusion is that there is no adequate theory which predicts range-velocity relations in the region in which electron pick-up is important and hence it is better to use the experimentally measured range-velocity relations and, if necessary, extrapolate from them.

Applications to High Energies: Correction for Electron Pick-up

Barkas (1952) has suggested a method of obtaining range-velocity relations at high energies.

At velocities greater than that at which electron pick-up begins, so that effective charge on the ion is in fact the Atomic Number, then

$$\frac{dE}{dR} = Z^2 . g(v) \qquad (A7)$$

where $g(v)$ is a function known from the theory of excitation and ionisation processes.

$$\frac{Z^2}{M}\, dR = v.g(v).dv$$

$$\frac{Z^2 R}{M} = G(v) + B_z \qquad (A8)$$

where $G(v)$ is a universal function and B_z is a constant.

This formula will hold for all ions at high energies but the constant B_z is dependent on the atomic number as it is a correction for all the factors that cause deviation from this relation at low energies, i.e. it corrects for the effects of electron pick-up, nuclear stopping and hard collisions.

If a plot of $\frac{Z^2 R}{M}$ is made against a function of velocity (e.g. $\frac{E}{M}$) then the graphs for different elements will appear as a series of parallel curves whose separation is given by the values of B_z e.g. for protons and alpha particles:

$$R(E_1) = R_2\left(\frac{M_2}{M_1} E_1\right) + B_2 - B_1$$

$$= R_2(4E) + 0.20 \text{ cm.} \qquad \text{(Blackett).}$$

Bethe (1950) stated that $B_2 - B_1$ was 0.20 cm. at low energies and 0.30 cm. at high energies.

The relation (A8) has been used for carbon ions of 120 MeV by Miller et. al. (1950) when good agreement between the calculated and experimental ranges was obtained.

References

Anthony 1936, Phys. Rev. 51, 726.

Barkas U.C.R.L. Report No.1937.

Bethe 1950, Rev. Mod. Phys. 22, 213.

Blackett 1925, Proc. Roy. Soc. A107, 349.

Blackett and Lees 1931-32, Proc. Roy. Soc. A134, 658.

Bøggild 1945, Danske, Vid. Sels. 18 No.8.

Bøggild, Arroe and Sigurgeirsson 1941, Phys. Rev. 71, 281.

Bøggild, Bromstrom and Lauritsen 1941, Phys. Rev. 59, 275.

Bøggild, Minnhagen and Neilsen 1949, Phys. Rev.

Bower, Bretscher and Gilbert 1938, Proc. Camb. Phil. Soc. 34, 290.

Briggs 1927, Proc. Roy. Soc. A114, 341.

Brunnings, Knipp and Teller 1941, Phys. Rev. 60, 657.

Eaton 1935, Phys. Rev. 48, 921.

Gilbert 1948, Proc. Camb. Phil. Soc. 44, 447.

Hansen and Wrenshall 1940, Phys. Rev. 57, 750.

Hughes and Eggler 1948, Phys. Rev. 73, 809.

Joliot 1936, J. de Phys. (7), 5, 219.

Knipp and Teller 1941, Phys. Rev. 59, 659.

Lillie 1952, Phys. Rev. 87, 716.

Livingston and Bethe 1937, Rev. Mod. Phys. 9, 261.

McCarthy 1938, Phys. Rev. 53, 30.

Miller, Hamilton, Purnam, Hayward and Rossi 1950, Phys. Rev. 80, 456.

O'Ceallaigh and Davis 1938, Proc. Roy. Soc. A167, 81.

Walker and Fremlin 1953, Nature 171, 189.

Wilson 1942, Proc. Roy. Soc. A177, 382.

Wrenshall 1940, Phys. Rev. 57, 1095.

Wood 1913, Phil. Trans. 26.

General Conclusions

It has been shown that by cloud chamber studies of the photo-emission of charged particles, it is possible to obtain results that could not be found by other techniques.

From the ranges of low energy photoprotons, an energy distribution was obtained which had a level structure. The details of the levels were confirmed by detailed balancing calculations from the inverse, (p,γ), reaction. This was the most definite evidence obtained up to that time, that photodisintegration reactions could proceed through energy levels.

A new technique of the microscopic measurement of recoil ranges was developed. This enabled the (γ,p) cross section to be measured at high energies. In connection with this, a survey was made of range-energy relations for heavy ions. It was found that a consistent picture was obtained for the elements from Boron to Neon and it was suggested that the range-velocity relations have a periodicity similar to that of the Periodic Table.

From the measurement of $(\gamma,star)$ events in neon, it was shown that the Isotopic Spin Selection Rules could be violated, probably due to the impurity of the levels involved at these high energies and high Atomic Numbers.

It was demonstrated that the photodisintegration results for light elements, could be interpreted on a Compound Nucleus model in

which the details of the levels and thresholds were important; this was in contrast to previous interpretations which had been based on statistical methods and in which only the Atomic Number was important. In particular the anomalously low (γ,n) cross section in N^{14} was explained by such detailed consideration.

The yield of alpha particles from Neon was shown to be much higher than from nitrogen or other neighbouring elements and this suggests that the alpha particle model of the nucleus may have some applicability.

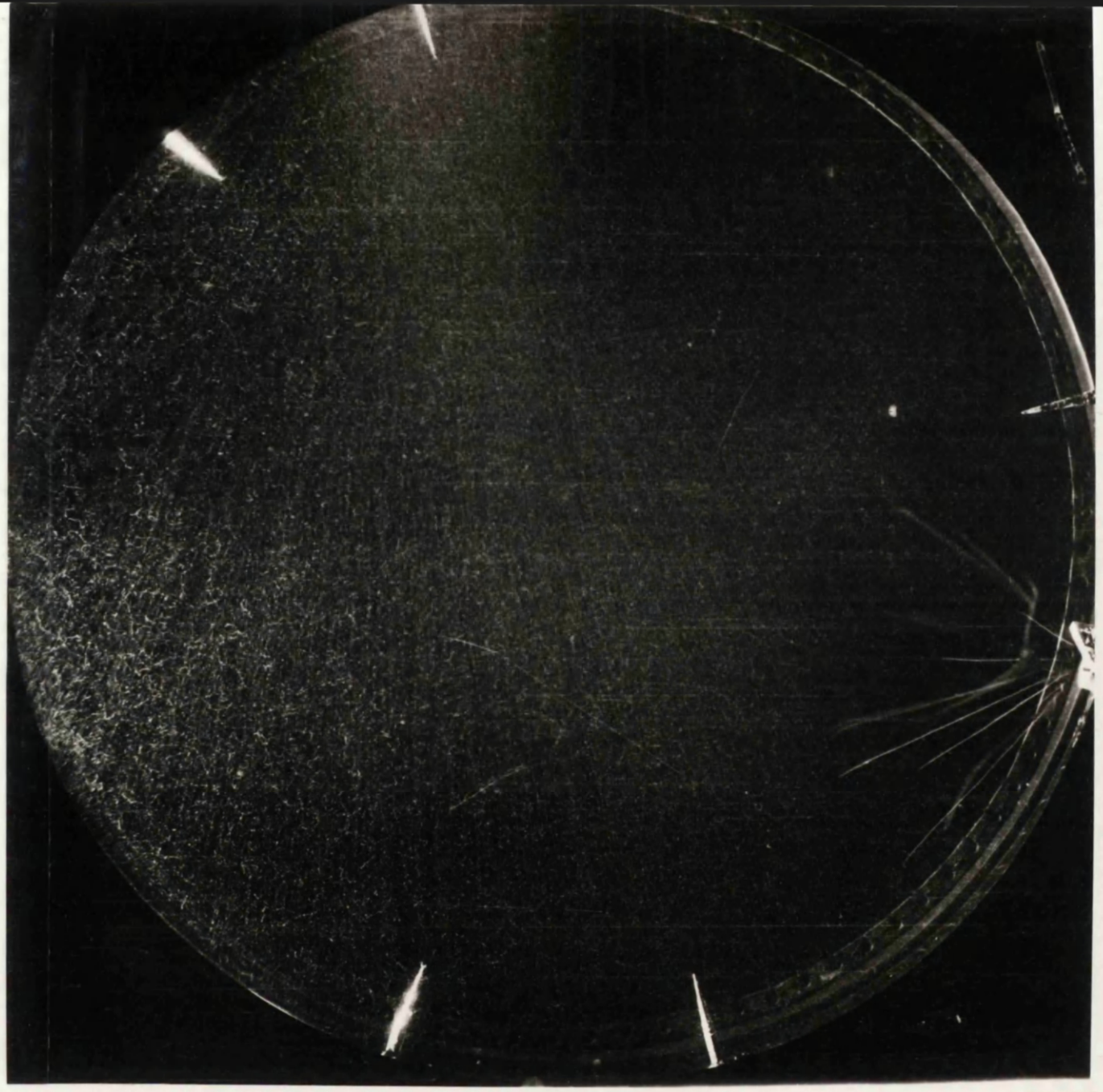

Plate II.1. $He^4(\gamma,p)H^3$ Event.

The X-ray beam entered at the top of the photograph, its interaction with the wall produced the background of electron tracks. The five spikes round the wall were to permit the alignment of the films. The radioactive alpha source is on the right hand side of the photograph. Note that both the proton and triton tracks are lighter than those of the radioactive alpha particles.

Plate II.2. (γ,α) Event in O^{16} or N^{14}

The recoil is long and heavily ionising. The fragment ionisation is heavier than that of a proton and is comparable with that of the radioactive alpha particles.

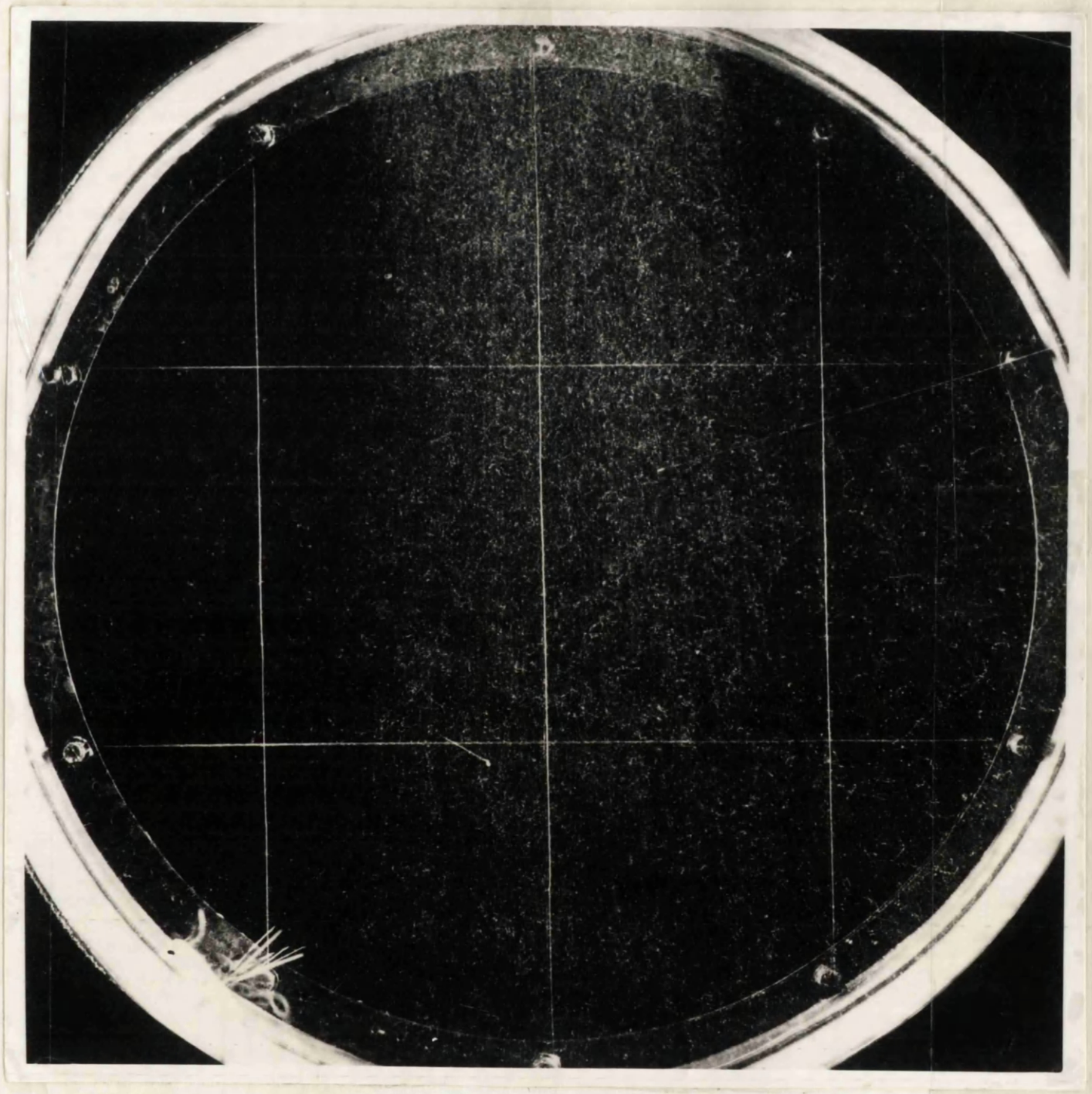

Plate III.1. $N^{14}(\gamma,p)C^{13}$ and $N^{14}(\gamma,pn)C^{12}$ Events

The (γ,p) flag has a long fragment which leaves at the right hand side of the photograph. In this flag the recoil and fragment are almost collinear whereas in the (γ,pn) event towards the foot of the photograph, the recoil is non-collinear with the fragment.

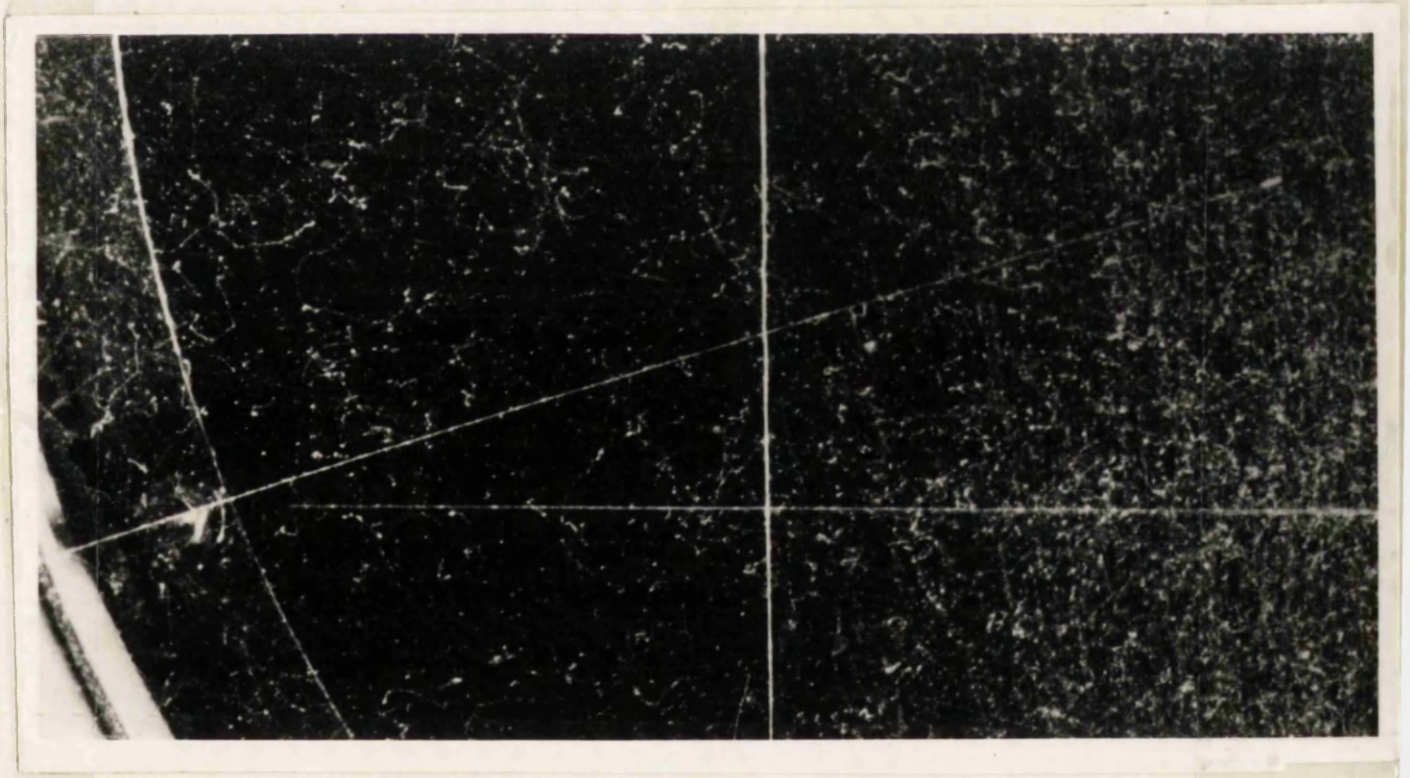

Plate III.2. $N^{14}(\gamma,p)C^{13}$

This is an enlargement of the event shown in Plate III.1 to show the detail of the recoil track.

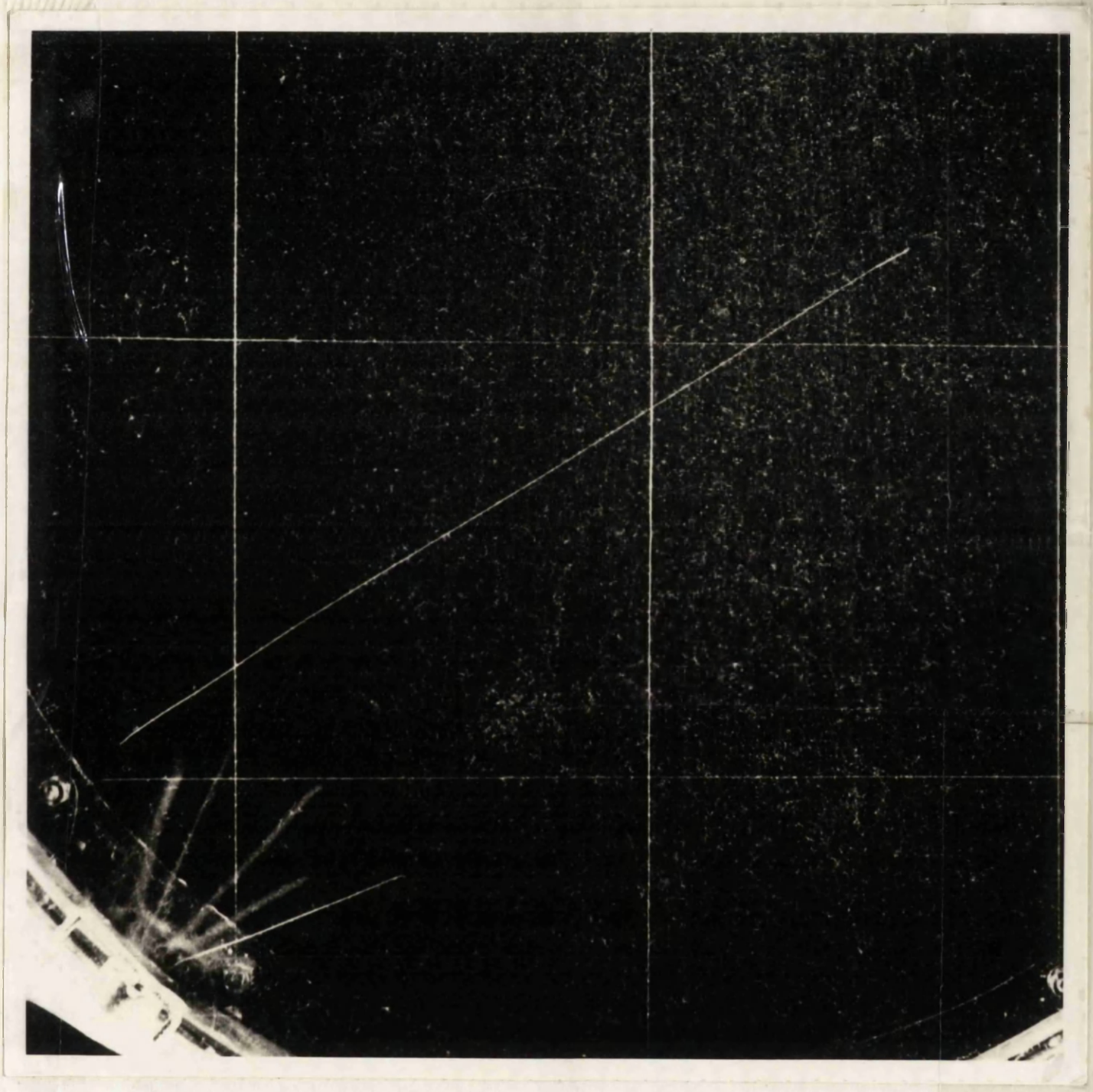

Plate IV.1. $Ne^{20}(\gamma,\alpha)\ O^{16}$ Flag.

The ionisation change at the origin is small and the fragment is heavily ionising with an intensity comparable with that of the radioactive alpha particles.

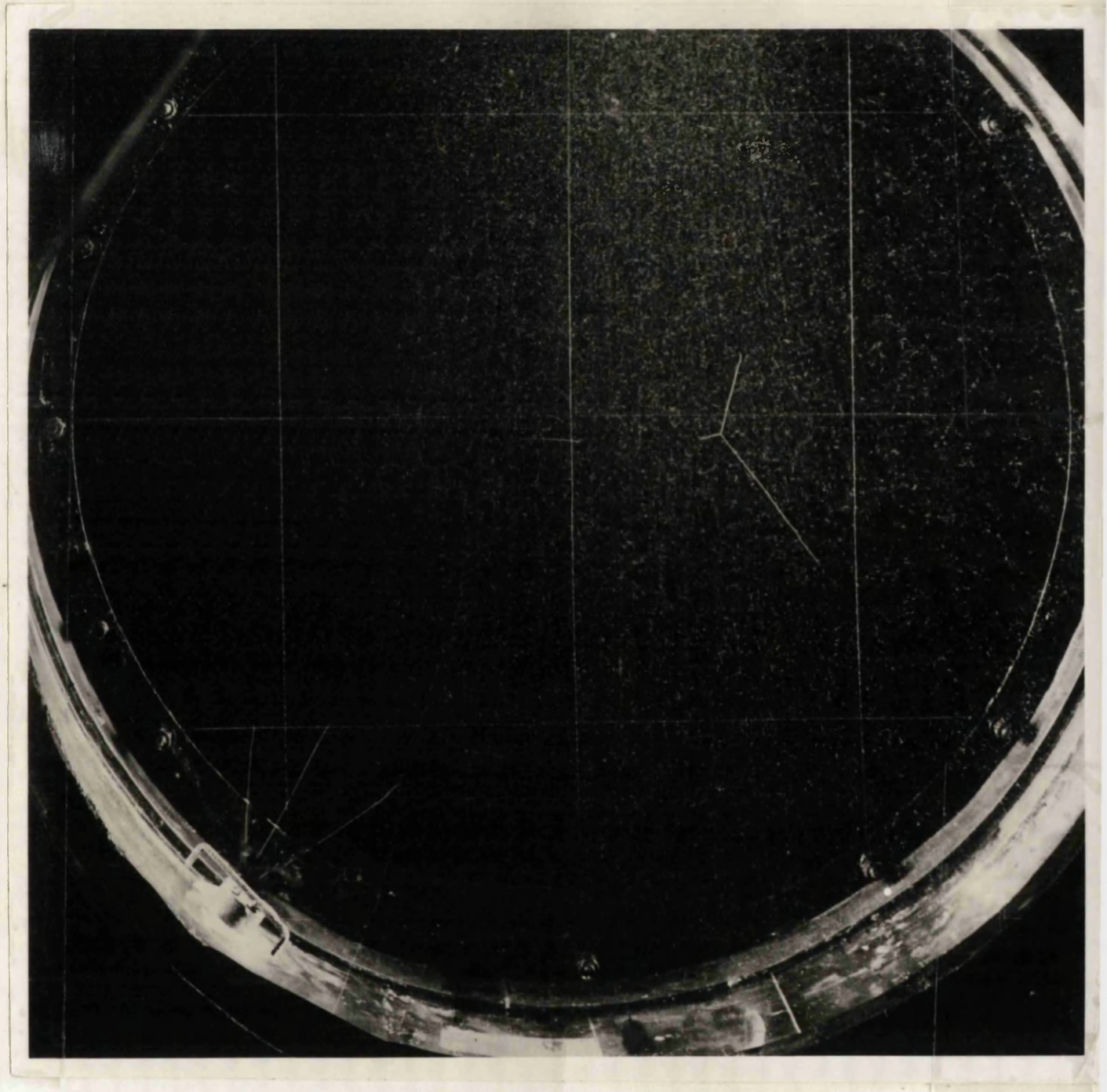

Plate IV.2. $Ne^{20}(\gamma,\alpha\alpha)C^{12}$ Star.

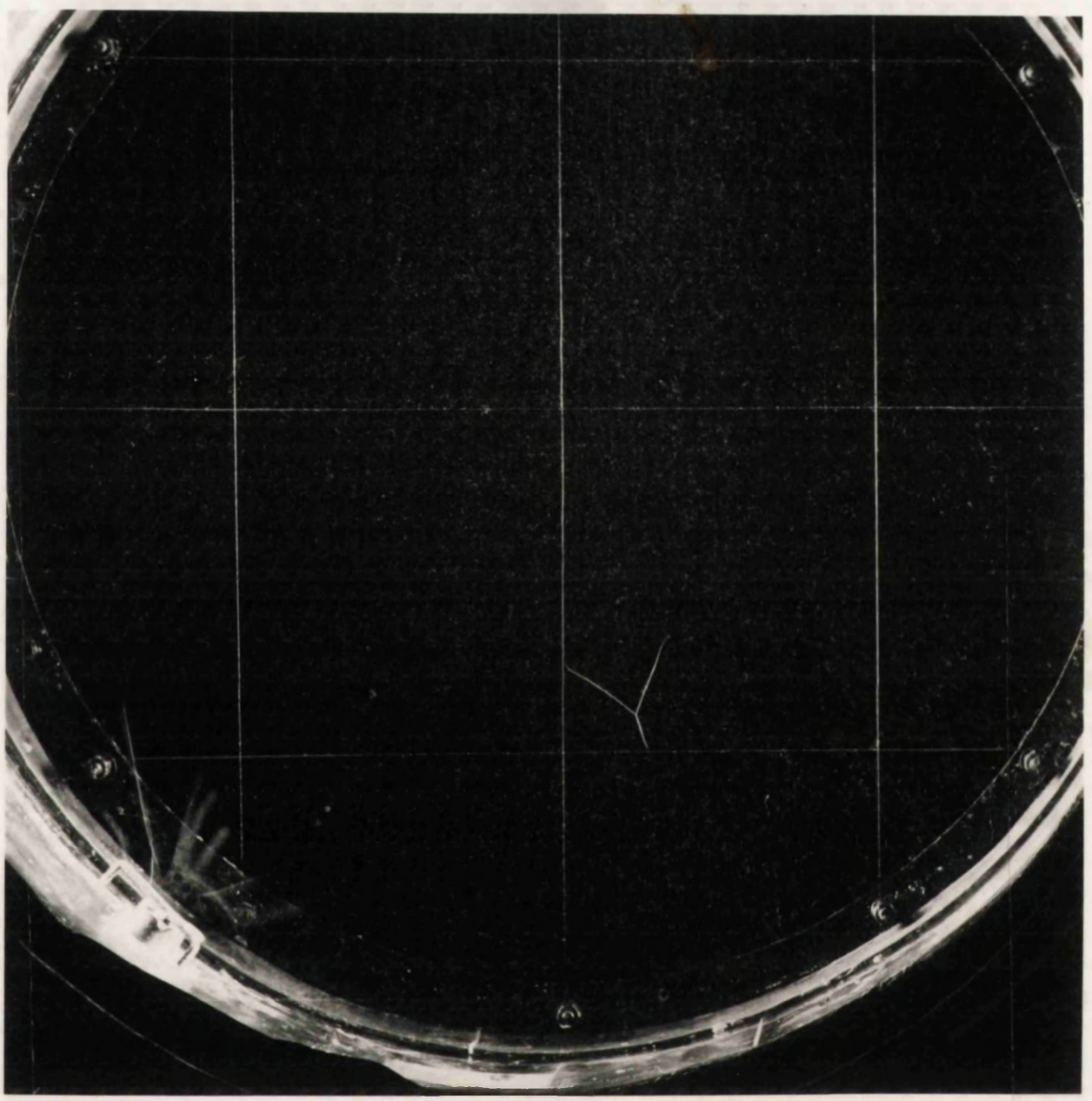

Plate IV.3. $Ne^{20}(\gamma,\alpha\alpha)C^{12}$ Star.

Plate IV.4. $Ne^{20}(\gamma,\alpha\alpha)C^{12}$ Star.

This is an enlargement of Plate IV.3.

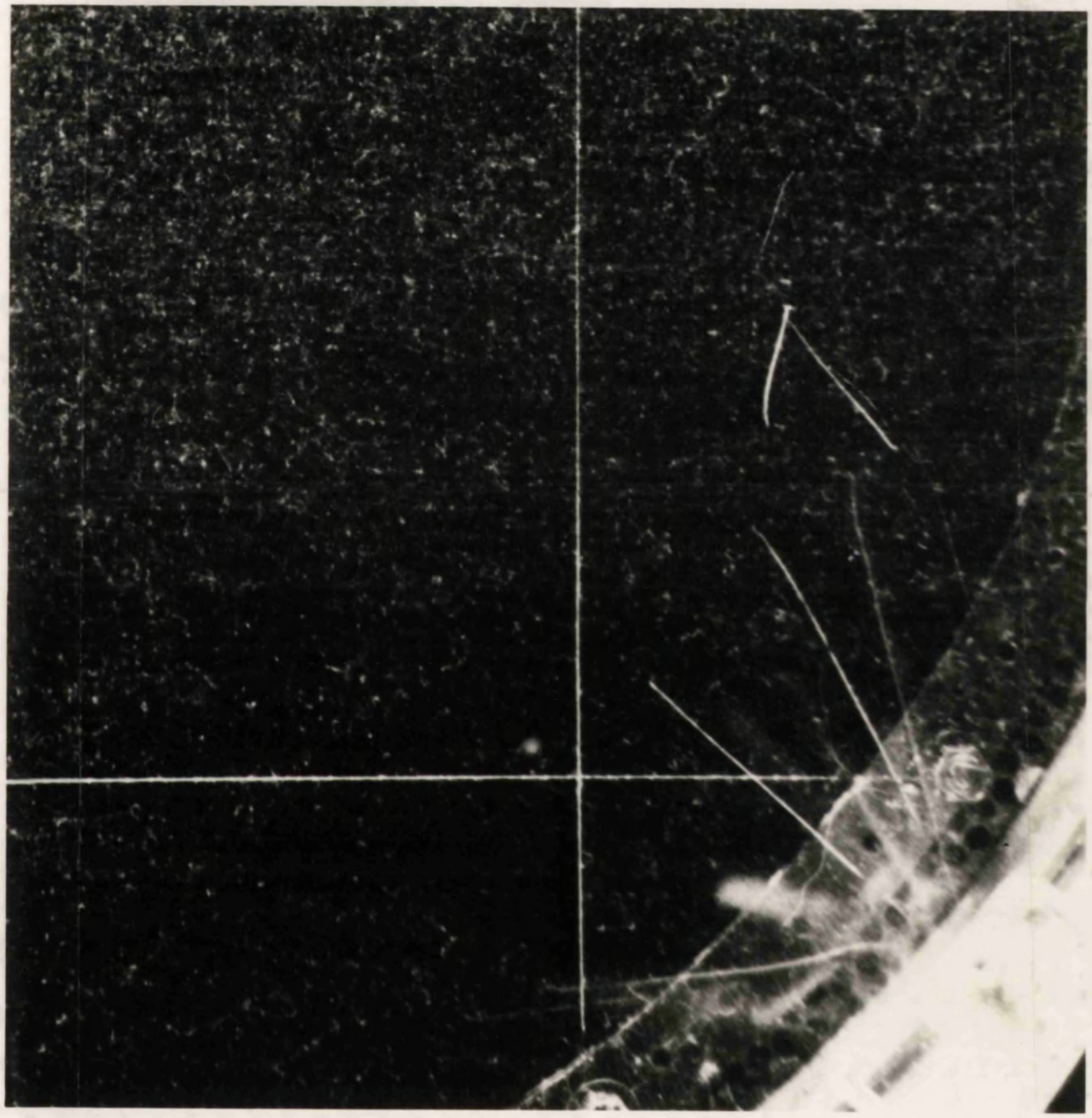

Plate IV.5. $Ne^{20}(\gamma, p)N^{15}$ Star.

The ionisation of the proton is considerably less than that of the other two tracks. That the proton has very low momentum is shown by the fact that the alpha and recoil tracks are almost in a straight line.